EVALUATION OF THE ROLE OF C-ABL IN IMATINIB-INDUCED TOXICITY IN CARDIOMYOCYTES

Dem Fachbereich Chemie der Technischen Universität Kaiserslautern
zur Verleihung des akademischen Grades
„Doktor der Naturwissenschaften“
genehmigte Dissertation

(D386)

vorgelegt von
Anja Nussher

Prof. Dr. Armin Wolf (Novartis Pharma AG/Technische Universität Kaiserslautern)
Prof. Dr. Wolfgang E. Trommer (Technische Universität Kaiserslautern)

Meinen lieben Eltern, Oma, Opa & Albert

Eröffnung des Promotionsverfahrens: 12.09.2008

Tag der wissenschaftlichen Aussprache: 26.02.2009

Prüfungskommission

Vorsitzender	Prof. Dr. Dr. Dieter Schrenk
1. Berichterstatter:	Prof. Dr. Wolfgang E. Trommer
2. Berichterstatter:	Prof. Dr. Armin Wolf

Die vorliegende Dissertation entstand zwischen Juni 2005 und Februar 2009 und wurde in der Novartis Pharma AG, Basel, Schweiz im Arbeitskreis „investigative Toxicology“ bei Prof. Dr. Armin Wolf erstellt.

Herrn Professor Armin Wolf danke ich für die Bereitstellung meines Themas.

Herrn Professor Wolfgang Trommer danke ich herzlich für die Zeit, die er sich für mich genommen hat und für seine bereitwillige Hilfe bei wissenschaftlichen Fragen.

Herrn Professor Dieter Schrenk danke ich für die Übernahme des Prüfungsvorsitzes an meiner Aussprache.

Table of Figures

Figure 1 Structure of imatinib mesylate. 6
Figure 2 Regulation of c-Abl kinase activity. 10
Figure 3 Structure of the Abl protein..... 11
Figure 4 Conformation changes in c-Abl to fully activated c-Abl. 13
Figure 5 A model for nuclear targeting in response to genotoxic stress..... 15
Figure 6 Pro- and anti-apoptotic signals of the UPR in normal cells..... 19
Figure 7 Apoptotic pathways. 22
Figure 8 Several pathways of sustained-ER stress which can lead to apoptosis..... 24
Figure 9 Schilling counting chamber 31
Figure 10 Bionas® *metabolic chip* SC1000 34
Figure 11 The luciferase reaction. 37
Figure 12 MTS and its formazan product. 38
Figure 13 Caspase 3/7 cleaves the luminogenic substrate containing the DEVD sequence. 39
Figure 14 LDH assay. 40
Figure 15 Reaction schematic for the bicinchoninic acid (BCA) containing protein assay. 41
Figure 16 Structure of doxorubicin. 55
Figure 17 ATP content in NRVCM after different time points. 57
Figure 18 ATP content in H9c2 after different time points. 59
Figure 19 MTS reduction in NRVCM after different time points. 60
Figure 20 MTS reduction in H9c2. 61
Figure 21 Caspase 3/7 activity in NRVCM. 63
Figure 22 Caspase activity in H9c2 induced by imatinib and doxorubicin. .. 65
Figure 23 LDH release in imatinib-treated NRVCM after 24 h. 66
Figure 24 Induction of eIF2α protein expression in NRVCM 24 h after imatinib treatment. 72
Figure 25 Expression profile of XBP1 in NRVCM treated for 24 h with imatinib..... 73
Figure 26 Induction of CHOP in NRVCM after imatinib treatment 24 h after incubation..... 74
Figure 27 Cytotoxicity tests in different kinds of fibroblasts 24 h after imatinib treatment. 78
Figure 28 Expression of eIF2α in different kinds of fibroblasts 24 h after imatinib incubation. 81
Figure 29 mRNA expression profile of XBP-1 spliced vs. unspliced after 24 h imatinib treatment in different kinds of fibroblasts. 82

Figure 30 CHOP expression profile 24 h after imatinib treatment in different kinds of fibroblasts. 83
Figure 31 Online cell measurement during 24 h of imatinib incubation on H9c2. 87
Figure 32 ROS generation in imatinib treated NRVCM. DCF assay. 92
Figure 33 Modulation of imatinib induced toxicity 24 h after treatment by different concentrations of the reactive oxygen scavenger DTT. 94
Figure 34 Modulation of imatinib-induced toxicity 24 h after treatment by different concentrations of the antioxidant NAC. 95
Figure 35 Modulation of imatinib induced toxicity 24 h after treatment by different concentrations of the tocopherol derivative TPGS. 96
Figure 36 Modulation of imatinib induced toxicity 24 h after treatment by different concentrations of the RNS scavenging PBN. 97
Figure 37 Structure of siRNA. 101
Figure 38 siRNA-mediated post-transcriptional gene silencing mechanism. The siRNA pathway to RNA interference. 102
Figure 39 mRNA expression of c-Abl 24 h after nucleofection of several siRNA directed against different regions in the c-Abl gene in H9c2. 106
Figure 40 Optimisation of lipofection in NRVCM. 107
Figure 41 Gene expression of IFN response markers in NRVCM 24 h after silencing. 108
Figure 42 Gene expression of c-Abl after silencing in NRVCM. 109
Figure 43 Protein expression of c-Abl after silencing c-Abl. 110
Figure 44 ATP content in silenced NRVCM 24 h after imatinib treatment... 115
Figure 45 MTS reduction in silenced NRVCM 24 h after imatinib treatment. 117
Figure 46 Caspase 3/7 activity in silenced NRVCM 24 h after imatinib treatment. 72 h. 119
Figure 47 Gene expression of ER stress-related genes on c-Abl silenced NRVCM 24 h after incubation. 121
Figure 48 Beating rate of NRVCM after silencing c-Abl with 80 nM c-Abl_10S siRNA and 24 h imatinib treatment. 123
Figure 49 Cytotoxicity (LDH release) of NRVCM after silencing c-Abl with 80 nM c-Abl_10S siRNA and treatment for 24 h with imatinib..... 123

Index of Tables

Table 1 Plate formats and their seeding conditions. 32
Table 2 Programs of the Bionas analyzer. 35
Table 3 Preparations for Gel Loads. 43
Table 4 Master Mix pipetting scheme for PCR assay. 49
Table 5 Temperature programs for One-Step RT-PCR. 49
Table 6 Calculations for desired transfection reagent. 51
Table 7 Settings for beating rate measurements. 54
Table 8 Table of significances of ATP contents after imatinib (IM) or doxorubicin (DX) treatment in NRVCM at the concentrations and time points indicated.. 58
Table 9 Table of significances of ATP contents after imatinib (IM) or doxorubicin (DX) treatment in H9c2 at the concentrations and time points indicated 59
Table 10 Table of significances of MTS reduction after imatinib (IM) or doxorubicin (DX) treatment in NRVCM at the concentrations and time points indicated. 60
Table 11 Table of significances of MTS reduction after imatinib (IM) or doxorubicin (DX) treatment in H9c2 at the concentrations and time points indicated 62
Table 12 Table of significances of caspase activity after imatinib (IM) or doxorubicin (DX) treatment in NRVCM at the concentrations and time points indicated. 63
Table 13 Table of significances of caspase activity after imatinib (IM) or doxorubicin (DX) treatment in H9c2 at the concentrations and time points indicated 65
Table 14 IC_{50}s [µM] of the cell viability in NRVCM and H9c2 after incubation of imatinib for the time points indicated. 70
Table 15 Table of significance levels of ATP content, MTS reduction, ADP/ATP ratio, caspase 3/7 activity and LDH release after imatinib (IM) treatment in different types of fibroblasts for 24 h. 79
Table 16 IC_{50}s [µM] of the cell viability in different kinds of fibroblasts after 24 h incubation of imatinib. 79
Table 17 Table of significances of acidification rates, cell impedance and respiration rates after compound treatment in H9c2 cells for 24 h. 88
Table 18 Silencing efficiencies of several siRNA oligos as determined by RT-PCR 24 h post nucleofection 106
Table 19 Silencing efficiencies of lipofected NRVCM. 107

Table 20 Table of conducted experiments of gene silencing investigations in NRVCM. 109
Table 21 Silencing efficiencies of c-Abl mRNA and protein in NRVCM. 111
Table 22 Achieved silencing efficiencies [%] of the used siRNAs in NRVCM at concentrations of 40 and 80 nM in mRNA and protein. 111
Table 23 List of designed shRNA chosen for lentiviral transfection. 129

Index of Abbreviations

µM	10^{-6} M, micromolar
mM	10^{-3} M, millimolar
nM	10^{-9} M, nanomolar
A.U.	arbitrary units
AAV	adeno-associated virus
Abl	Abelson tyrosine kinase
Ad	adenovirus
ADP	adenosine-5'-diphosphate
AGP	α acid glycoprotein
ALL	acute lymphatic leukaemia
A-MuLV	Abelson murine leukemia virus
Apaf1	apoptotic protease-activating factor 1
Arg/Abl2	Abl-related gene
ArgBP2	Arg binding protein 2
ATF	activating transcription factor
Atm	ataxia telangiectasia mutated kinase
ATP	adenosine-5'-triphosphate
ATTC	American Type Culture Collection
AUC	area under the curve
Bad	Bcl-2-associated death promoter
Bax	Bcl-2 associated X protein
BCA	bicinchoninic acid
Bcl-2	B-cell lymphoma 2
Bcr	breakpoint cluster region
BD	binding domains
Bid	BH3 interacting domain death agonist
BiP	binding immunoglobulin protein
c-Abl	cellular Abl (in mammals)
caspase	cysteine-dependent aspartate-directed protease
Cbl	casitas B-cell lymphoma
CHF	congestive heart failure
CHOP	C/EBP-homologous protein
CL	cardiolipin
c_{max}	maximum plasma concentrations
CML	chronic myeloid leukaemia
CTC	US National Cancer Institute Common Toxicity Criteria
CTL	cytotoxic T-cell lymphocyte
CYP450	cytochrome P450
cyt c	cytochrome c
DCF	2′,7′-dichlorofluorescein
H_2DCFDA	2',7'-dichlorofluorescin diacetate
DED	death effector domain
DISC	death-inducing signalling complex
DMEM	Dulbecco's modified essential medium
DNA	deoxyribonucleic acid
DNA-PK	DNA-dependent protein kinase
ds	double stranded

DTT	dithiothreitol
DX	doxorubicin
EC_{50}	50 % efficacy concentration
EGFR	epidermal growth factor receptor
eIF2α	eukaryotic initiation factor 2 α subunit
ER	endoplasmatic reticulum
FADD	Fas-associated protein with death domain
FasL	Fas ligand
FasR	Fas receptor
FGFR	fibroblast growth factor receptor
GAPDH	glycerinaldehyde-3-phosphate-dehydrogenase
GIST	gastrointestinal stromal tumours
h	hour(s)
HBSS	Hank's buffered salt solution
HIV	human immunodeficiency virus
IC_{50}	50 % inhibitory concentration
IFN	interferon
IM	imatinib mesylate
IRE1	inositol-requiring gene 1
INT	2-[4-iodophenyl]-3-[4-nitrophenyl]-5-phenyltetrazolium chloride
JNK	c-Jun N-terminal kinase
LDH	lactate dehydrogenase
miRNA	micro RNA
MLV	oncoretroviral murine leukaemia virus
mM	10-3 M, millimolar
mPMS	1-methoxy 5-methyl-phenazinium methyl sulphate
mRNA	messenger RNA
mtDNA	mitochondrial DNA
MTS	5-[3-(carboxymethoxy)phenyl]-3-(4,5-dimethyl-2-thiazolyl)2(4-
NAC	N-acetylcysteine
nDNA	nuclear DNA
NES	nuclear export signal
NF-κB	nuclear factor kappa-light-chain-enhancer of activated B cells
NLS	nuclear localisation signal
nM	10^{-9} M, nanomolar
NOX	NADPH oxidases
NRVCM	neonatal rat ventricular cardiomyocytes
OAS1	2', 5'-oligoadenylate synthetase 1
PBN	α-phenyl-tert-butyl nitrone
PBS	phosphate buffered salt solution
PDGFRα/β	platelet-derived growth factor receptor α / β
PERK	PKR-like endoplasmatic reticulum kinase
P-gp	multidrug transporter permeability-glycoprotein
Ph^+	Philadelphia chromosome
PKC	protein kinase c
PKR	protein kinase
PPD	PAZ/PIWI domain proteins
PxxP	proline-rich region
Rb	retinoblastoma protein
RIG-1	retinoic acid-inducible gene 1

RISC	RNA-inducing silencing complex
ROS	reactive oxygen species
RTK	receptor tyrosine kinase
SAPK	stress-activated protein kinase
SCF	stem cell factor
SH	Src homology domains
shRNA	short hairpin RNA
siRNA	small (short) interfering RNA
siRNP	siRNA-protein complex
SOD	superoxide dismutase
$t_{1/2}$	half-life
TG	thapsigargin
TIE-2	tyrosine kinase with immunoglobulin and EGF homology-2
TKI	tyrosine kinase inhibitor
TNF	tumour necrosis factor
TPGS	d-α-tocopheryl polyethylene glycol 1000 succinate
TRL	Toll-like receptors
Tyr	Tyrphostine
UPR	unfolded protein response
UTR	untranslated region
UV	ultra violet
VEGFR	vascular endothelial factor receptor
VDUP-1	vitamin D_3-upregulated protein-1
XBP1	X-box protein 1

TABLE OF CONTENTS

Table of Figures ii
Index of Tables iv
Index of Abbreviations vi

1 Summary 1
Zusammenfassung 3

2 Introduction 5

2.1 Imatinib 6
2.1.1 Dosing and Application 6
2.1.2 Absorption, Distribution, Metabolism and Excretion 7
2.1.3 Tolerability 8
2.1.4 Inhibition Efficacy 8
2.1.5 Binding & Inhibition of c-Abl Kinase Activity by Imatinib 10

2.2 Abelson tyrosine kinase 11
2.2.1 Protein Architecture 12
2.2.2 Localisation 13

2.3 Signalling dependent on c-Abl 14
2.3.1 The Cell Cycle 14
2.3.2 Genotoxic Stress Response 15
2.3.3 Oxidative Stress 16
2.3.4 Endoplasmatic Reticulum Stress Response 18
2.3.5 Apoptosis 21
2.3.6 Cardiotoxicity 24

3 Purpose of the Study 25

4 Materials & Methods 26

4.1 General Materials 26
4.1.1 Chemicals & Reagents 26
4.1.2 Software 26

4.2 Cell Culture 26
4.2.1 Basal media & Buffer 27
4.2.2 Supplements of Media 27
4.2.3 Cells 28
4.2.4 Fibroblast Cells 30
4.2.5 FR 30
4.2.6 RFL -6 31
4.2.7 Subculturing Cells 31
4.2.8 Mycoplasma Screening 32

4.3 Online Cell Measurement 33
4.3.1 Preparation of Medium 33
4.3.2 Cleaning of Chips 33
4.3.3 Preparation of Chips 34
4.3.4 Programs of Bionas 34

4.4 Biochemical assays 36
4.4.1 Incubation schemes 36
4.4.2 ATP Content 37
4.4.3 ADP/ATP ratio 37
4.4.4 MTS Reduction Capacity 38
4.4.5 Caspase 3/7 Activity 39
4.4.6 Lactate Dehydrogenase Release 40
4.4.7 ROS detection assay 41
4.4.8 Protein Determination 41
4.4.9 Semi-quantitative Protein Determination 42

4.5 Molecular Biology 46
4.5.1 Total RNA Extraction 46
4.5.2 Quantification of RNA 46
4.5.3 Integrity of RNA 46
4.5.4 Reverse Transcription 47
4.5.5 Real-Time Polymerase Chain Reaction (PCR) 47

4.6 RNAi 50
4.6.1 Transfections 50
4.6.2 siRNA 50
4.6.3 Set-up for Lentiviral Transfection of NRVCM 53
4.6.4 DNA purification 53

4.7 Beating rate 54

5 Results & Discussion 55

5.1 Cytotoxic & Apoptotic Potential of Imatinib 55
5.1.1 Background 55
5.1.2 Results 57
5.1.3 Discussion 67

5.2 Evaluation of Imatinib-Induced Endoplasmatic Reticulum Stress in NRVCM 72
5.2.1 Background 72
5.2.2 Results 72
5.2.3 Discussion 74

5.3 Evaluation of the Specificity of Imatinib-Induced Toxicity 77
5.3.1 Background 77
5.3.2 Results 78
5.3.3 Discussion 84

5.4 Evaluation of the Reversibility of Imatinib-Induced Effects in H9c2 cells 86
5.4.1 Background 86
5.4.2 Results 87
5.4.3 Discussion 89
5.5 Evaluation of Imatinib-Induced Reactive Oxygen Species Formation in NRVCM 92
5.5.1 Background 92
5.5.2 Results 92
5.5.3 Discussion 97
5.6 Gene Silencing of c-Abl by RNAi 101
5.6.1 Background 101
5.6.2 Results 106
5.6.3 Discussion 112
5.7 Influence of c-Abl silencing on Imatinib-mediated Impaired Cellular Function on NRVCM 114
5.7.1 Background 114
5.7.2 Results 114
5.7.3 Discussion 124
5.7.4 Set-up of Stable Silencing in NRVCM 128
5.7.5 Background 128
5.7.6 Results 128
6 Conclusion 130
7 Bibliography 132
8 Appendix 153
8.1 Acknowledgements 153
8.2 Curriculum Vitae 156

1 SUMMARY

It was recently reported that imatinib causes cell death in neonatal rat ventricular cardiomyocytes (NRVCM) by triggering endoplasmic reticulum (ER) stress and collapsed mitochondrial membrane potential. Retroviral gene transfer of an imatinib-resistant mutant c-Abl into NRVCM appeared to alleviate imatinib-induced cell death and it was concluded that the observed imatinib-induced cytotoxicity is mediated through direct interactions of imatinib with c-Abl. The imatinib effects were described as being specific for cardiomyocytes only, which are relevant also for the *in vivo* situation in man. [Kerkelä *et al.* 2006]

The goal of the present study was to reproduce the published experiments and to further explore the dose-response relationship of imatinib-induced cell death in cardiomyocytes. Additional markers of toxicity were investigated. The following biochemical assays were applied: LDH release (membrane leakage marker), MTS-reduction (marker of mitochondrial integrity), ATP cellular contents (energy homoeostasis) and caspase 3/7 activity (apoptosis). The endoplasmatic reticulum (ER) stress markers eIF2α (elongation initiation factor 2α), XBP1 (X Box binding Protein 1), and CHOP (cAMP response element-binding transcription factor (C/EBP) homologous protein) were determined at the transcriptional and protein level. Online monitoring of cell attachment of, oxygen consumption and acidification of the medium by rat heart cells (H9c2) seated on chips (Bionas) allowed the determination of the onset and reversibility of cellular functions. Image analysis measured the spontaneous beating rates after imatinib treatment. The role of imatinib-induced reactive oxygen species was evaluated directly by 2',7'-Dichlorofluorescein fluorescence and indirectly by means of interference experiments with antioxidants. The specificity of imatinib-induced effects were specific to cardiomyocytes was evaluated in fibroblasts derived from rat heart, lung and skin. The specific role of c-Abl in the imatinib-induced cellular toxicity was investigated by specific gene silencing of c-Abl in NRVCM.

The results demonstrated that imatinib caused concentration-dependent cytotoxicity, apoptosis, and ER stress in heart, skin and lung fibroblasts, similar or stronger to those observed in cardiomyocytes. Similar to the results from cardiomyocytes, ER stress markers in fibroblasts were only increased at cytotoxic concentrations of imatinib. This effect was not reversible; also, reactive oxygen species did not participate in the mechanism of the imatinib-induced cytotoxicity in NRVCM.

SUMMARY

Small interfering RNA (siRNA)-mediated reduction of c-Abl mRNA levels by 51 % and c-Abl protein levels by 70 % had neither an effect on the spontaneous beating frequency of cardiomyocytes nor did it induce cytotoxicity, apoptosis, mitochondrial dysfunction or ER stress in NRVCM. Incubation of imatinib with c-Abl siRNA-transfected NRVCM suggested that reduced c-Abl protein levels did not rescue cardiomyocytes from imatinib-induced cytotoxicity.

In conclusion, results from this study do not support a specific c-Abl-mediated mechanism of cytotoxicity in NRVCM.

ZUSAMMENFASSUNG

Vor kurzem wurde berichtet, dass die Inkubation von Imatinib zum Zelltod von neonatalen ventrikulären Kardiomyozyten der Ratte (NRVCM) führt, indem es Stress im endoplasmatischen Retikulum (ER Stress) auslöst und das mitochondriale Membranpotential zum Zusammenbruch führt. Der durch Imatinib induzierte Zelltod schien bei einer c-Abl-Mutanten, welche resistent gegen Imatinib ist und retroviral transfiziert wurde, in NRVCM vermindert zu werden. Daraus wurde geschlossen, dass die beobachtete, durch Imatinib induzierte Zytotoxizität direkt durch die Beeinflussung von c-Abl mit Imatinib vermittelt wird. Des Weiteren wurden die Effekte von Imatinib als spezifisch auf Kardiomyozyten beschrieben, welche folglich auch für die *in vivo* Situation im Menschen relevant ist. [Kerkelä *et al.* 2006]

Die vorliegende Studie nahm es sich zum Ziel, die publizierten Experimente zu reproduzieren und Dosis-Wirkungs-Beziehungen von Imatinib-induziertem Zelltod in Kardiomyozyten auszuweiten. Außerdem wurden zusätzliche Toxizitätsmarker untersucht. Dazu wurden folgende biochemische Untersuchungen durchgeführt: LDH-Freisetzung (Enzymaktivität der Laktatdehydrogenase im Überstand), MTS-Reduktion (Aktivität von mitochondrialen Enzymen), ATP-Gehalt in Zellen (Energiehomöostase) und Caspase 3/7-Aktivität (Apoptose). Marker für den ER Stress wurden auf transkriptionaler und Proteinebene untersucht: eIF2α (elongation initiation factor 2α), XBP1 (X Box binding Protein 1), und CHOP (cAMP response element-binding transcription factor (C/EBP) homologous protein). Die Zellanhaftung, der Sauerstoffverbrauch und die Ansäuerung des Mediums wurden bei Rattenkardiomyozyten (H9c2) kontinuierlich gemessen (Bionas), welche auf Chips kultiviert waren. Mit dieser Methode kann man das Einsetzen der Toxizität als auch die Reversibilität zellulärer Funktionen untersuchen. Das spontane Schlagen der Kardiomyozyten nach der Behandlung mit Imatinib wurde anhand einer Bildanalyse gemessen. Die Fluoreszenz von 2',7'-Dichlorofluorescein gab direkt Aufschluss über den Einfluss von reaktiven Sauerstoffspezies (ROS). Indirekt wurde die Bildung von ROS über Interferenz-Experimenten mit Antioxidantien beurteilt.

Die Spezifität von Imatinib-induzierten Effekten zu Kardiomyozyten wurde in Fibroblasten der Ratte bestimmt, welche vom Herzen, der Lunge und der Haut entstammten. Die spezielle Rolle von c-Abl in der von Imatinib induzierten Zelltoxizität wurde anhand spezifischen Genesilencing von C-Abl in NRVCM untersucht.

Die Ergebnisse zeigten, dass Imatinib konzentrationsabhängige Zytotoxizität, Apoptose und ER Stress in Herz-, Haut- und Lungenfibroblasten hervorrief, ähnlich oder stärker als sie in Kardiomyozyten beobachtet wurden. Ähnlich zu den Ergebnissen, welche von Kardiomyozyten erhalten wurden, zeigten sich ER Stress-Marker in Fibroblasten nur bei zytotoxischen Konzentrationen von Imatinib erhöht. Dieser Effekt stellte sich als nicht reversibel heraus. Auch konnte keine Teilnahme von reaktiven Sauerstoffspezies in dem Mechanismus von Imatinib-induzierter Zytotoxizität in NRVCM nachgewiesen werden.

Die small interfering RNA (siRNA)-vermittelte Verminderung der c-Abl-mRNA-Gehalte um 51 % und c-Abl-Proteingehalte um 70 % hatten weder einen Effekt auf die spontane Schlagfrequenz von Kardiomyozyten, noch wurden Zytotoxizität, Apoptose, mitochondriale Fehlfunktion oder ER Stress in NRVCM induziert.

Die Inkubation von Imatinib mit c-Abl siRNA-transfizierten NRVCM lässt nicht darauf schließen, dass reduzierte Proteingehalte von c-Abl Kardiomyozyten vor Imatinib-induzierter Toxizität bewahren.

Zusammengefasst lässt sich sagen, dass die Ergebnisse der vorliegenden Studie einen spezifischen c-Abl-vermittelten Mechanismus der Zytotoxizität in NRVCM nicht unterstützen.

2 INTRODUCTION

Cancer is, after cardiovascular diseases, the second major cause of death in most developed countries. And global cancer deaths are suggested to increase by 45 % until 2030 (projected number: 11.5 million) compared to 2007 (7.9 million) [Mathers *et al.* 2006]. Life expectancy has extended over the last century due to several factors – and thus, cancer increases as age-related disease [EUFIC 1998; WHO 2006].

Diagnosis of cancer was – and still is – feared and considered often as a death sentence. Over a long time cancer was known to be incurable, even after removing the tumour. Treatments for cancer went through a slow process of development. Only two centuries ago, alternative/additional treatments to surgery were developed. Chemo- and radio-therapy improved the outcome but were accompanied with heavy adverse events [Anonymous 2009]. Most cancer treatments target general processes of cell division, thereby damaging also normal cells and causing intolerable side effects.

Cancer treatment was revolutionised in 2001 by imatinib mesylate (formerly known as STI571), a small molecular drug. Unique in cancer treatment so far, this drug targets the active aberrant kinase and prevents thereby the progression to cancer effectively. The key to its success, the high specificity, also limits the use in different kinds of cancers. The most prominent cancer types imatinib is used for are rare gastrointestinal stromal tumours (GIST) and the rare chronic myeloid leukaemia (CML). [Waalen 2001]

CML is unique among malignancies in that the malady (at least in the stable chronic phase, the early stage of the disease) appears to be the result of a single major biochemical defect [Sawyers 1999]: A gene encoding the Abelson tyrosine kinase (Abl) at q34 on chromosome 9 is fused with q11 on chromosome 22, the breakpoint cluster region (Bcr). The resulting fusion chromosome 22 is known as Philadelphia chromosome (Ph). [Rowley 1973]

The protein expressed of the chimeric fusion gene named Bcr-Abl is a constitutively highly activated kinase found in 90-95 % of cases of CML (Ph^+ CML). This fusion protein is essential for initiation, maintenance and progression of CML. Additional genetic and epigenetic abnormalities are required for progression of the disease [Ren 2005].

As a selective inhibitor of tyrosine kinase activity, imatinib raises the hope of improved cancer treatment with less severe adverse events. Its unique way of action that underlies its success will be described in the next sections.

2.1 Imatinib

The small molecular drug imatinib mesylate (formerly known as STI571 now traded under the name Glivec or Gleevec in the United States) inhibits selectively the tyrosine kinase activity of Abl1, Bcr-Abl, platelet-derived growth factor receptor-α and -β (PDGFRα/β), Abl2 and c-Kit [Carroll *et al.* 1997; Heinrich *et al.* 2000]. In carcinogenic cells the activity of these tyrosine kinases is highly up-regulated.

Imatinib gained approval by the FDA within two and a half months, although "normal" FDA applications can take up to 18 months [Waalen 2001]. Indeed, imatinib has been proven to be successful and superior to historical interferon-α (IFN-α) or chemotherapy results [Sawyers 1999]. The superiority of imatinib to the former gold standard IFN-α plus cytarabine in all standard indicators for CML within a median follow-up of 19 months was shown in a crossover study [O'Brien *et al.* 2003]. A large proportion of the IFN-α-treated patients have changed to the imatinib group.

Imatinib has been developed from the lead compound of inhibitors against protein kinase C (PKC) [Zimmermann *et al.* 1996; Zimmermann *et al.* 1997]. Based on a 2-phenylaminopyrimidine backbone (Figure 1), a 3' pyridyl group at the 3' position of the pyrimidine improves activity in cellular assays. Further enhancement against tyrosine kinases is achieved by the benz-amide group at the phenyl ring. Addition of a "flag-methyl" group ortho to the diaminophenyl ring reduces activity against PKC. The water solubility and oral bioavailability is augmented with N-methylpiperazine. [Deininger *et al.* 2005]

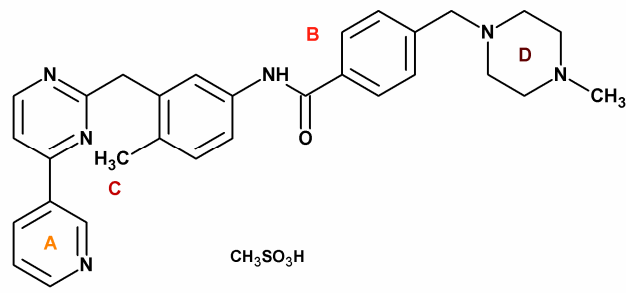

Figure 1 The structure of imatinib mesylate. The backbone of imatinib is a 2-phenylaminopyrimidine. **A.** The 3'-pyrimidine group accounts for improved activity in cellular assays. **B**. The benzamide group to the phenole ring enhances the activity against tyrosine kinases. **C.** A methyl group strongly reduces the activity against PKC. **D.** The water solubility and oral bioavailability is increased with the addition of a N-methylpiperazine group. (adapted from [Deininger *et al.* 2005])

2.1.1 Dosing and Application

Imatinib has been approved for the treatment of adult and paediatric patients newly diagnosed with Ph^+ CML, for whom bone marrow transplantation is not considered as first line treatment, in chronic phase after failure of interferon-α therapy, in accelerated phase or blast crisis. It has also been approved for the

treatment of acute lymphatic leukaemia (ALL, more aggressive than CML), c-Kit-positive unresectable and/or metastatic malignant GIST [Novartis 2005].
Imatinib is taken as a daily pill with a meal and a big glass of water, once or twice daily according to the dose. Generally, 400 mg or 600 mg once daily are recommended for adult patients. Doses of 800 mg should be taken twice daily, each dose of 400 mg. For paediatric patients, the dosing is chosen according to the body surface and the phase of the disease. In the chronic phase of CML 400 mg/d, while in the blast crisis as well as in the advanced phase 600 mg/d are recommended. For treatment of more aggressive leukaemia like Ph^+ ALL, a 600 mg/d in combination with chemotherapy is recommended. Imatinib therapy should be continued indefinitely as discontinuation is reported to result in a relapse. [Cortes *et al.* 2004]

2.1.2 Absorption, Distribution, Metabolism and Excretion

The pharmacokinetics was evaluated in a range of 25 to 1000 mg after a single dose and in steady state. Within this range, the area under the curve (AUC) increased proportionally with the dose. After repeated administration, the accumulation in the steady state was increased 1.5 – 2.5 fold. [Novartis 2005]
The absorption of imatinib occurs within 1-2 h in healthy volunteers after a single dose of imatinib [Gschwind *et al.* 2005]. Within 2-4 h the absorption occurs after oral administration in CML patients [Novartis 2005]. Thus, absorption is rapid and complete with imatinib as the main compound in plasma. Maximal plasma concentrations (c_{max}) of imatinib were found to range from 0.921 ± 0.095 µg/mL (1.87 ± 0.19µM) in healthy volunteers [Gschwind *et al.* 2005]. In CML patients the c_{max} was reported to be 2.3 µg/mL (4.6 µM). The mean absolute bioavailability is 98 % [Novartis 2001].
23 % of imatinib was found to be distributed in red blood cells, therefore 77 % of imatinib and its metabolites are present in the plasma [Gschwind *et al.* 2005] [Novartis 2005]. Most of imatinib portion found in plasma (95 %) is bound to plasma proteins, mainly to albumin, to a lesser extent to α acid glycoprotein (AGP) and a small extent to lipoprotein [Novartis 2005]. The amount of imatinib and its metabolites decreased multi-exponentially with a terminal half-life longer than two days in healthy volunteers [Gschwind *et al.* 2005]. In repeated dose studies the pharmacokinetics didn't change significantly. Within one week steady-state was reached [Peng *et al.* 2004].
Imatinib is metabolised mainly by the cytochrome P450 (CYP) isoform CYP3A4 to its main active metabolite *N*-desmethyl-imatinib with similar potency to imatinib. In plasma, an area under the curve (AUC_{0-24}) of 9 % for *N*-desmethyl-

imatinib and 65 % for imatinib was found. In CML patients the AUC of the main metabolite is about 15% of that of the parent compound. [2001]
The excretion is slow, only 25 % of the dose is eliminated after two days, mainly via the faeces. 25 % are eliminated unchanged and the remainder as metabolites [2001]. In CML patients the mean plasma half-life ($t_{1/2}$) ranges from 14.5 to 23.3 h [Peng *et al.* 2004]. In healthy volunteers the $t_{1/2}$ of imatinib is 13.5 ± 0.9 h [Gschwind *et al.* 2005].

2.1.3 Tolerability

Imatinib has been shown to be well tolerated after a single dose under fasting conditions in healthy volunteers without serious adverse events [Gschwind *et al.* 2005].
In paediatric patients imatinib treatment is generally well tolerated. The incidences of grade 3 and 4 events (classified according to the US National Cancer Institute Common Toxicity Criteria (CTC)), are low; most frequently nausea and vomiting is reported. Overall, the tolerability is similar to that in adult patients but with lower incidences of musculoskeletal pain and no reports about peripheral oedema. The latter is more frequent in patients aged ≥ 65 years [Novartis 2001].
Adverse events of imatinib in adult CML patients are usually of mild to moderate severity. Most common adverse events include nausea (43 %), oedema (39 %) and diarrhoea (25 %). Severe anaemia (CTC grade 3) was found at doses ranging from 600 – 1000 mg in some patients [Druker *et al.* 2001]. No cardiotoxic events were found during clinical trials [Deininger *et al.* 2005] and no maximal tolerated dose was identified [Druker *et al.* 2001].
Compared to the former gold standard therapy, treatment with interferon-α plus cytarabine, imatinib-receiving patients have a significantly lower incidence of neutropenia and thrombopenia (CTC grade 3 and 4) [Buchdunger *et al.* 1996].

2.1.4 Inhibition Efficacy

In kinase activity assays imatinib potently inhibits all Abl tyrosine kinases (IC_{50} = 0.025-0.2 µM, substrate phosphorylation). Serine/threonine kinases are not affected and the intracellular domain of the epidermal growth factor receptor is also not inhibited. Weak or no inhibition of the kinase domain is observed with the receptors for vascular endothelial factor 1 and 2, fibroblast growth factor 1, tyrosine kinase with immunoglobulin and EGF homology-2, c-MET and non-receptor tyrosine kinases of the SRC family. These results are confirmed in cell lines expressing constitutively active forms of Abl: V-Abl [Buchdunger *et al.* 1996], $p210^{Bcr\text{-}Abl}$ [Druker *et al.* 1996], $p185^{Bcr\text{-}Abl}$ [Carroll *et al.* 1997; Beran *et al.*

1998] and translocated ets leukaemia-Abl [Carroll *et al.* 1997]. With a concentration of up to 10 µM of imatinib the growth of parental or v-Src-transformed cells is not affected. The 50 % inhibitory concentration (IC_{50}s) values of the Abl kinase activity by imatinib ranges from 0.1 to 0.35 µM. Similar results are found in other cell lines derived from leukaemia patients positive for Ph^+ [Gambacorti-Passerini *et al.* 1997; Beran *et al.* 1998; Deininger *et al.* 2000] while Ph^--cell lines remain unaffected [Carroll *et al.* 1997; Gambacorti-Passerini *et al.* 1997]. Imatinib does not only affect the proliferation of Ph^+ cells but also induces apoptosis [Druker *et al.* 1996; Deininger *et al.* 1997].

After 30 months, imatinib achieves a haematological response in 95 % of newly diagnosed CML patients (interferon-α plus cytarabine: 56 %), a major cytogenetic response of 83 % (interferon-α plus cytarabine: 16 %) and a complete cytogenetic response of 68 % (interferon-α plus cytarabine: 5.4 %) [Novartis 2005]. Imatinib's efficacy is represented by the annual rates of disease progression to the accelerated or blast phase among patients with chronic CML after 5 years of follow-up: 1.5 %, 2.8 %, 1.6 %, 0.9 % and 0.6 % over the respective 5 years. In this study, 65 % of patients in the interferon-α plus cytarabine switched to the imatinib group while only 3 % of the imatinib group had crossed over to the alternative method. [Druker *et al.* 2006]

2.1.5 Binding & Inhibition of c-Abl Kinase Activity by Imatinib

Imatinib binds to the activation loop of the c-Abl kinase outside of a highly conserved ATP binding site. The kinase gets trapped in an inactive conformation [Schindler *et al.* 2000]. Usually the activated kinase switches between different states in a phosphorylation-dependent manner in order to control the catalytic activity [Johnson *et al.* 1996].

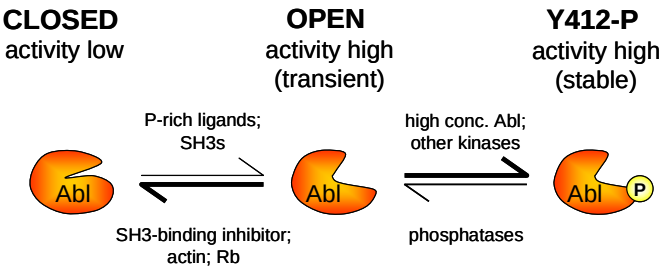

Figure 2 Regulation of c-Abl kinase activity. The catalytic domain of c-Abl kinase switches its conformation dynamically from the inactive closed to the open kinase active conformation. This equilibrium normally favours the closed form with low specific activity. When phosphorylated at Tyr 412, the open form is stabilised and thus the equilibrium is shifted towards the active form. (adapted from [Harrison 2003])

When fully active, the loop is stabilised in an open conformation by phosphorylation on residues within the loop (see Figure 2). This conformation, also called “active” conformation, is very similar in all kinases. In contrast, the conformations in the inactive state of the kinases are very distinct [Schindler *et al.* 2000]. And here the specificity of imatinib is founded: it binds to and stabilises c-Abl in its more unique inactive conformation with no ATP bound.

Interestingly, the concentration at which 50 % of the kinase is inhibited (IC_{50}) is approximately 200-fold lower for the active tyrosine-phosphorylated kinase compared to the inactive one [Hubbard *et al.* 1998]. This seems paradox as imatinib is shown to inhibit effectively the kinase activity of the constitutively *active* Abl-oncogenes when the *inactive* form is greatly favoured.

This phenomenon can be explained by switching from a static to a dynamic approach. Even in the activated state of c-Abl the conformation of the catalytic domain flips between open and closed, the phosphorylation is transient. With the inhibitor occurring, the system will balance the conformations to the inactive form by stably binding and withdrawing it from the equilibrium. [Smith *et al.* 2002]

2.2 Abelson tyrosine kinase

The Abl gene is the human homologue of the oncogene v-Abl of the Abelson murine leukaemia virus which has been incorporated at some point in evolution [Abelson *et al.* 1970]. In mammals the Abelson tyrosine kinase (Abl1) is often referred to as cellular Abl (c-Abl). Together with Arg (Abl-related gene; Abl2), its only paralogue, c-Abl builds the Abl family of non-receptor tyrosine kinases (non-RTK) which are closely related to Src kinases. [Hanks 2003]

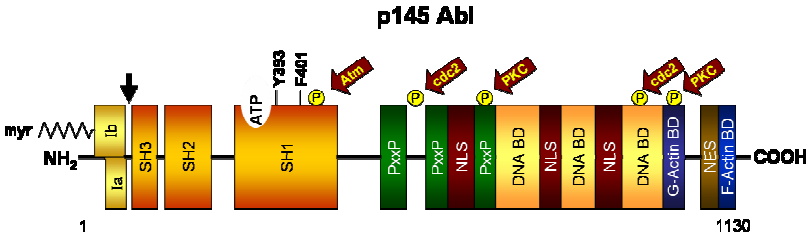

Figure 3 Structure of the Abl protein. Two isoforms are denoted with the first exon at the NH3-terminus. Ib is 19 kb longer and contains a myristoylation (myr) site for anchoring at the membrane. Three SRC-homology (SH) domains are located close to the NH3 terminus. The major site for autophosphorylation within the kinase domain is Y393. Phenylalanine 401 (F401) is highly conserved in PTKs containing SH3 domains. Proline-rich regions (PxxP) dominate the centre and are capable to bind to SH3 domains, besides three nuclear localisation signals (NLS) are found, two of them located closer to the c-terminus as well as a nuclear export signal (NES) is located to the C-terminus. At this end, binding domains (BD) for G-actin as well as F-actin are located. (modified from [Deininger *et al.* 2000])

The difference to Src kinases is in an additional C-terminal region that contains nuclear localisation (NLS) and export (NES) signals, as well as binding sites for cellular proteins like signalling adapters and actin (Figure 3). Towards the NH2-terminus three Src homology domains (SH1-SH3) are located. The tyrosine kinase function is designed by SH1 while SH2 and SH3 are responsible for interactions with proteins [Cohen *et al.* 1995]. The structural domains are illustrated within the protein. The two possible isoforms (Ia and Ib) in human c-Abl emerge after varying splicings of the first exon [Laneuville 1995; Smith *et al.* 2002]. The Ib isoform of c-Abl is 19 residues longer, contains a myristoylation signal and seems to be expressed in all cell types [Renshaw *et al.* 1988].

2.2.1 Protein Architecture

Protein kinases are known for a variety of activation mechanisms [Blume-Jensen *et al.* 2001] including binding of another molecule (second messengers, other protein subunits), dissociation from an inhibitor or phosphorylation/de-phosphorylation. Like many kinases, c-Abl is activated by the phosphorylation of a residue on a mobile segment near the catalytic cleft, the “activation segment” [Johnson *et al.* 1996]. The activation is carried out in a two step process in protein kinases(Figure 4): (1) a structural transition from a “closed” to “open” conformation with rearrangement of structural elements essential for substrate binding and catalysis involved, followed by (2) stabilising the open confirmation by the means of phosphorylation of the activation segment [Hubbard *et al.* 1998]. The first step is in equilibrium between the open and the closed formation, normally favouring the closed one. With the step to phosphorylation the equilibrium shifts towards the open conformation. As a result, the kinase is fully activated [Smith *et al.* 2002].

As a member of the Src kinases, this circle of activation/inhibition is essentially the same for c-Abl but bears some differences that finally lead the two kinases to adopt dissimilar conformations in their auto-inhibited state. The differences cause various conformations even in conserved parts of the catalytic site. [Harrison 2003]

The catalytic activity of c-Abl is very tightly regulated *in vivo* [Pendergast 2002]. A complex mechanism regulates and stabilises inactive c-Abl including intra-molecular inhibition by the SH3 domain [Van Etten *et al.* 1995; Barila *et al.* 1998; Brasher *et al.* 2001], and N-terminal domains [Pluk *et al.* 2002], regulatory tyrosine phosphorylation [Van Etten *et al.* 1995; Brasher *et al.* 2001] and binding of cellular inhibitors [Pendergast *et al.* 1991; Wen *et al.* 1997].

The intra-molecular complex inhibiting c-Abl involves the catalytic kinase domain as well as the SH2 and SH3 domains including all other segments towards the N-terminus of the protein. [Courtneidge 2003; Harrison 2003; Hantschel *et al.* 2004]

C-Abl builds a regulatory apparatus out of three critical components (illustrated in Figure 4): The “switch”, the kinase-activation loop and the coupling of its conformational state to a transition between active and inactive conformations. The “clamp”, an assembly of both SH2 (large lobe) and SH3 (small lobe) domains represents the “regulatory apparatus” on the back side of the kinase. The “latch”, the N-myristoyl group [Hantschel *et al.* 2003]; binds to a deep hydrophobic pocket in the large lobe. If the myristoyl group is not in place, the binding site for the SH2 domain is destroyed [Schindler *et al.* 2000].

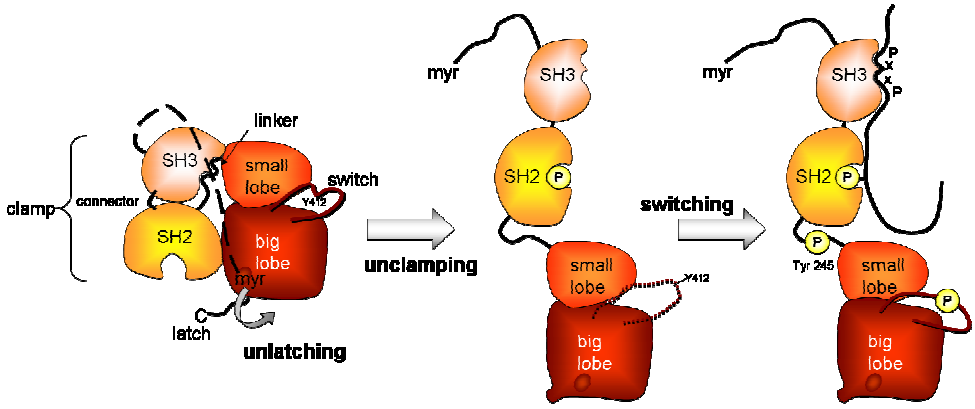

Figure 4 Conformation changes in c-Abl to fully activated c-Abl. The SH2-SH3 fixes the bilobed kinase domain in the inactive state. The N-terminal end anchors with its myristoyl group in a hydrophobic pocket of the SH2 domain. By release of the myristoylated N-terminus, the assembled state is unlatched and can progress to unclamping. When unclamped by competing SH2 or SH3 ligands, the kinase domain can in turn be switched into its active conformation by phosphorylation of Y412 in the activation loop (shown in dark red/black). Phosphorylation of 245 in the linker further sets the switch in c-Abl. (adapted from [Harrison 2003])

With removal, the clamp is unlocked by destabilising the SH2-interaction [Xu *et al.* 1999]. The SH2 and SH3 modules are in charge of hiding/presenting the catalytic cleft. For this purpose, a connector in between them allows flexing. With the assembly of the two modules the capacity to flex is blocked by spanning the two lobes and contacting the hinge between them directly [Nagar *et al.* 2003].

The terminal inactivation of activated c-Abl is mediated by an ubiquitation-dependent degradation in the proteasome [Echarri *et al.* 2001]. Adaptor proteins regulate various cellular events like cell adhesion, migration, proliferation, cell survival and cell cycle as well as cytoskeletal organisation [Pawson *et al.* 1997; Buday 1999; Flynn 2001]. A member of the vinexin adaptor protein family Arg binding protein 2 (ArgBP2) promotes c-Abl to the proteasome. ArgBP2 is expressed ubiquitously, in the heart at high level. ArgBP2 is located in the nucleus as well as on stress fibres [Wang *et al.* 1997], just like c-Abl [Van Etten *et al.* 1989]. ArgBP2 negatively regulates c-Abl kinase via recruiting casitas B-cell lymphoma (Cbl, an ubiquitin ligase) [Thien *et al.* 2001] to the c-Abl complex. Hence, c-Abl phosphorylates Cbl which finally leads to a Cbl-mediated ubiquitination and degradation of c-Abl [Soubeyran *et al.* 2003].

2.2.2 Localisation

Within the cell the localisation of c-Abl is strictly regulated [Hantschel *et al.* 2004; Wong *et al.* 2004] because c-Abl mediates apoptosis or survival dependent on its localisation [Yoshida *et al.* 2005].

Localisation of c-Abl is different depending on the cell type and its function. For example, in fibroblasts c-Abl is predominantly located in the nucleus mediating

apoptosis while most of c-Abl is cytoplasmic in primary haematopoietic cells and neurons. In sharp contrast, transformed c-Abl is like Bcr-Abl, the molecular defect in CML, solely located to the cytoplasm and recruits survival. Enforced entrapment of Bcr-Abl in the nucleus subsequently induces apoptosis [Vigneri *et al.* 2001].

A NES and three NLSs control the shuttle between cytoplasm and nucleus independently of the c-Abl kinase activity [Shaul 2000; Yoshida *et al.* 2005]. In both the cytoplasm and the nucleus c-Abl is associated to certain proteins.

14-3-3 proteins are in charge of inhibition of the apoptotic response in the cytoplasm. Once these proteins are lowered, c-Abl shuttles into the nucleus [Yoshida *et al.* 2005] and interacts with the retinoblastoma tumour suppressor protein (Rb) inhibiting its activity [Welch *et al.* 1993]. The consequences will be explained in chapter 2.3.1.

2.3 Signalling dependent on c-Abl

The c-Abl protein holds a complex role of a central module. Depending on external (e.g. growth factors) as well as internal signals (e.g. oxidative stress), it influences processes of the cell cycle and apoptosis. [Schwartzberg *et al.* 1991; Tybulewicz *et al.* 1991]

2.3.1 The Cell Cycle

In resting or early G_1 cells, c-Abl is bound to Rb, a potent inhibitor of the tyrosine kinase activity [Welch *et al.* 1993]. In complex with Rb, c-Abl can be recruited to a DNA-binding complex in the nucleus [Welch *et al.* 1995]. At the G_1/S transition the c-Abl-Rb-complex becomes disrupted by the cell cycle-regulated phosphorylation of Rb, resulting in activated and released nuclear c-Abl which allows the cells to enter the S phase [Welch *et al.* 1993; Welch *et al.* 1995]. An enhancement of nuclear c-Abl activity can be achieved by exposing cells in the S-phase to DNA-damaging agents such as ionising radiation [Liu *et al.* 1996]. For this effect, an ataxia telangiectasia mutated kinase (Atm) is required [Baskaran *et al.* 1997].

2.3.2 Genotoxic Stress Response

When cells are exposed to ultraviolet irradiation or agents damaging the DNA, genotoxic stress affect the cell. The cell responses differently to genotoxic stress including cell-cycle arrest, activation of DNA repair and in the worst case, induction of apoptosis.

Genotoxic stress activates the proapoptotic mitogen activated protein kinase pathways and c-Jun N-terminal kinase/stress-activated protein kinase (JNK/SAPK). [Kharbanda *et al.* 1998]

JNK/SAPK in turn phosphorylates 14-3-3 proteins in the cytoplasm causing the dissociation of the c-Abl-14-3-3 complex [Yoshida *et al.* 2005] in the cytoplasm. As a result, c-Abl transiently accumulates in the nucleus, inducing apoptosis [Huang *et al.* 1997; Yuan *et al.* 1997].

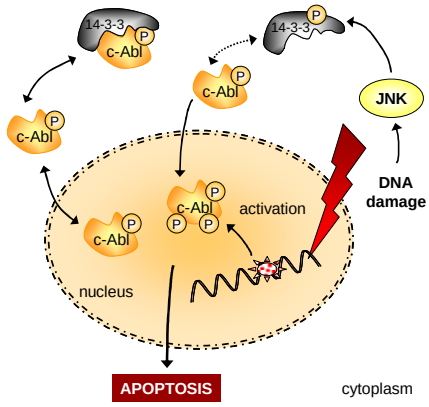

Figure 5 A model for nuclear targeting in response to genotoxic stress. On the left side c-Abl is illustrated in the cell under normal conditions, shuttling between the cytoplasm and the nucleus. In the cytoplasm the 14-3-3 protein binds and traps it. On the right side DNA damage abrogates the cytoplasmic sequestration of c-Abl by JNK-mediated phosphorylation. Dissociated c-Abl targets the nucleus while nuclear c-Abl is activated and apoptosis is induced. (adapted from [Yoshida *et al.* 2005])

Nuclear c-Abl is activated by mechanisms dependent on DNA-dependent protein kinase (DNA-PK) as well as of Atm [Baskaran *et al.* 1997]. In turn, c-Abl phosphorylates and activates proteins in the nucleus associated with DNA-damage-induced cell death like p73 and Rad9 [Kharbanda *et al.* 1995; Kharbanda *et al.* 2000] and p53 [Gong *et al.* 1999; Yuan *et al.* 1999].

C-Abl is activated in response to genotoxic stress [Kharbanda *et al.* 1995] and is essential for DNA damage-induced apoptosis [Huang *et al.* 1997].

It was recently shown that c-Abl targets and phosphorylates caspase 9 in proximity to the caspase recruitment domain in response to genotoxic stress. In turn, Caspase 9 auto-processes and activates caspase 3 [Raina *et al.* 2005]. Caspases are hallmarks of apoptosis and will be explained in chapter 2.3.5.

2.3.3 Oxidative Stress

Reactive oxygen species (ROS) are naturally occurring products of cellular metabolism and can be harmful or beneficial for living systems. They are free radicals which are oxygen-defined molecules with one or more unpaired electrons which accounts for their high reactivity and therefore short half-life. [Valko *et al.* 2004; Valko *et al.* 2006]

At low/moderate concentrations they benefit the system by being part of diverse cellular signalling pathways, e.g. in the defence against infectious agents and by induction of the mitogenic response. The deleterious effect of free radicals is termed oxidative stress. [Kovacic *et al.* 2001; Valko *et al.* 2001; Ridnour *et al.* 2005]

The transient production of hydrogen peroxide (H_2O_2) is an important signalling event triggered by the interaction of a variety of cell surface receptors with their ligands [Chen *et al.* 1995; Lo *et al.* 1995; Bae *et al.* 1997; Zafari *et al.* 1998; Sattler *et al.* 1999; Sattler *et al.* 2000].

NADPH oxidases (NOX) are prominent sources of receptor-activated H_2O_2 [Park *et al.* 2004]. They reduce molecular oxygen to superoxide, which undergoes dismutation, either spontaneously or catalytically, to form H_2O_2. H_2O_2 leads to a sequence of events that includes phosphorylation of c-Abl, oligomerisation, and Ca^{2+}-dependent translocation, resulting in the membrane co-localisation of activated c-Abl and NOX5 proteins [El Jamali *et al.* 2008].

In addition, ROS can be produced by irradiation with UV light/x-rays/γ-rays or they can be catalysed by metal ions. During inflammation neutrophils and macrophages produce ROS, and they are also generated during oxidative phosphorylation [Cadenas 1989].

ROS such as hydrogen peroxide, superoxide and hydroxyl radical are naturally occurring products of oxygen metabolism in all aerobic organisms. An imbalance between the production of ROS and the detoxification system of the cell causes oxidative stress which results in damage of lipids, proteins and DNA. Additional ROS are caused by detoxification reactions of the cytochrome P450 system [Scholz *et al.* 1990]. Depending on the scale of damage, oxidative stress may be handled by the cell, retaining its normal state. Increased oxidative stress can trigger apoptosis, while severe damage caused by oxidation leads to necrosis [Lennon *et al.* 1991].

ROS leads to activation of protein kinase C δ (PKCδ), which triggers the ROS-induced activation of c-Abl and also the translocation of c-Abl to mitochondria. In the mitochondria, c-Abl triggers cytochrome c (cyt c) release that contributes to apoptosis [Sun *et al.* 2000]. In addition, c-Abl induces a loss of mitochondrial

transmembrane potential leading to both apoptosis and necrosis [Ha *et al.* 1999].

In mitochondria ROS can also damage mitochondrial DNA (mtDNA) that encodes genes essential for oxidative phosphorylation. Once damaged, the loss of electron transport, mitochondrial membrane potential and ATP generation can result in lethal cell injury. Beside the production of energy, mitochondria synthesise iron-sulphur-clusters. Iron, like oxygen, is essential for life but together they generate ROS. An increase of iron concentration causes oxidation of proteins as well as mitochondrial and nuclear DNA damage [Karthikeyan *et al.* 2003]. Oxidative phosphorylation is reduced which subsequently leads to an increased generation of H_2O_2 in mitochondria. The mtDNA of mammalian cells is much more sensitive to H_2O_2-induced damage compared to nuclear DNA (nDNA). Also, liberated iron may lead to DNA damage even at physiological concentrations of H_2O_2 [Yakes *et al.* 1997]. Oxidative mtDNA damage triggers expression of faulty genes, lack of key electron transport enzymes and subsequent ROS generation to finally result in cell death. This cascade is also called the mitochondrial catastrophe thesis. [Fariss *et al.* 2005]

ROS have a short half-life, thus molecules in proximity to ROS-producing sites in the inner mitochondrial membrane are targets for oxidation. One of these is cardiolipin (CL), an unsaturated phospholipid located exclusively on the inner mitochondrial membrane of eukaryotic cells [Tuominen *et al.* 2002]. CL anchors the cyt c protein to the mitochondrial membrane where it participates in the electron transport of the respiratory chain [Fariss *et al.* 2005]. ROS induces CL peroxidation followed by the caspase pathway [Iverson *et al.* 2004]. The dissociation of cyt c from CL is also expected to be caused by ROS, making cyt c ready for entering the cytoplasm upon permeabilisation of the outer membrane [Ott *et al.* 2002].

2.3.4 Endoplasmatic Reticulum Stress Response

The endoplasmatic reticulum (ER) is responsible for protein synthesis and proper folding of secreted and surface proteins. Translated on polysomes which are bound to the membrane, they are translocated in their extended, unfolded state through the translocon into the ER. The ER is an oxidising compartment favouring the formation of disulphide bonds and stabilises thereby the protein folding and assembly (reviewed in [Ron 2002]). Highly charged N-linked glycans are often added to the peptides. As a consequence, the ways a protein can fold is limited, thus aids to keep the correct way of folding. ER molecular chaperones and folding proteins aid and monitor the maturation of nascent proteins. They associate with newly synthesised proteins in order to prevent their aggregation and to support the correct folding and assembly under ATP consumption [Ellgaard *et al.* 1999; Ma *et al.* 2004]. Secretory proteins also need Ca^{2+} for proper maturation. If any of these aspects are changed, unfolded proteins can accumulate in the ER and impair its functions (reviewed in [Ron 2002]).

Proteins improperly matured are retained in the ER or sent to cytoplasm for degradation dependent on 26S proteasome, ER and cytosolic chaperones [Brodsky *et al.* 1999]. Alterations in homeostasis are sensed by the ER and signals are transduced to the nucleus and cytoplasm. Hence, eukaryotic cells respond to the accumulation of unfolded or excess proteins in the ER with transcriptional activation of genes that encode proteins residential in the ER and repression of protein synthesis [Mori 2000] which is referred to as the unfolded protein response (UPR) [Gething *et al.* 1992].

The UPR serves to limit the accumulation of unfolded proteins, preserves the solubility of those that are present and targets them for degradation. Primarily, the UPR activation protects the ER. However, it also acts to limit the damage to other organelles and, in extreme cases, to ultimately protect the organism by triggering apoptosis in cells experiencing prolonged stress [Kozutsumi *et al.* 1988].

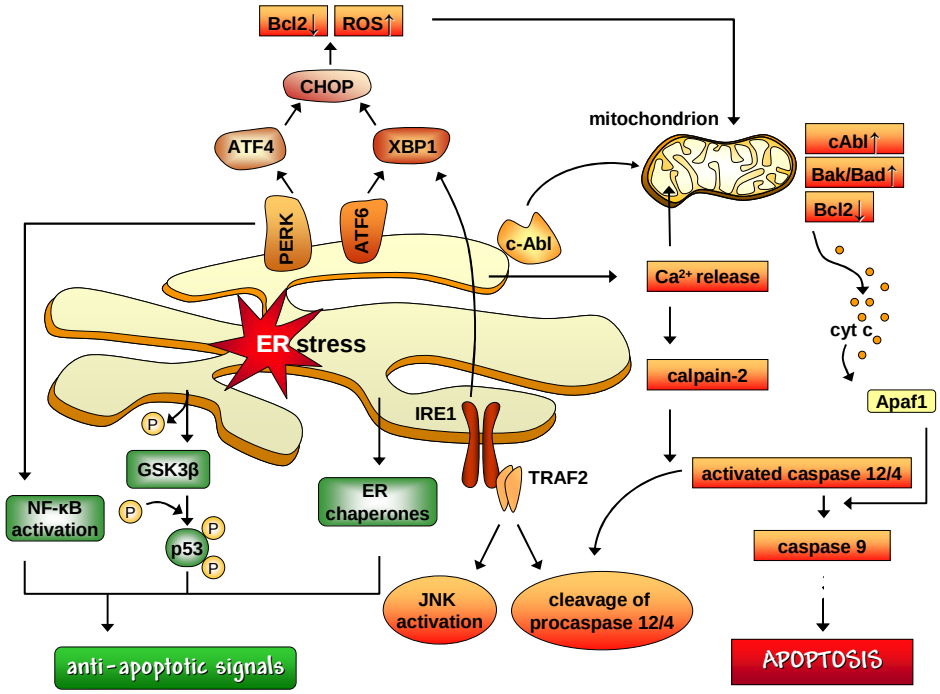

Figure 6 Pro- and anti-apoptotic signals of the UPR in normal cells. ER stress activates pathways dependent or independent on mitochondria. When CHOP is induced and c-Abl is translocated to the mitochondrial membrane during ER stress, pro-apoptotic members of the Bcl2-family (Bak/Bad) are up-regulated while the anti-apoptotic member Bcl2 is down-regulated. Subsequently, the mitochondrial membrane is damaged and cyt c is released to the cytosol. The activation of IRE1 recruits tumour-necrosis factor receptor associated factor 2 (TRAF2) which activates pro-caspase 12 (in humans 4) thereby signalling an apoptotic response independent of mitochondria. On caspase 9 and 3 both pathways are united and lead to cell death. Anti-apoptotic responses triggered by ER stress can be mediated by glycogen synthase kinase-3(beta) (GSK3beta) which phosphorylates p53 when activated leading to its degradation. Activation of NF-kB induces also anti-apoptotic responses. Apaf1: apoptotic protease activating factor 1; ATF: activating transcription factor; JNK: c-Jun N-terminal kinase; NF-kB: nuclear factor k-B; PERK: PKR-like kinase; ROS: reactive oxygen species; XBP1: X-box binding protein 1. (adapted from [Ma *et al.* 2004])

Possible pathways triggered upon ER stress are illustrated in Figure 6. In the early response to ER stress, PKCδ is suggested to be activated by ROS and recruited to the ER by ER stress sensing proteins such as c-Abl [Qi *et al.* 2008]. PKCδ translocates rapidly to the ER where it builds a complex with and becomes phosphorylated by c-Abl [Yuan *et al.* 1998; Sun *et al.* 2000]. The complex translocates to mitochondria dependent on the phosphorylation of PKCδ and its catalytic activity. Together they activate JNK which in turn triggers the intrinsic pathway of apoptosis by translocating the pro-apoptotic proteins of the Bcl-2 family, Bax (Bcl-2-associated X protein) and Bad (Bcl-2-associated death promoter) to the mitochondrium causing subsequent release of cyt c of the mitochondrium [Qi *et al.* 2008].

Accumulation of unfolded proteins in the ER [Kozutsumi *et al.* 1988] emerges the dissociation of BiP (binding immunoglobulin protein) from the luminal domains of UPR transducers, namely IRE1 (inositol-requiring gene 1), PERK

(PKR-like endoplasmatic reticulum kinase) and ATF6 (activating transcription factor 6) [Bertolotti *et al.* 2000; Shen *et al.* 2002] and causes dimerisation followed by activation of the kinases.

Activated IRE1 features an endonuclease which removes 26 bases from the X-box protein 1 (XBP1) transcript. The resulting transcription factor bears a more potent transactivation domain than the one encoded by the unspliced form of XBP1 [Yoshida *et al.* 2001]. During the UPR a transient inhibition of protein synthesis is initiated by PERK. By activating the eukaryotic translation factor 2α subunit (eIF-2α) [Shi *et al.* 1998; Harding *et al.* 1999], a G_1 arrest is induced that prevents the propagation of cells experiencing ER stress. However, this block of translation induces at the same time the synthesis of activating transcription factor 4 (ATF4) [Harding *et al.* 2000] and transactivates downstream proteins like GADD34 [Ma *et al.* 2003] which reverses the translation effect by phosphorylating eIF-2α and C/EBP-homologous protein (CHOP). CHOP subsequently triggers apoptosis [McCullough *et al.* 2001]. PERK also regulates positively anti-apoptotic proteins like B-cell lymphoma 2 (Bcl-2) during ER stress via activation of the nuclear factor kappa-light-chain-enhancer of activated B cells (NF-κB) [Jiang *et al.* 2003].

The release of BiP from ATF6 induces the translocation of ATF6α/ATF6β transcription factors to the Golgi where they are cleaved during UPR activation [Ye *et al.* 2000]. Thereby the cytosolic transcription-factor domain is liberated. The ER-localised transmembrane protein ATF6 induces XBP1-transcription which is subsequently spliced by the activated IRE1 endonuclease domain [Haze *et al.* 1999]. The spliced form of XBP1 is a highly active transcription factor and up-regulates ER chaperones as well as folding proteins [Yoshida *et al.* 2001; Calfon *et al.* 2002]. The transcription-factor domain of ATF6 is liberated from the membrane and transported to the nucleus [Ma *et al.* 2004].

In addition, IRE1 activates JNK/SAPK (c-Jun N-terminal kinase) and induces gene transcription [Shamu *et al.* 1996; Tirasophon *et al.* 1998; Urano *et al.* 2000].

2.3.5 Apoptosis

Apoptosis is a programmed cell death which is initiated upon specific stimuli under consumption of ATP. This form of cell death is genetically controlled and evolutionarily conserved, essential for normal embryonic development and for the maintenance of tissue homeostasis in adults [Fariss *et al.* 2005]. Characteristic changes in morphology include cell shrinkage, plasma membrane blebbing, chromatin condensation and typically, the fragmentation of DNA into multiples of 180bp. Ultimately, the cells break into small apoptotic bodies which are cleared through phagocytosis by proximal cells [Delhalle *et al.* 2003]. A variety of biochemical changes accompanies this transformation, such as the externalisation of phosphatidylserine at the cells surface [Homburg *et al.* 1995; Martin *et al.* 1995] and other alterations that promote recognition by phagocytes [Pradhan *et al.* 1997; Savill 1997].

Apoptotic cell death is triggered by extrinsic (receptor-mediated) and intrinsic (mediated by mitochondria) signalling pathways, both illustrated in Figure 7. The external pathway may also affect the intrinsic pathway via caspase 8 in order to amplify the apoptotic response [Aouad *et al.* 2004]. A specialised family of cysteine-dependent aspartate-directed proteases [Lazebnik *et al.* 1994] termed caspases [Alnemri *et al.* 1996] is the hallmark of apoptosis [Thornberry *et al.* 1998]. Caspases are synthesised as inactive zymogens (pro-caspases) and get activated by a specific cleavage [Thornberry *et al.* 1997]. They are classified into two families, the initiator caspases (e.g. caspase 8, 9) and the effector caspases (e.g. caspase 3, 7) [Shi 2002].

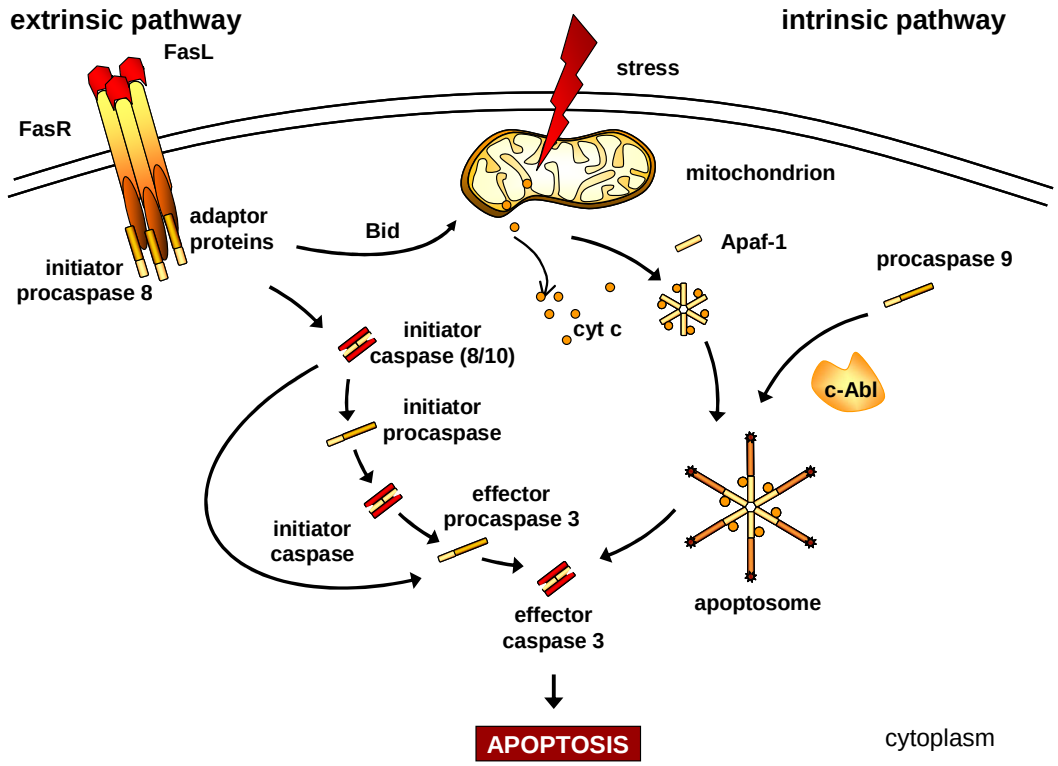

Figure 7 Apoptotic pathways. The extrinsic pathway illustrated on the left side is initiated by ligands, in this case the Fas-ligand. Fas-receptors trimerise and adaptor proteins (FADD) associate to their death domain. FADDs recruit initiator pro-caspases to the complex and activate them to cleave effector pro-caspases or to translocate a member of the proapoptotic Bcl-2 family (Bid) to the mitochondria. Hereafter the intrinsic pathway is triggered. Cytochrome c (cyt c) is released to the cytosol to build under ATP consumption the apoptosome which cleaves and activates effector caspases resulting in self-destruction of the cell. (adapted from [Delhalle *et al.* 2003])

Death receptors are a family of cell-surface receptors like the tumour necrosis factor (TNF) receptor or Fas [Ashkenazi *et al.* 1998; Pan *et al.* 1998]. They represent the Extrinsic Pathway, connecting death-promoting extracellular signals (cytokines of the TNF family like TNF-α, FasL) to execution of apoptosis [Locksley *et al.* 2001]. Binding of a ligand to its receptor initiates trimerisation of the receptor, adaptor proteins are recruited to the death domains of both receptor and adaptor proteins. In the case of the FasR, the adaptor protein is FADD (Fas-associated protein with death domain). FADD and pro-caspases 8 and 10 inherit a death effector domain (DED), both DEDs interact and the caspases are subsequently recruited to the receptor complex which is called death-inducing signalling complex (DISC) [Delhalle *et al.* 2003]. The active caspase 8 either directly activates the effector caspase 3 or initiates the translocation of BH3 interacting domain death agonist (Bid) in the case that the recruitment of pro-caspase 8 to DISC is weak [Scaffidi *et al.* 1998]. Bid translocates to the mitochondrion and triggers the release of cyt c from the mitochondrium [Gross *et al.* 1999]. Cyt c is located and associated to cardiolipin (CL) in the inner mitochondrial membrane [Tuominen *et al.* 2002]: Proapoptotic

Bcl-2 family proteins located to the cytoplasm induce the release of cyt c to the cytoplasm in a CL-dependent manner [Lutter *et al.* 2000].

Intracellular signals, like damaged DNA by ultraviolet irradiation or the exposure of the cell to chemotherapeutic drugs induce the intrinsic pathway which is mediated by the mitochondrium. These stress factors make the mitochondrium release diverse proteins from the intermembrane space [Green *et al.* 2004]. This critical event can also be initiated through the action of the pro-apoptotic members of the Bcl-2 family proteins. Cyt c readily binds to the apoptotic protease-activating factor 1 (Apaf-1). As a result, its conformation is changed ATP-dependently and the proteins oligomerise to bind pro-caspase 9, building the apoptosome [Li *et al.* 1997; Zou *et al.* 1997]. Caspase 9 was found to associate and be activated by c-Abl in the response to genotoxic stress [Raina *et al.* 2005]. As part of the apoptosome the activated caspase 9 cleaves and activates effector caspases 3 and 7. Known for their rapid catalytic turnover they degrade a large number of cellular proteins which will ultimately kill a cell [Thornberry *et al.* 1998].

2.3.6 Cardiotoxicity

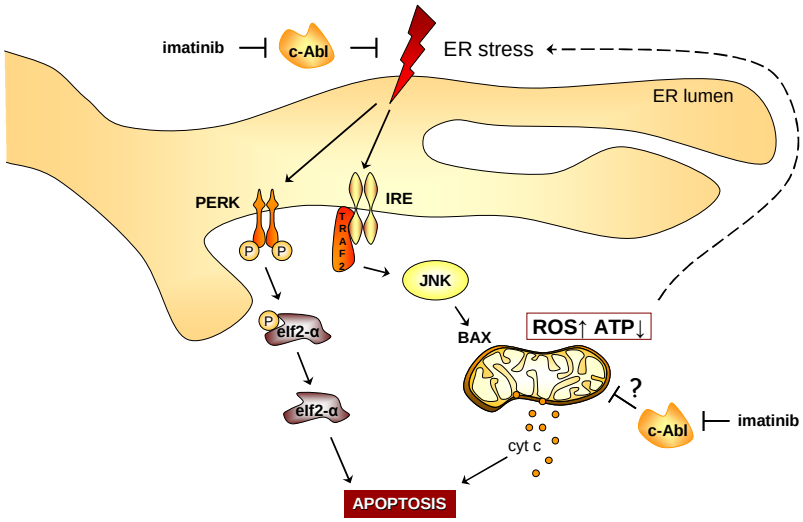

Figure 8 Several pathways of sustained-ER stress which can lead to apoptosis. Activation of PERK results in dephosphorylation of eIF2α, thereby promoting apoptosis. IRE1-TRAF2-mediated JNK-signalling is also activated by ER stress. Bax is translocated to the mitochondrial membrane resulting in cytochrome c release and collapse of the mitochondrial membrane potential. C-Abl may suppress the ER stress response indirectly by preventing mitochondrial collapse or directly via an as yet undefined mechanism. Kerkelä and co-workers suggest imatinib to promote apoptosis and heart damage by inhibiting c-Abl. ROS: reactive oxygen species; ATP: adenosine triphosphate. (adapted from [Mann 2006])

The event of cardiac toxicity in imatinib-treated patients was unknown until recently. Heart failure was reported for the first time in 2006 in imatinib-medicated patients [Park *et al.* 2006]. In the same year another group has reported about imatinib-treated patients, who have developed left ventricular dysfunction and even congestive heart failure (CHF) [Kerkelä *et al.* 2006]. During imatinib treatment the ejection fraction was decreased to less than the half as compared to the ejection fraction before medication. These observations led Kerkelä and co-workers to investigate the toxicity of imatinib in cardiomyocytes. From results obtained in NRVCM they concluded on an imatinib-mediated mechanism of cardiotoxicity in which mitochondria play a central role. The mitochondrial dysfunction and the consequent energy drop were implicated to be a crucial factor in cardiotoxicity; and to be the consequence of an imatinib-induced ER stress. According to this mechanism, the collapsed mitochondrial membrane potential is leading to cyt c release and induction of apoptotic cell death. C-Abl seems to play a central role in this mechanism, since the retroviral transfection of a c-Abl mutant form was shown to be cytoprotective against the imatinib-induced cytotoxicity.

3 PURPOSE OF THE STUDY

The purpose of the present thesis was to reproduce the data published by Kerkelä and co-workers and to investigate the role of c-Abl in the imatinib-induced cardiotoxicity more in detail. With a refined experimental design, by using additional markers of cytotoxicity and the utilisation of various control systems as well, the results should allow better understanding of the underlying mechanism of imatinib-induced toxicity in NRVCM. The following issues were targeted:

- Assessment of the cytotoxic and apoptotic effects induced by imatinib in cardiomyocytes in the different cardiac cell models NRVCM and the embryonic cell line H9c2.
- Establishment of dose- and time-dependent response-relationships of imatinib in cardiomyocytes by investigating various cytotoxic key parameters in NRVCM and H9c2 cells.
- Assessment of the reversibility of imatinib-induced effects by means of online monitoring of cellular attachment, oxygen consumption and pH in H9c2 cells.
- Evaluation of the specificity of the observed imatinib-induced effects in cardiomyocytes by investigations with cardiac, pulmonary and dermal fibroblasts.
- Investigation of the potential role of reactive oxygen species in the mechanism of imatinib-induced cytotoxicity in NRVCM.
- Evaluation of imatinib-induced toxicity in cardiomyocytes after specific gene silencing of c-Abl using the siRNA approach.
- Evaluation of cardiomyocyte function and toxicity after specific c-Abl knock down in combination with imatinib treatment.
- Set up of a stable lentiviral c-Abl silencing in NRVCM.

4 MATERIALS & METHODS

4.1 General Materials

4.1.1 Chemicals & Reagents

DL-Dithiothreitol (DTT)	*SIGMA-Aldrich*
Ethanol, absolute	*Merck KGaA*
Hydrogen peroxide, 30%	*Fluka*
N-Acetyl-L-Cysteine (NAC)	*Sigma*
α-phenyl-tert-butyl nitrone (PBN)	*Sigma*
PBS tablets	*Sigma*
D-α-tocopheryl polyethylene glycol 1000 succinate (TPGS)	*Eastman*

4.1.2 Software

GraphPad Prism version 5.00 for Windows	*GraphPad Software*
Microsoft Excel 2002	*Microsoft Corporation*

The software used for calculation of the results was Microsoft Excel and GraphPad Prism. The latter was also used to create the graphs.

4.2 Cell Culture

TrypLE Express	*Gibco*
Trypan Blue Stain 0.4 %	*Gibco*

centrifuge	*GPR*	*Beckman*
incubators	*cytoperm 2*	*Heraeus*
light microscope	*DM IRB*	*Leica*

Laboratory materials used for biochemical assays were purchased from Eppendorf (tubes, pipettes & tips), Costar (culture flasks, plates: Corning cellBIND; graduated pipettes) and BD Biosciences.

All cells were cultured at 37℃ with 5% CO_2 and 95% humidity. Cell culture medium was used prewarmed. For trypsinization of adherent cells 1 mL/75cm^2 TrypLE Express was used on PBS washed cells. To inactivate trypsin, 4 times the amount of serum-containing culture medium was added to the trypsinised cells.

4.2.1 Basal media & Buffer

HBSS	*- Ca^{2+}*	*Gibco*
	- Mg^{2+}	
DMEM high glucose		*Gibco*
DMEM:F12 (1:1)		*Gibco*
EMEM		*Gibco*
HAM's F12		*Gibco*
L-15		*Invitrogen*

4.2.2 Supplements of Media

equine serum	*HyClone*
fetal bovine serum	*HyClone*
HEPES 1M	*SIGMA*
ITSX	*Invitrogen*
MEM Non Essential Amino Acids (NEAA) (100x)	*Invitrogen*
$NaHCO_3$ 1M	*Merck*
oxycarbon (95 % O_2; 5 % CO_2)	*Carbagas*
Penicillin / Streptomycine / L-Glutamine (100x)	*Gibco*
Primocin	*InVivoGen*

4.2.3 Cells

Cell lines were purchased at the American Type Culture Collection (ATCC). Cells were cultured, thawed or frozen according to the recommendations given by the supplier.

4.2.3.1 Preparation of NRVCM

isolation medium (oxygenated)	*L-15*	*-*	*-*
preplating medium (oxygenated)	*DMEM:F12* *- with L-Glutamine* *- 15 mM HEPES* *- without Phenol Red*	*fetal bovine serum* *horse serum* *$NaHCO_3$* *primocin* *ITSX*	*25%* *25%* *1x* *1x* *1x*
culture medium NRVCM	*DMEM:F12* *- with L-Glutamine* *- 15 mM HEPES* *- without Phenol Red*	*fetal bovine serum* *horse serum* *BrdU* *NaHCO3* *primocin* *ITSX*	*2 %* *2 %* *100µM* *1x* *1x* *1x*

Trypsin	*1000 µg/vial*	*Worthington Biochemical Corporation*
Soybean Trypsin Inhibitor,	*2000 µg/vial*	*Worthington Biochemical Corporation*
Purified Collagenase	*1500 units/vial*	*Worthington Biochemical Corporation*
BrdU		*Sigma*

special stirrer with helical tool	*tool: Novartis*	*TecNoMara*
stirrer	*LAB-EGG*	*Faust Laborbedarf*

To isolate and purify NRVCM, no Ca^{2+} or Mg^{2+} containing HBSS or medium were used until the cells have reached the step of preplating. Cells were handled carefully, therefore only 25 mL pipettes were used and centrifugation was conducted without using brakes.

4.2.3.1.1 Heart Extraction

For primary cell culture 0-2 day old pups of neonatal Wistar rats were used. The pups of up to 8 litters were swiftly decapitated and fixed on a cork plate. The ribcage was cut horizontally so that the heart lied open. With the bend part of tweezers the heart was removed and transferred immediately into ice-cold HBSS on ice. One tube collected the hearts of one litter.

4.2.3.1.2 Isolation of NRVCM

The hearts were swirled and washed once with fresh HBSS. The vessels and atria were cut off. Ventricles were transferred to a 10 cm petri dish (PD) filled with HBSS on ice. Once all hearts were cut, they were equally distributed to the PDs (10-12 hearts per PD), squeezed and HBSS was aspirated. With the bend side of small scissors the hearts were minced into pieces of less than 1 mm^2. Trypsin in HBSS was added resulting in 100 u trypsin/10 mL HBSS. The PDs were sealed with parafilm and placed at 4℃ over ni ght (16-22 h).

The subsequent steps were conducted under sterile conditions:
The content of a PD was transferred into a Blue Max tube and 0.9 mL trypsin inhibitor was added per tube. After 10' at 37℃ in the water bath, 10 mL of collagenase II solution (dissolved in prewarmed and oxygenated L-15 medium) was added and kept for 45' in the water bath while stirring. New Blue Max tubes were prepared with a 70 µM mesh cell strainer on top. Cell strainers were rinsed with 2 mL of oxygenated L-15.
Cells were slowly pipetted up and down 10-15 times with a 25 mL pipette then left undisturbed for 3-4 minutes to let the cells settle. 10 mL supernatant were taken and transferred to the prepared tubes. 15 mL fresh oxygenated L-15 was added and cells were again resuspended. This step was repeated once. The strainer was rinsed again with 2 mL L-15 then the cells were left undisturbed at RT for 20'.
After centrifugation at 100 *g* w/o brake at RT for 5' the supernatant was discarded. Cells were resuspended in oxygenated prewarmed preplating medium and plated in a T150 flask (25 mL medium). The flasks were incubated for 30 min then turned topsy-turvy for another 30 min to allow more fibroblasts to attach to the surface.
Finally the cells were centrifuged again at 100 *g* for 5' w/o brake, pooled, resuspended in 10 mL prewarmed culture medium and counted with 1:1 Trypan Blue.
Plates were prepared beforehand with half the volume of the final medium and stored at the incubator. The other half was added with the cell suspension.

4.2.3.2 H9c2 (2-1)

DMEM	*fetal bovine serum*	*10 %*
- high glucose		

H9c2 is a rat cardiac cell line derived from embryonic BD1X rat heart tissue. It is a subclone of the original cell line, exhibiting many of the properties of skeletal muscle. To avoid fusion of myoblastic cells forming multinucleated myotubes and loss of myoblastic cells the cells were subcultured before confluence. [Kimes *et al.* 1976]

H9c2 were cultured in high glucose DMEM supplemented with 10 % fetal bovine serum.

To avoid differentiation, H9c2 were subcultured before reaching confluence at 70-80 % confluency.

4.2.4 Fibroblast Cells

4.2.4.1 Cardiac Fibroblasts

DMEM:F12	*fetal bovine serum*	*10 %*
- with L-Glutamine	*$NaHCO_3$*	*1x*
- 15 mM HEPES	*primocin*	*1x*
- without Phenol Red	*ITSX*	*1x*

After the preplating step of NRVCM heart fibroblast culture was established. For NRVCM culture unsettled cells were used; remaining attached cells on the flasks were mainly fibroblasts. They were grown for fibroblast culture. To further purify the culture, fibroblasts were passed for three times, until less than 10% of the cells displayed myocyte markers (e.g. α-sarcomeric actin), indicating the homogeneity of this cell system. Cells at passage four were seeded for drug treatment.

4.2.5 FR

EMEM	*fetal bovine serum*	*10 %*
- 2mM L-glutamine	*Non Essential Amino Acids (NEAA)*	*1 %*
	sodium pyruvate	*1mM*
	penicillin	*100 U/mL*
	streptomycine	*50 U/mL*

FR is a rat skin fibroblast cell line (passage 12+) derived from Sprague-Dawley rat. It was isolated as a skin biopsy from a rat foetus, 18 days of gestation. The

fibroblasts were seeded for drug treatment after three consecutive passages of amplification.

4.2.6 RFL -6

Ham's F12K	*fetal bovine serum*	*20 %*
	penicillin	*100 U/mL*
	streptomycine	*50 U/mL*

RFL-6 cells are lung fibroblast cells from Sprague-Dawley rats derived from the 18th day of gestation. These cells are provided in passage 12+.
After three consecutive passages of amplification the fibroblasts were plated for drug treatment.

4.2.7 Subculturing Cells

Cells were detached with the means of 1 mL/75cm^2 TrypLE™ Express and incubated at 37 C for some minutes. Detachment was observed visually and enhanced by tapping the flask. Serum-containing medium stopped the activity of trypsin and cells were centrifuged, diluted in culture medium and counted in a Schilling cell counting chamber (Figure 9). All four 5 x 5 squares in the corners were counted with cells only accounted that were on the upper & left line but omitting cells lying on the lower & right line of each square.

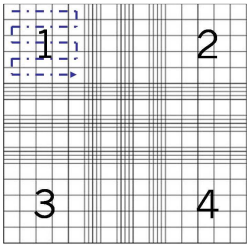

Figure 9 Schilling counting chamber

With trypan blue the viability of the cells was determined. Viable cells are capable to eliminate Trypan Blue, hence viable cells are bright whereas dead cells are coloured blue.
The sum of viable cells multiplied with 2500 and the dilution factor d results in the cell density per mL.

To determine viability, $cells/mL = \sum_{i=1}^{4} x_i * d * 2500$ viable and dead cells were counted separately in each field.

$$viability\ [\%] = \frac{100 * \sum_{i=1}^{4} x_i\ viable\ cells}{\sum_{i=1}^{4} x_i\ all\ cells}$$

NRVCM cells were diluted 1:20 (1:10 in medium, 1:1 with trypan blue) for counting. The cell suspension was adjusted to 0.903*10^6 cells/mL. Cells were incubated four days after plating.

H9c2 cells were adjusted to a concentration of $5*10^4$ cells/mL. Two days after plating, cells were treated. To maintain H9c2 in culture, $1.7*10^6$ cells/T150 are seeded being ready after 2 days or splitted 1:4 over the weekend.
All fibroblast cells are plated at a density of $2*10^5$ cells/mL. One day after plating, the cells are treated with the incubation medium.
The volume of each format is listed in Table 1. This corresponds to a ratio between volume to surface of about 0.3 mL/cm^2, so the conditions of each format are aligned.

Table 1 Plate formats and their seeding conditions.

plate format	*prelayed*	*cell suspension*	*end volume*	*assays*
96 well plate	50 µL	50 µL	100 µL	MTS, LDH, ATP, CAS
24 well plate	300 µL	300 µL	600 µL	beating rate
12 well plate	500 µL	500 µL	1000 µL	PCR
6 cm PD	-	4 mL	4 mL	Western Blot

4.2.8 Mycoplasma Screening

To screen for contaminations of mycoplasma the Venor®*GEM* kit was used. This kit is a nucleic acid amplification assay on the basis of PCR. To run this test, the supernatant of cells AT 80 % confluence is taken and prepared according to the manufacturer's advice.
All the cells used were free of contamination.

4.3 Online Cell Measurement

microscope	*Wild M8*	*Leica*
Triton X-100		*Serva*

The Bionas 2500 analyzing system offers online a label-free and non-invasive measurement of cell adhesion, cellular oxygen exchange and extra-cellular acidification. This delivers indirectly data about the adhesion & confluence (impedance), the metabolism rate (acidification via glycolysis) and cellular respiration (oxygen consumption) to generate ATP in the oxidative phosphorylation.

4.3.1 Preparation of Medium

DMEM high glucose powder		*Gibco*
+ L-Glutamine		
+ Pyruvate		
- $NaHCO_3$		
pH electrode	*Hydrus 500*	*Fisherbrand*
osmometer		

In order to measure the acidification of the medium caused by cellular metabolism, it is crucial to reduce buffers in the medium to a minimum. In addition, proliferation had to be avoided. Therefore the medium was prepared with powder. 5 L were prepared with 5 mL FBS and 5 mL HEPES resulting in 0.1 % FBS and 1 mM HEPES. The pH was adjusted to 7.4

4.3.2 Cleaning of Chips

Bionas metabolic chip SC1000	*Bionas*
quicktips	*Aichele Medico*

Used chips (a picture onto the electrodes in the hutch is shown in Figure 10) were rinsed with ddH_2O, the water jet was directed on the electrodes. The chips were cleaned mechanically with a Q tip. After rinsing the chips again with ddH_2O the chips were air-dried and stored for next experiments. A microscope equipped with a goose neck was used to check for resting cells on the surface.

4.3.3 Preparation of Chips

Figure 10 Bionas® *metabolic chip* SC1000

Chips were wiped with 70 % EtOH and placed in quadriPERM plates under sterile conditions.
The hutches were filled with 500 µL EtOH (70 %) and incubated for 10 min at RT. The hutches were washed three times with culture medium. Filled with 100 µL culture medium chips were placed into the incubator. In the meantime, cells were detached and adjusted to 10^6 cells/mL. 100 µL of cell suspension were added to each chip by pipetting up and down to distribute the cells evenly on the surface.
The next day the cells were attached in a monolayer and ready to be inserted into the machine.

4.3.4 Programs of Bionas

Bionas 2500 analyzing system	Bionas autosampler AS 600	Bionas
	Bionas 2500 basic unit	
	Bionas power unit PU 300	
Bionas 1500 *recording* and *analyzing software*		Bionas

4.3.4.1 Disinfection

The cell confluence on the chips was checked with a microscope. Prior to inserting cells on chips the whole Bionas® 2500 analyzing system was disinfected as indicated in Table 2. During the disinfection step old chips (dummies) were used. The medium of the chips was changed to 200 µL running medium and placed carefully into the holder after disinfection was finished. With gentle joggling the correct position of the chips was assured.
In a table the wafer number as well as the batch number of the chips used and the compounds in the running medium was registered.

4.3.4.2 Measurement

For H9c2 cells, the measurement step included 7 h of adaptation to the flow, the incubation time endures 24 h and recovery of the cells 6 h. The optimal condition for H9c2 cells were 4’ stop, 6’ go with a flow rate of 1 (14 µL/min).

4.3.4.3 Cleaning

Each measurement was finalised with 2 h of 0.2 % Triton X-100 in running medium. This is recommended as QC by Bionas. Finally, the tubes were cleaned with ddH_2O.

Table 2 Programs of the Bionas analyzer.

program	*liquid*	*go cycle [min]*	*stop cycle [min]*	*AS position*	*flow rate [14 µL/min]*	*time*
disinfection	EtOH	-	-	1	100	3’
	EtOH	-	-	1	4	15’
	PBS	-	-	2	4	15’
	running medium	4	6	3	4	15’
measurement	running medium	4	6	3	1	7h
	incubation	4	6	4	1	24 h
	running medium	4	6	3	1	6h
end	killing	4	6	5	1	2h
	ddH_2O	-	-	6	1	12’

4.4 Biochemical assays

Cytofluor Microtiterplate reader	CytoFluor Multi-Well Plate Reader Series 4000	PerSeptive Biosystems
SpectraMax 250		Molecular Devices
shaker	TITRAMAX 1000	Heidolph Instruments
TECAN	Genios Pro	TECAN
Magellan	TECAN	
SoftMaxPro	absorbance multiplate reader	
Cytofluor	Cytofluor	

4.4.1 Incubation schemes

Four days after plating NRVCM, the next day (fibroblasts) or 48 h after plating (H9c2) the inner 60 wells of 96 well microtiter plates were incubated according to the following schemes. Outer wells were cell-free but filled with incubation medium.

Stocks of the compounds were prepared with a resulting end-concentration of 10 mM in ddH_2O and stored in aliquots at -20°C.

4.4.1.1 Cytotoxicity assays

Master Mix for 14 plates, time- and dose-dependence:

	100 µM	**75 µM**	**50 µM**	**30 µM**	**20 µM**	**10 µM**	**5 µM**	**1 µM**	**0.1 µM**	**0 µM**
[µL]	70	52,5	35	21	20	3500	700	700	700	0
source	stock	stock	stock	stock	stock	20µM	50µM	10µM	1µM	
DMEM [µL]	6930	6947,5	6965	6979	9980	3500	6300	6300	6300	7000

4.4.1.2 Antioxidants

Stock solutions of 100 mM and 10 mM (TPGS) were prepared freshly in ddH_2O. Double-concentrated incubation medium was prepared and diluted with medium (pre-incubation) or imatinib-medium, double-concentrated) 1:1. Antioxidants were pre-incubated for 4.5 h, then aspirated and cells were co-incubated with 0 and 50 µM imatinib for 24 h in addition.

Double-concentrated incubation medium was prepared as following: 7 mL medium was prelayed, 560 µL (DTT, NAC), 210 µL (PBN) or 2100 µL (TPGS) removed. The removal was substituted by the antioxidant (stock solution). Each antioxidant was then diluted 1:1 in medium (3.5 mL).

Pre-incubation medium was then diluted again 1:1 with medium and added onto the plates. After 4.5 h of incubation, the co-incubation medium was added. It consists of the double-concentrated incubation medium of antioxidant mixed 1:1 with 100 µM imatinib (in medium).

4.4.2 ATP Content

CellTiter-Glo Luminescent Cell Viability Assay Promega

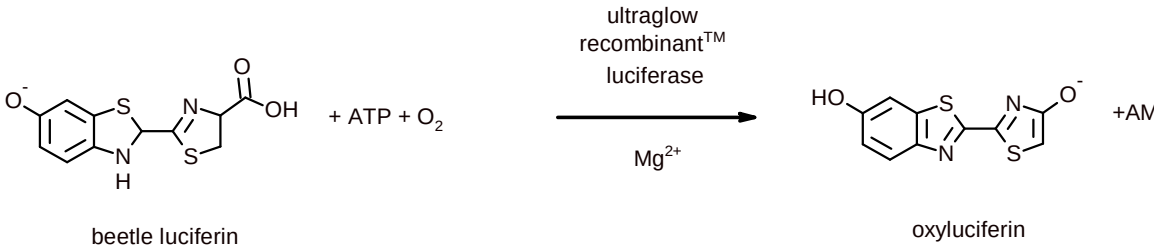

Figure 11 The luciferase reaction. Luciferase catalyses the mono-oxygenation of luciferin in the presence of Mg^{2+}, ATP and molecular oxygen.

The present ATP is quantified signalling the presence of metabolically active cells. This assay contains a thermostable luciferase (recombinant firefly luciferase) generating a stable “glow-type” luminescent signal. The reaction is shown in Figure 11.

By means of Cell Titer-Glo Luminescent Cell Viability Assay the amount of viable cells in culture was determined according to the manufacturer’s instructions. Cells are plated in black 96 well plates with a clear bottom. At the end of incubation 100 µL of freshly prepared reagent (up to some days old) was added to a well of a black 96 well plate, placed on a shaker for 2 min and kept in the dark for 8 min. The plate was read with TECAN, Magellan, 100 ms/well or with HT Synergy microplate reader.

As blank value, the reagent in culture medium was taken and subtracted from each value.

4.4.3 ADP/ATP ratio

ApoSENSOR ADP/ATP Ratio Assay Kit BioVision

With changes in the ADP/ATP ratio different modes of cell death and viability are possible to distinguish. Proliferating cells have increased levels of ATP and decreased levels of ADP. In contrast, in apoptotic cells the ratio is inverted. The decrease in ATP and increase in ADP are much more pronounced in necrosis than apoptosis. With bioluminescent detection of the ADP and ATP levels a rapid screening of apoptosis, necrosis, growth arrest, and cell proliferation is possible simultaneously in mammalian cells. The assay utilizes the enzyme luciferase to catalyse the formation of light from ATP and luciferin. The ADP level is measured by its conversion to ATP that is subsequently detected using the same reaction.

NRVCM were plated in clear-walled 96 well plates and treated for 24 h. At the end of the incubation, the medium was removed and 100 µL of nuclear

releasing buffer (NRB) was added for 5 minutes at RT with gentle shaking. The ATP level was measured after adding 1 µL of ATP-monitoring enzyme diluted in 50 µL of NRB per well of cell lysate. The luminescence was read immediately with a 10 s integration (data A). After 10-15 min the plate was read again (data B). Then 1 µL of ADP-converting enzyme diluted in 50 µL of NRB was added and read immediately showing the ADP level (data C). The ADP/ATP ratio is calculated as

$$ADP/ATP\,ratio = \frac{data\,C - data\,B}{data\,A}$$

The results obtained were interpreted as follows:

cell fate	*ADP level*	*ATP level*	*ADP/ATP*
proliferation	very low	high	very low
growth arrest	low	slightly increased	low
apoptosis	high	low	high
necrosis	much higher	very low	much higher

4.4.4 MTS Reduction Capacity

CellTiter 96 Aqueous Non-Radioactive Cell Proliferation Assay Promega

To monitor the number of viable cells in proliferation or chemosensitivity assays the Cell Titer 96® AQ_{eous} Non-Radioactive Cell Proliferation Assay was used according to the manufacturer's instructions. This assay is based on the principle established by Malich and co-workers [Gregor Malich 1997]. Active cells reduce the yellow MTS into a formazan product that is brown and soluble in tissue culture medium (see Figure 12).

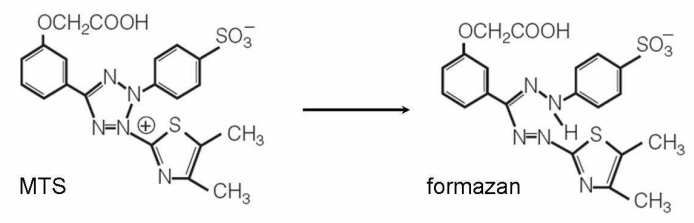

Figure 12 MTS and its formazan product.

Cells were plated in clear 96 well plates omitting the outer wells for the MTS assay. 10 µL of the volume was added 2 h (NRVCM), 1.5 h (fibroblast cells) or 1 h (H9c2) prior to the end of incubation to the cells and were replaced into the incubator. A multiplate reader was used to read the absorbance at 490 nm representing the quantity of the formazan product and which is proportional to viable cells in culture.

4.4.5 Caspase 3/7 Activity

Caspase-Glo 3/7 Assay Promega

The Caspase-Glo 3/7 Assay measures active forms of effector caspases 3 and 7. Based on a luminogenic caspase-3/7 substrate containing a tetrapeptide sequence (DEVD), the reagent is optimized for caspase activity, luciferase activity and cell lysis. Cells are lysed, then caspases are cleaved resulting in cleavage of the substrate hence the luciferase generates a luminescent signal (Figure 13). Luminescence is generated by a thermostable luciferase (Ultra-Glo™ Recombinant Luciferase, firefly).

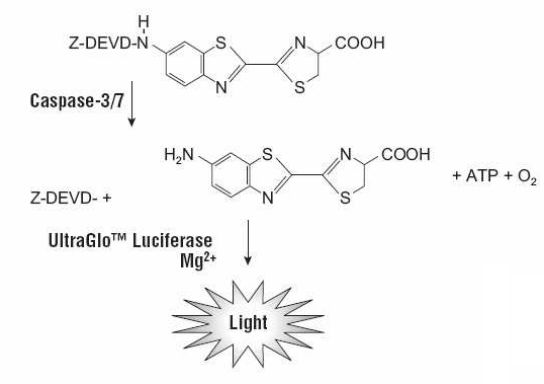

Figure 13 Caspase 3/7 cleaves the luminogenic substrate containing the DEVD sequence. The release of a substrate for luciferase (amino-luciferin) activates the luciferase and results in production of light.

The Caspase-Glo 3/7 Assay was performed according to the manufacturer's instructions. With this assay the cleavage and therefore activation of caspases 3 and 7 was monitored. Caspases are the hallmark of apoptosis, thus, activation of caspases indicate that apoptosis is triggered. The cells are plated in black 96 well plates with a clear bottom. Briefly, at the end of incubation 100 µL reagent is added per well, put on a shaker for 2', then kept in the dark for 28'. The luminescence was measured with TECAN GENios, Magellan, 100 ms/well at a wavelength of 560 nm (250 ms integration time, gain 125) or monitored in HT Synergy.

As blank solution the reagent in culture medium was taken and subtracted from each particular value.

4.4.6 Lactate Dehydrogenase Release

Cytotoxicity Detection Kit (LDH) Roche

Cell-free supernatant is incubated with the substrate mixture from the kit. The more cells are damaged or killed, the more LDH is released to the supernatant. A coupled enzymatic reaction determines the amount of LDH. During this reaction, the tetrazolium salt INT is reduced to formazan (see Figure 14). The release of LDH into the medium was determined using a LDH Cytotoxicity Detection Kit according to the manufacturer's instructions in 96 well plates. At the end of the treatment, 50 µL of supernatant was removed from each well and transferred into a clear flat bottom 96 well plate. 50 µL of reconstituted reaction mixture was then added into each well. After 10 min incubation at room temperature, the plate was read at a wavelength of 490 nm with a microtiter plate reader. Supplemented medium was used as a blank and subtracted as background. Measurements are expressed as percentage of LDH release in culture medium in relation to total LDH from lysed control cells by Triton X-100.

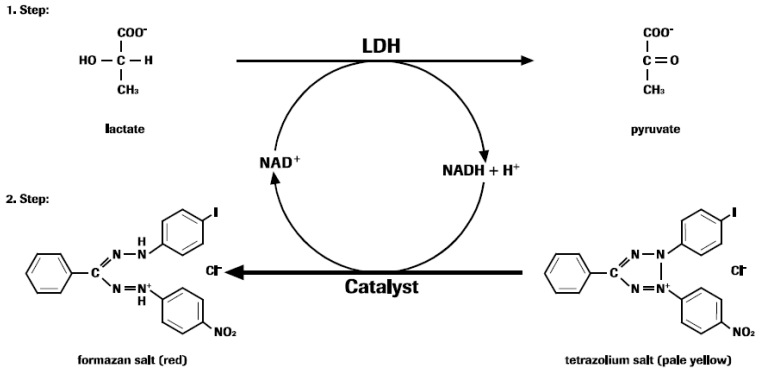

Figure 14 LDH assay. In the first step, released lactate dehydrogenase (LDH) reduces NAD^+ to $NADH^+$ H^+ by oxidation of lactate to pyruvate. In the second enzymatic reaction 2 H are transferred from $NADH^+$ H^+ to the yellow tetrazolium salt INT (2-[4-iodophenyl]-3-[4-nitrophenyl]-5-phenyltetrazolium chloride) by a catalyst.

4.4.7 ROS detection assay

2',7'-Dichlorofluorescin diacetate Sigma

The diacetate form of the membrane-permeable dye (reduced DCF, DCF-DA) enters the cell. Esterases cleave the acetate groups of DCF-DA thus trapping the reduced probe (DCFH) intracellularly. ROS present in the cell oxidise DCFH which results in the fluorescent product DCF [Wenzel *et al.* 2006].
The generation of ROS was assessed using the reagent 2',7'-Dichlorofluorescin diacetate (DCF). DCF-DA was co-incubated with the compounds in PBS for one hour or added 30 min prior to the end of incubation (24 h) at the final concentration of 10 µM.

4.4.8 Protein Determination

MicroBCA Protein Assay Reagent Kit Pierce
Albumin, Bovine Sigma

The Pierce Micro BCA™ Protein Assay Kit detects and quantifies total protein based on bicinchoninic acid (BCA). BCA is used to detect Cu^{1+} which is formed in an alkaline environment by proteins reducing Cu^{2+}. Two molecules BCA chelate and one Cu^{1+} results in a purple coloured reaction product with a strong absorbance at 562 nm. This is linear with increasing protein concentrations.

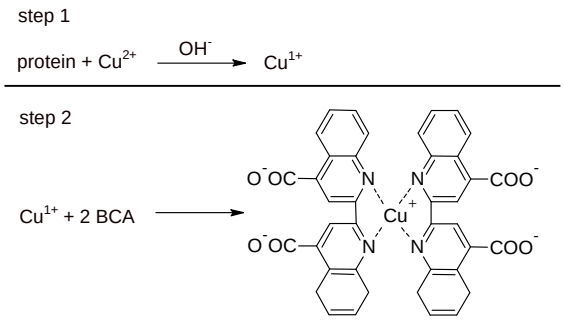

Figure 15 Reaction schematic for the bicinchoninic acid (BCA) containing protein assay.

100 µL of the standards (0, 5, 10, 15, 20, 30, 40, 50, 60 µg/mL BSA) and the diluted samples (1:200 for WB) are pipetted in triplicates on a clear 96 well plate. 100 µL of the reagent is added to the standard and the samples, briefly placed on the shaker, sealed and incubated at 60℃ for 30 min. The plate is read on a multiplate reader at 490 nm absorbance. Determination of the protein amount was calculated by the software automatically.

4.4.9 Semi-quantitative Protein Determination

4.4.9.1 Buffers

Blocking Buffer	LI-COR
HBSS	Gibco
- Ca^{2+}	
- Mg^{2+}	
PBS in ddH_2O, *filtrated*	made of tablets
PBST, filtrated	0.1% Tween 20 in PBS
Tween® 20	Sigma-Aldrich™
wash buffer	Blocking Buffer : PBST 1:1

4.4.9.2 SDS-gel Electrophoresis

CelLytic M Cell Lysis Reagent	Sigma
E-PAGE™ Loading Buffer 1 (4X)	Invitrogen
LI-COR Molecular Weight Markers	LI-COR
MagicMark™ XP Western Standard	Invitrogen
Nupage Sample Reducing Agent	Invitrogen
Phosphatase inhibitor cocktail 1	Sigma
Phosphatase inhibitor cocktail 2	Sigma
Protease inhibitor cocktail	Sigma
SeeBlue® Plus2 Pre-stained Standard	Invitrogen
WB washer	GE healthcare
Centrifuge 5417 R	eppendorf
vacuum pump Vacuskan R	Skan

The E-PAGE protein electrophoresis system of Invitrogen was used to determine the levels of a specific protein.

Cells plated in 6 cm PDs were washed twice with cold PBS and lysed in 100 µL lysis buffer containing phosphatase and protease inhibitors. Cells were scraped with a cell scraper and transferred into an Eppendorf tube. Over 10 minutes cell lysates were vortexed every two minutes, then centrifuged at 20 000 *g* at 4℃ for 10 minutes. The supernatant was transferred to a new tube and the protein content measured with the Micro BCA Protein kit.

The protein level was adjusted to 10-15 µg/20 µL (up to 1.33 µg protein per µL) with ddH_2O. Generally, a mix of 200 µL end volume was prepared, consisting of 130 µL of the diluted protein plus 20 µL NuPAGE Sample Reducing Agent and

50 µL E-PAGE Loading Buffer. The samples were vortexed and heated to 70℃ for 10 minutes, shaking at 850 rpm.

Table 3 Preparations for Gel Loads.

reagent	*reduced, for 10 µL*	*reduced, for 200 µL*
protein sample	x	x
E-PAGE Loading Buffer 1 (4x)	2.5 µL	50 µL
NuPAGE Sample Reducing Agent (10x)	1 µL	20 µL
ddH_2O	ad 10 µL	ad 200 µL

As Molecular Weight Standard a mixture of MagicMarkXP Western Protein Standard and Molecular Weight Markers was loaded: 1 µL of each marker plus 13 µL ddH_2O. 15 µL of marker and sample preparations were loaded per lane and the gel was run in the Mother E-Base for 30 min. When the electrophoresis had finished, the gel was cut and briefly washed in ddH_2O.

4.4.9.3 Semi-dry Blot of Electrophoresis Gel

E-PAGE™ 48 Protein Electrophoresis System	Invitrogen
Mother E-Base™	Invitrogen
E-Base device	Invitrogen
iBlot device	Invitrogen

According to the manufacturer's instructions the iBlot device was prepared and the proteins were blotted for 7.5 minutes onto a membrane. The membrane was cut and marked to keep the correct directions.

4.4.9.4 Blocking of unspecific Binding Sites

blocking buffer, final	Blocking Buffer : PBS 1:1

Unspecific binding sites were blocked with incubation in Odyssey Buffer & PBS (1:1) for an hour rocking at room temperature (RT).

4.4.9.5 Incubation of the Membrane with Primary Antibodies

primary antibodies	host	dilution	size [kDa]	supplier
α-tubulin	mouse	1:100 000	50	Sigma
β-actin	mouse	1:200 000	42	Sigma
c-Abl (K-12) :sc 131	rabbit	1:1000	120	Santa Cruz
CHOP	mouse	1:500	31	abcam Ltd
eIF2α	rabbit	1:1000	40	Cell Signaling Technology
eIF2α (phospho)	rabbit	1:500	40	Cell Signaling Technology
GAPDH	rabbit	1:50000	37	Cell Signaling Technology
JNK1/2	rabbit	1:5000	JNK1: 46 JNK2: 54	Sigma
JNK1/2 (phospho)	mouse	1:1000	p-JNK1: 46 p-JNK2: 54	Sigma
XBP-1 (COOH terminus)	rabbit	1:500	30	Biolegend
E-PAGE 48 8% Gels				Invitrogen
iBlot Transfer Stacks				Invitrogen

The membrane was directly transferred into a solution of Odyssey Buffer & PBST (1:1) and primary antibodies (anti c-Abl, rabbit 1:1000; anti β-actin, mouse 1:200 000). The membrane was incubated rocking over night at 4℃. The next morning, the membrane was washed 5 x for 5’ rocking at RT in PBST.

4.4.9.6 Incubation of the Membrane with Secondary Antibodies

secondary antibodies	host	dilution	supplier
anti-Mouse IgG-IRDye680	goat	1:15 000	LI-COR
anti-Rabbit IgG-IRDye680	goat	1:15 000	LI-COR
anti-Mouse IgG-IRDye800CW	goat	1:15 000	LI-COR
anti-Rabbit IgG-IRDye800CW	goat	1:15 000	LI-COR

Finally, the membrane was incubated with secondary antibodies which bind specifically to the primary antibody attached to the protein of interest. The secondary antibody labelled with IRDye800CW (green) was chosen for the detection of the protein of interest since its signal detection is more sensitive. The secondary antibody coloured in red was labelled with IRDye680 and used for the control protein (anti-rabbit, anti-mouse, 1:15 000) in Odyssey Buffer & PBST (1:1) for 1 h rocking at RT. After the final wash of 5 x for 5’ rocking at RT in PBST and 5 x 5’ rocking at RT in PBS, the membrane was dried in the dark.

4.4.9.7 Detection of Protein Bands

Odyssey *Infrared Imaging System*	LI-COR Biosciences
Odyssey 2.1 software	LI-COR Biosciences

As soon as the bands were dry, the membrane was scanned by the Odyssey Infrared Imaging System.

4.5 Molecular Biology

Laboratory materials for molecular biology were acquired from Rainin (pipettes & tips), Falcon and Eppendorf.

bacteria shaker	Forma Orbital Shaker	Thermo Electron Corporation
bench	VS120 AFX	Skan
centrifuges		
table centrifuge	5424	Eppendorf
	Avanti J-E	Beckman
incubator	KBP 6087	Termaks

4.5.1 Total RNA Extraction

MagNA Pure LC RNA Isolation Kit – High Performance		Roche
RNA extraction robot	MagNA Pure LC	Roche

Total RNA were extracted according to the MagNA Pure LC RNA Isolation Kit – High Performance as described by the manufacturer.
The plate formats used were 24-well plates for cell lines and 12-well plates for NRVCM. At the end of incubation, cells were washed twice with 300 µL PBS (RT). To lyse cells 100 µL of each PBS and MagNA Pure Lysis buffer were added. Plates were rocked to avoid foaming and transferred into Eppendorf tubes. Cell lysates were kept at -80℃ until RNA extraction.
Total RNA was extracted according to the manufacturer's protocol. The RNA was eluted in 50 µL Elution Buffer and the quantity as well as RNA integrity was checked each time as quality control.

4.5.2 Quantification of RNA

nanodrop	ND-1000 Spectrophotometer	NanoDrop®

The samples were quantified spectrophotometrically using a Nanodrop. 260/280 nm ratio in the range of 1.8 to 2.3 was used as a QC standard.

4.5.3 Integrity of RNA

8 µL of total RNA were run on an agarose gel (1.2 %) stained with ethidium bromide. Intact total RNA resulted in a clear, sharp 28S and 18S rRNA bands. Only samples of good quality (2:1 ratio of 28S:18S) were kept for further analysis.

4.5.4 Reverse Transcription

High Capacity cDNA Archive Kit		Applied Biosystems
CAS 1200™ Automated Sample Setup		Corbett Robotics
Peltier Thermal Cycler	Dyad	Bio-Rad
Alpha unit Block		Bio-Rad
Corbett Robotics		Corbett

300 ng of total RNA were used in the reverse transcription reaction which was performed according to the manufacturer's instructions (ABI).

4.5.5 Real-Time Polymerase Chain Reaction (PCR)

TaqMan Fast Universal PCR Master Mix (2x)	Applied Biosystems
TaqMan Universal PCR Master Mix (2x)	Applied Biosystems

4.5.5.1 Primers and Probes

primers & probes for c-Abl		Applied Biosystems
primers & probes for ArgBP2		Applied Biosystems
primers & probes for eIF2α		Applied Biosystems
primers & probes for CHOP (*here: DDiT3)*		Applied Biosystems
primers & probes for XBP1		Applied Biosystems
XBP1 spliced & unspliced		Microsynth
forward primer	5'-GAGTCCAAGGGGAATGGAG-3'	
reverse primer	5'-TTGTCCAGAATGCCCAAAAG-3'	
XBP1 spliced probe	5'-CTGCACCTGCTGCGGACT-3'	Applied Biosystems
XBP1 unspliced probe	5'-TCAGACTACGTGCGCCTCT-3'	Applied Biosystems

2 µL of the cDNA were used for PCR. For each gene of interest a Master Mix was prepared as listed in

Table 4. All samples were monitored for 18S, the housekeeping gene which all samples were adjusted to. The samples were placed into the PCR machine. Depending on the Master Mix used, the fast or normal program was chosen as indicated in Table 5. Generally, all detectors used were FAM (absorbance = 530 nm, blue), except for XBP-1 spliced which was measured in the same sample as unspliced XBP-1. To be able to differentiate between the two forms, unspliced XBP-1 was measured with VIC (absorbance = 554 nm, green).

Table 4 Master Mix: Pipetting scheme for PCR assays.

	1 sample [µL]	*1 sample for XBP1 [µL]*	
Master Mix (2x)	10	10	
TGEA (20x, Taqman Gene Expression Assay)	1	FW spliced (1:10)	1.6
		RV spliced (1:10)	1.6
		probe spliced (1:100)	2.7
		probe unspliced (1:100)	2.7
DEPC H_2O	7	-	
cDNA template (samples)	2	2	
final reaction volume	20	21.8	

Table 5 Temperature programs for One-Step RT-PCR.

	normal		fast	
	time	*temperature [°C]*	*time*	*temperature [°C]*
	2 min	50		
	10 min	95	20 s	95
40 cycles	*15 s*	*95*	*1 s*	*95*
	1 min	*60*	*20 s*	*60*

The RT-PCR was performed according to the TaqMan (Fast) Universal PCR Master Mix Protocol.

4.5.5.2 Analysing PCR data

The relative quantification of gene expression changes was determined using the standard curve method. Results are presented in Arbitrary Units (A.U.) as the ratio between the number of molecules for the gene of interest and the number of molecules for 18S (normalized gene expression). For siRNA experiments the expression data are presented as % of control values representing a fold-expression change versus the control group.

XBP1 spliced and unspliced were calculated as follows: The difference in cycle threshold (ΔCT) was evaluated by the CT of XBP1 minus CT of 18S, for each sample and both XBP1 spliced and unspliced. ΔΔCT was calculated by subtraction of the average of the ΔCT of GFP (incubated with 0 µM) from the ΔCT of the gene of interest. Fold change resulted by calculating $2^{-\Delta\Delta CT}$. The ratio of spliced versus unspliced XBP1 (fold change) was shown in the graph.

4.6 RNAi

4.6.1 Transfections

RNase AWAY Molecular BioProducts

All transfections were conducted under sterile, RNase-free conditions.

4.6.2 siRNA

siRNA	supplier	ordering number	sequence
GFP-22 modified with 3'-Alexa Fluor 488	QIAGEN	1781802_10	GCA AGC TGA CCC TGA AGT TCA
Rn_Abl1_1_HP siRNA	QIAGEN	SI01484287	TAC CTA TGG CAT GTC ACC TTA
Rn_Abl1_2_HP siRNA	QIAGEN	SI01484294	CTC GAT GGA ACT CCA AGG AAA
Rn_Abl1_3_HP siRNA	QIAGEN	SI01484301	TGG GTG TAC TTT GTA GAC TTA
Rn_Abl1_4_HP siRNA	QIAGEN	SI01484308	CCG GAC GGC AGC CTA AAT GAA
Rn_Abl1_1	Novartis Pharma	129354	TTG ATC TCC TTC ATC ACT GCG
Rn_Abl1_2	Novartis Pharma	129355	TTC ATT TAG GCT GCC GTC CGG
Rn_Abl1_3	Novartis Pharma	129356	TTA TAG GCC AGG CTC TCG GGT
Rn_Abl1_4	Novartis Pharma	129357	TTT AGT GAT GCT GAG AGT GTT
Rn_Abl1_5	Novartis Pharma	129358	TTC ACG GCC ACA GTG AGG CTG
Rn_Abl1_6	Novartis Pharma	129359	TCA GAG GCA GTG TTG ATC CTG
Rn_Abl1_7	Novartis Pharma	129360	TTT CTC TGG GCA GCC TTC CGG
Rn_Abl1_8	Novartis Pharma	129361	TTG GCC ACC TGC TCA GAC CTG
Rn_Abl1_9	Novartis Pharma	129362	TTT CCC AGA GCA ATA CTC CAA
Rn_Abl1_10	Novartis Pharma	129363	TGA TTA TAA CCT AAG ACC CGG

Thermomix thermomixer comfort Eppendorf

4.6.2.1 Nucleofection of H9c2

Cell Line Nucleofector Kit L amaxa

Transfection of H9c2 was performed with the nucleofector of amaxa according to the protocol provided.
Cells of about 80 % confluency were harvested and counted in TryPLE Express/medium – suspension. The needed amount of cells was centrifuged at 100 *g* for 5' and resuspended in Nucleofection Buffer, adjusted to $3.6*10^5$ cells/100 µL. 100 µL of cell suspension was pipetted down and up in an Eppendorf tube with 1.5 µL of 20 µM siRNA prelayed and transferred into a cuvette (4 mm gap). Electroporation was performed with the nucleofection programme C-20. After 10' left undisturbed at RT, 400µL of prewarmed culture medium is added. Finally, cells were transferred into a tube prelayed with prewarmed culture medium appropriate to result in $0.36*10^6$ cells / 2.1 mL. Cuvettes of the same siRNA were pooled and then plated.

4.6.2.2 Lipofection of NRVCM

lipofectamine 2000 Invitrogen

On day 3 after plating, NRVCM were changed to 90 % of normal medium volume of primocin-free culture medium.
On day four, the transfection reagent was prepared according to the manufacturer's instructions. OptiMEM was prewarmed and added to the siRNAs and lipofectamine 2000, respectively, placed in Eppendorf tubes. Two different concentrations of siRNA were investigated, 40 and 80 nM, both of them with 2 µL/mL lipofectamine 2000. For calculations for each preparation, see table below:

Table 6 Calculations for desired transfection reagent.

$$siRNA\,(20\mu M)\ [\mu L] = \frac{transfection\ reagent\,[\mu L]}{2 * x}$$

transfection reagent	*OptiMEM supplemented with siRNA and lipofectamine 2000*	
desired end-concentration of siRNA	40 nM	x = 25
	80 nM	x = 12.5
desired end-concentration of lipofectamine 2000	2 µL/mL	x = 25

The Eppendorf tubes prepared were filled up with prewarmed OptiMEM to half the volume of the transfection reagent. Tubes were tapped and centrifuged for

4-5 seconds, then left undisturbed for 5'. Each siRNA containing tube was pooled with a lipofectamine 2000 containing tube. Again, tubes were tapped and centrifuged briefly for 4-5 sec. After 20 minutes at RT, the transfection reagent was ready to use and stable for up to 6 h. 10 % of transfection reagent was added, cells were investigated 16, 24, 48, 80 and 72 h post transfection. 24 h after transfection, medium was changed.

4.6.3 Set-up for Lentiviral Transfection of NRVCM

4.6.3.1 Medium & Supplements for Bacteria

Luria Bertani (LB) medium	Invitrogen
LB Agar, powder (Lennox L Agar)	Invitrogen
kanamycin sulphate 50 mg/mL	amresco
ampicillin sodium salt 100 mg/mL	amresco

4.6.3.2 Designing shRNAs

By means of the BLOCK-iT™ RNAi Designer provided by Invitrogen (available online at https://rnaidesigner.Invitrogen.com/rnaiexpress/) the most efficient siRNAs were modified to result in shRNAs. The resulting sequences were synthesised by Microsynth.

4.6.3.3 Cloning shRNAs into the pENTR™/U6 vector

BLOCK-iT U6 RNAi Entry Vector Kit	Invitrogen
Gateway LR Clonase II Enzyme Mix	Invitrogen

The oligos produced by Microsynth were annealed according to the protocol given in BLOCK-iT U6 RNAi Entry Vector Kit from Invitrogen. Annealed shRNAs were further processed as written in the manual: The ds oligos were cloned into a pENTR/U6 vector and finally the expression clone was generated performing an LR recombination reaction between the pENTR/U6 entry clone and the pLenti6/BLOCK-iT-DEST vector according to the BLOCK-iT Lentiviral RNAi Expression System manual provided from Invitrogen.

4.6.4 DNA purification

mini prep	QIAGEN

DNA purification was performed according to the QIAGEN mini prep kit. DNA was diluted in DEPC water, the quantity was measured with nanodrop and stored at -20℃. Sequencing of the harvested DNA was performed by Solvias, Bioanalytics.

4.7 Beating rate

camera	3CDD color vision camera module	Donpisha
heating stage	HT 200	Minitüb GmbH F.R.
light microscope	DMIL	Leica

NRVCM were spontaneously beating after 24 h in culture. Once they were connected, the effect of imatinib on their contraction rate was measured.

The frequency of contraction of NRVCM was determined by automated image analysis with software specifically designed by Dr. Wilfried Frieauff. A Leitz MIAS image analysis system connected to a Leica DM/IL phase contrast microscope with 40x objective and a stabilised lamp power supply were used to perform measurements. On the microscope a heating stage (37°C) was fixed and a Donpisha 3CDD vision camera mounted on the microscope for capturing images. Images were digitised to 8 bit grey value and 512 x 512 pixel resolution. Within a small frame beating cells were selected and the measurement was started. The first image was stored automatically as a reference image. In intervals of 80 ms a new image was recorded. The absolute grey difference between the current and the original reference image was computed. A thresholding for the total numbers of pixels in the different picture was used to indicate sufficient grey value change. Thus, during 15 sec 187.5 single measurements were performed. These data were stored and further processed by a programme in Excel developed by Dr. Wilfried Frieauff and plotted against time and the maxima of the resulting curves (frequency of contraction) were given automatically. Light intensity wasn't changed during a series of measurements. Plates were measured after being placed under the heating stage for some minutes for adaption to the light. Each well was measured in the middle and at two opposite borders. The settings are listed in Table 7.

Table 7 Settings for beating rate measurements.

analysis	*sensitivity*	*smoothing*	*control options*	*valid peaks*
15 s	20	2	valid maxima	% from average as limit

5 RESULTS & DISCUSSION

5.1 Cytotoxic & Apoptotic Potential of Imatinib

5.1.1 Background

All studies were performed either in NRVCM or the cell line H9c2. NRVCM is an *in vitro* cardiac cell model which is frequently used in experimental research to explore mechanisms of cardiac toxicity. Cardiomyocytes in culture possess many biochemical and physiological characteristics of cells in the living heart [Wenzel *et al.* 1970; Acosta *et al.* 1984; Limaye *et al.* 1999; Estevez *et al.* 2000; Kerkelä *et al.* 2006], for instance, they start to contract spontaneously after 2-3 days in culture. Impairment of beating rates can be used as organotypic and functional assays to evaluate a compound's potential cardiotoxic effects [Estevez *et al.* 2000].

By means of *in vitro* experiments in cardiomyocytes, a broad range of biochemical, physiological, pharmacological and morphological investigations can be performed to study the mechanisms of cardiotoxicity of drugs and chemical compounds [Sutherland *et al.* 2000]. NRVCM have also been used in the studies of Kerkelä to explore the mechanisms of the imatinib on cytotoxicity, apoptosis and on ER stress as well as on mitochondrial functions.

The cell line H9c2 is derived from embryonic rat heart tissue. It is a well established *in vitro* model, which was used in addition to the primary cardiomyocytes culture for mechanistic investigations [Menna *et al.* 2007; Han *et al.* 2008; Will *et al.* 2008].

Doxorubicin, the reference compound for cardiotoxicity, is a member of the anthracycline family [Ito *et al.* 2006], one of the most effective anti-cancer drugs ever developed [Weiss *et al.* 1982]. Doxorubicin is one of the first ones isolated from *Streptomyces peucetius* and bears aglyconic and sugar moieties as illustrated in Figure 16. The tetra cyclic ring with adjacent quinone-hydroquinone groups in rings C-D, in ring D the methoxy substituent at C-4 and a short side chain at C-9 with a carbonyl at C-13 represent the aglycone moiety. A glycosidic bound to C-7 of ring A attaches the sugar daunosamine and consists of a 3-amino-2,3,6-trideoxy-L-fucosyl moiety. [Minotti *et al.* 2004]

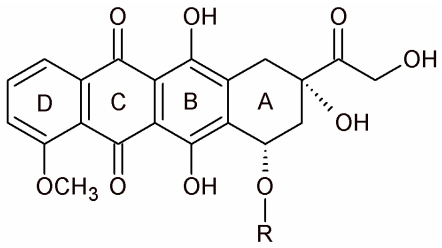

Figure 16 Structure of doxorubicin. R: Daunosamine

The highly efficient anthracylines are hampered in the clinical use by causing toxicity in cardiac cells. The incidence of cardiomyopathy and CHF was shown to

be dependent on the drug's dose. As the incidence of cardiotoxicity sharply increases at 550 mg/m^2 doxorubicin, an empirical dose limit of 500 mg/m^2 doxorubicin was set [Lefrak *et al.* 1973; Minotti *et al.* 2004].

In terms of the evaluation of cardiotoxic effects of new compounds under culture conditions, doxorubicin is often used as a control cardiotoxic reference compound.

Doxorubicin can cause toxicity by different mechanisms:

1) intercalation into DNA, emerging inhibited synthesis of macromolecules;
2) generation of free radicals, causing DNA damage or lipid peroxidation;
3) DNA binding and alkylation;
4) DNA cross-linking;
5) interference with DNA unwinding or DNA strand separation and helicase activity;
6) direct membrane effects;
7) initiation of DNA damage via inhibition of topoisomerase II; and
8) induction of apoptosis in response to topoisomerase II inhibition.

The type of toxicity depends from the *in vitro* applied concentrations. *In vitro* experiments with doxorubicin are very often performed at too high concentrations which may induce unspecific toxicity, others than mediated via topoisomerase II inactivation for instance. [Gewirtz 1999; Minotti *et al.* 2004]

The maximum plasma concentrations (c_{max}) of doxorubicin in patients after standard bolus infusions of 75 mg/m^2 are about 5 µM [Greene *et al.* 1983] which drop rapidly into the range into the range of 1-2 µM [Speth *et al.* 1987] until reaching a trough level of 25-250 nM. Similar concentrations were found after continuous infusion [Greene *et al.* 1983; Kokenberg *et al.* 1988].

Maximum plasma concentrations reported in imatinib-treated patients are below 6 µM [Druker *et al.* 2001; Pappas *et al.* 2005; Peng *et al.* 2005] when given up to twice-daily doses of 1000 mg. In children a c_{max} of 12.6 µM at a dose of 800 mg/m^2 was found [Pollack *et al.* 2007]. Therefore, concentrations exceeding 13 µM have to be considered as physiologically not achievable.

In the present study concentrations of doxorubicin and imatinib were investigated in a broad concentration range. The goal was establish clear concentration-response relationships to various toxicological endpoints in order to find potential links between toxicity and the different cellular mechanisms of action.

5.1.2 Results

The time- and concentration-dependent cardiotoxicity of imatinib was evaluated in NRVCM and in H9c2. Cellular ATP content, MTS reduction, caspase 3/7 activity and LDH release were measured as markers for cytotoxicity and apoptosis, respectively. Doxorubicin was used as reference compound.

5.1.2.1 ATP Content of NRVCM and H9c2 Cells after Imatinib treatment

Changes in the ATP content may reflect changes of the cell amount as well as effects on the respiratory chain.

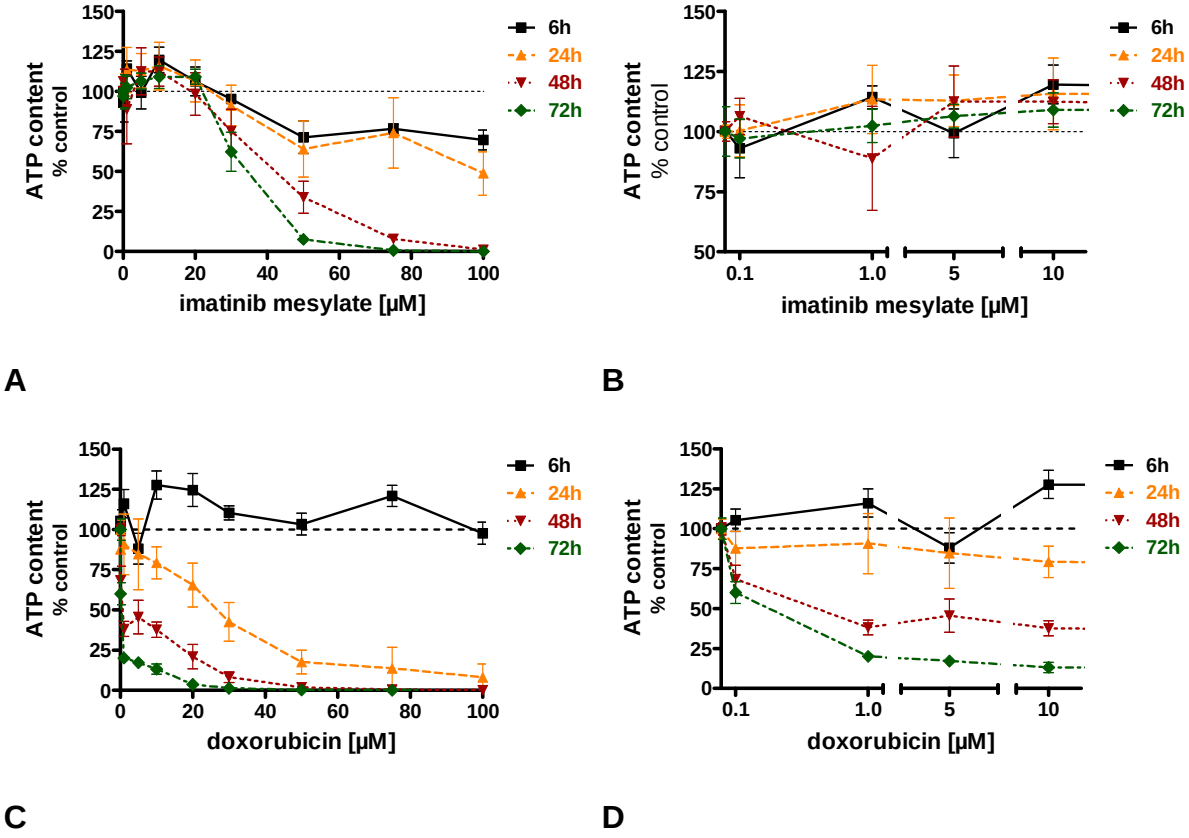

Figure 17 ATP content in NRVCM after different time points. A. Imatinib concentrations ranging from 0.1 – 100 µM. **B.** Detailed view into 0.1 – 10 µM. **C.** Doxorubicin concentrations ranging from 0.1 – 100 µM. **D.** Detailed view into 0.1 – 10 µM. All data were normalised to 100 %, represented by compound-free incubation. Mean ± SD of 3 independent experiments (6 h: n = 1).

Table 8 Table of significances of ATP contents after imatinib (IM) or doxorubicin (DX) treatment in NRVCM at the concentrations and time points indicated. Level of significance: * P < 0.05, ** P < 0.001, *** P < 0.0001.

		0.1 µM	1 µM	5 µM	10 µM	20 µM	30 µM	50 µM	75 µM	100 µM
IM	**6h**	ns	ns	ns	*	ns	ns	**	**	***
	24 h	ns	ns	ns	*	ns	ns	**	**	***
	48 h	ns	ns	ns	ns	ns	***	***	***	***
	72 h	ns	ns	ns	ns	*	***	***	***	***
DX	**6h**	ns	ns	ns	**	**	ns	ns	*	ns
	24 h	ns	ns	ns	**	***	***	***	***	***
	48 h	***	***	***	***	***	***	***	***	***
	72 h	***	***	***	***	***	***	***	***	***

Imatinib caused a time- and dose-dependent decline of the ATP content in NRVCM (Figure 17 A, B). After short time incubation of 6 h significant decreases were only achieved at the concentration of 50 µM imatinib. Increased incubation times reduced the toxic concentrations. Significant ATP decreases after 48 h were achieved at 30 µM and after 72 h at 20 µM imatinib.

Doxorubicin (Figure 17 C, D) also induced a dose- and time-dependent decrease of the ATP content in NRVCM. In contrast, significant ATP-decreases were found already at 10 µM after 24 h treatment of doxorubicin. Similar to imatinib, increased incubation time decreased the toxic concentration. After 48 and 72 h of incubation, the effective concentration of doxorubicin was 0.1 µM. Here the intracellular ATP level dropped to 25 % of the control values.

The cytotoxicity induced by doxorubicin in NRVCM was more pronounced and occurred at earlier time-points as compared with imatinib. The maximum effects found at 30 µM imatinib treatment were comparable to those obtained after 0.1 µM doxorubicin treatment.

The significance levels of both compounds can be found in Table 8.

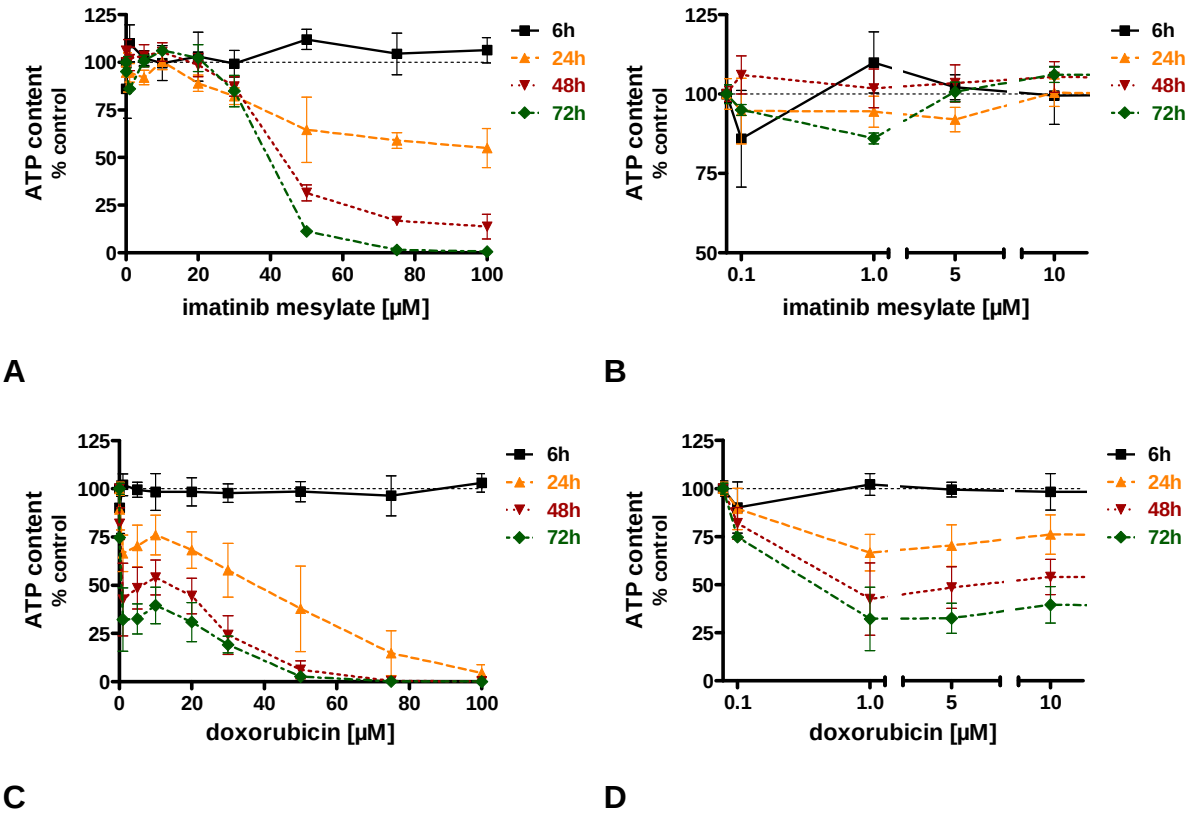

Figure 18 ATP content in H9c2 after different time points. A. Imatinib concentrations ranging from 0.1 – 100 µM. **B.** Detailed view into 0.1 – 10 µM. **C.** Doxorubicin concentrations ranging from 0.1 – 100 µM. **D.** Detailed view into 0.1 – 10 µM. All data were normalised to 100 %, represented by compound-free incubation. Mean ± SD of 3 independent experiments (6 h: n = 1).

Table 9 Table of significances of ATP contents after imatinib (IM) or doxorubicin (DX) treatment in H9c2 at the concentrations and time points indicated. Level of significance: * P < 0.05, ** P < 0.001, *** P < 0.0001.

		0.1 µM	1 µM	5 µM	10 µM	20 µM	30 µM	50 µM	75 µM	100 µM
IM	6h	**	ns	ns	ns	ns	ns	*	ns	ns
	24 h	ns	ns	ns	ns	*	***	***	***	***
	48 h	ns	ns	ns	ns	ns	***	***	***	***
	72 h	ns	***	ns	ns	ns	***	***	***	***
DX	6h	*	ns	ns	ns	ns	ns	ns	ns	ns
	24 h	ns	***	***	***	***	***	***	***	***
	48 h	**	***	***	***	***	***	***	***	***
	72 h	***	***	***	***	***	***	***	***	***

The pattern observed in H9c2 cells was similar to that found in NRVCM (Figure 18 A, B and Table 9). Doxorubicin as well as imatinib caused a concentration- and time-dependent decrease of ATP levels. However, 6 h treatment of imatinib and doxorubicin had no effect on the cells. Also, toxicity at similar concentrations was slightly less in H9c2. Significant toxicity of imatinib was found to be induced at concentrations above 30 µM, independent on incubation time. In general, both compounds were less effective in H9c2 cells than in NRVCM.

5.1.2.2 MTS Reduction of NRVCM and H9c2 Cells after Imatinib treatment

With the MTS assay mitochondrial functionality was investigated, as it is reduced enzymatically by mitochondrial enzymes.

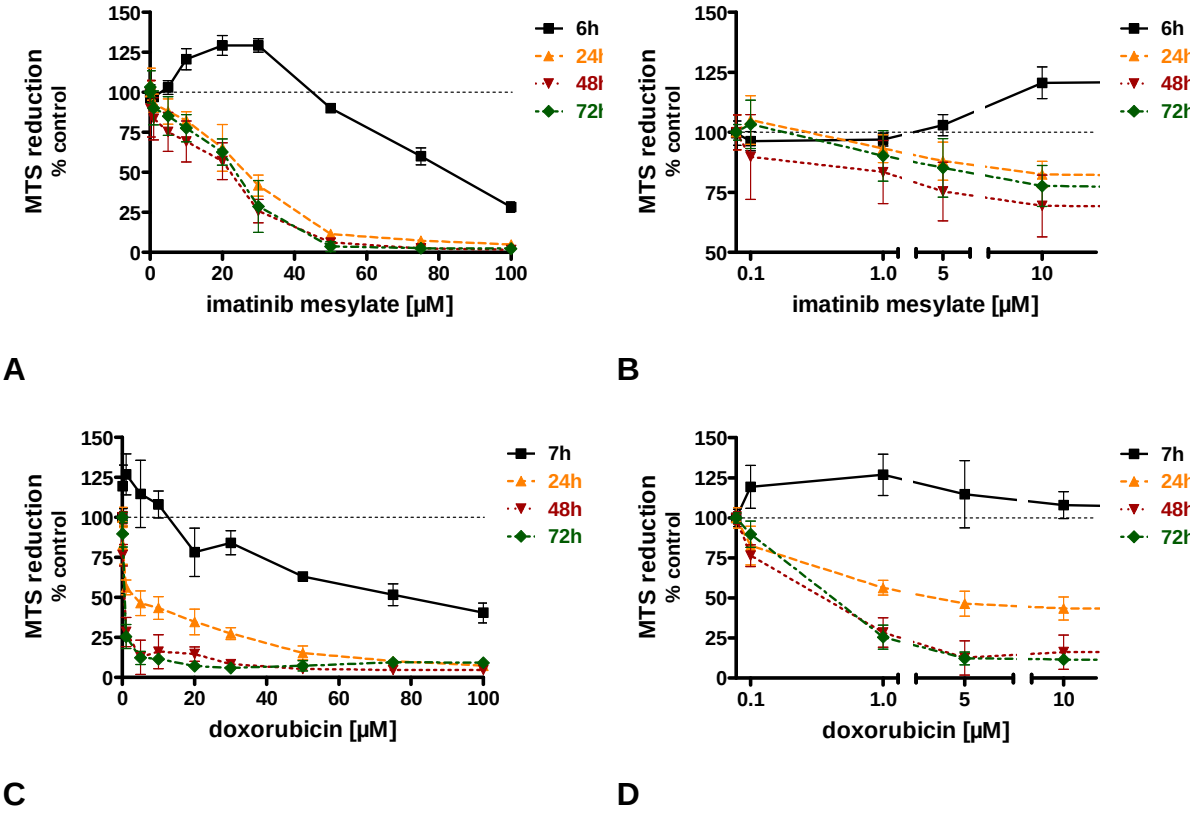

Figure 19 MTS reduction in NRVCM after different time points. A. Imatinib concentrations ranging from 0.1 – 100 µM. **B.** Detailed view into 0.1 – 10 µM. **C.** Doxorubicin concentrations ranging from 0.1 – 100 µM. **D.** Detailed view into 0.1 – 10 µM. All data were normalised to 100 %, represented by compound-free incubation. Mean ± SD of 3 independent experiments (6 h: n= 1).

Table 10 Table of significances of MTS reduction after imatinib (IM) or doxorubicin (DX) treatment in NRVCM at the concentrations and time points indicated. Level of significance: * P < 0.05, ** P < 0.001, *** P < 0.0001.

		0.1 µM	1 µM	5 µM	10 µM	20 µM	30 µM	50 µM	75 µM	100 µM
IM	6h	ns	ns	ns	***	***	***	ns	***	***
	24 h	ns	ns	**	***	***	***	***	***	***
	48 h	ns	**	***	***	***	***	***	***	***
	72 h	ns	ns	*	***	***	***	***	***	***
DX	6h	ns	ns	ns	ns	ns	ns	**	***	***
	24 h	***	***	***	***	***	***	***	***	***
	48 h	***	***	***	***	***	***	***	***	***
	72 h	***	***	***	***	***	***	***	***	***

Imatinib treatment for 6 h of NRVCM caused a dose-dependent increase of MTS reduction capability (Figure 19, A, B), reaching a maximum effect of about 130 % of control at the concentration of 30 µM. Increased imatinib concentrations led to dose-dependent decreases of MTS reduction. At 100 µM imatinib the maximum

inhibitory effect was achieved (28 % of the control). The bi-phasic curve characteristics disappeared at incubation times longer than 6 h. After 24, 28 and 72 h the concentration-responses were very similar. Here the effective imatinib concentrations was 5 µM with significant changes compared to the control. Significance levels compared to the control are found in Table 10.

Impaired MTS reduction after doxorubicin treatment of NRVCM occurred earlier and at lower concentrations than with imatinib (Figure 19 D, E). Statistically significant decreases compared to the control were found after 6 h incubation at concentrations above 50 µM doxorubicin (Figure 19 D, E and Table 10). At all other time points all concentration-dependent decreases were observed. The lowest effective concentration was 0.1 µM doxorubicin.

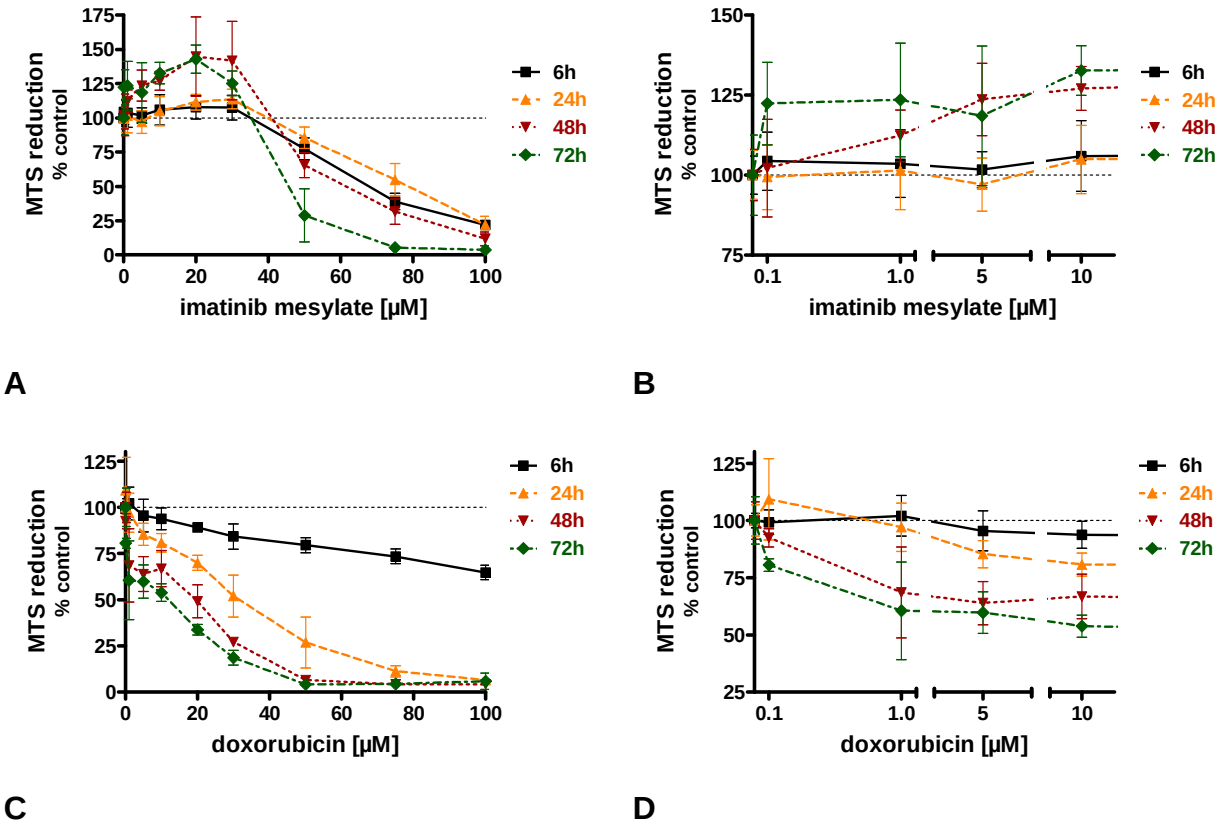

Figure 20 MTS reduction in H9c2. A. Imatinib concentrations ranging from 0.1 – 100 µM. **B.** Detailed view into 0.1 – 10 µM. **C.** Doxorubicin concentrations ranging from 0.1 – 100 µM. **D.** Detailed view into 0.1 – 10 µM. All data were normalised to 100 %, represented by compound-free incubation. Mean ± SD of 2-4 independent experiments.

Table 11 Table of significances of MTS reduction after imatinib (IM) or doxorubicin (DX) treatment in H9c2 at the concentrations and time points indicated. Level of significance: * P < 0.05, ** P < 0.001, *** P < 0.0001.

		0.1 µM	1 µM	5 µM	10 µM	20 µM	30 µM	50 µM	75 µM	100 µM
IM	**6h**	ns	ns	ns	ns	ns	ns	***	***	***
	24 h	ns	ns	ns	ns	ns	*	**	***	***
	48 h	ns	ns	**	**	***	***	***	***	***
	72 h	*	*	ns	***	***	*	***	***	***
DX	**6h**	ns	ns	ns	ns	**	***	***	***	***
	24 h	ns	ns	*	***	***	***	***	***	***
	48 h	ns	***	***	***	***	***	***	***	***
	72 h	**	***	***	***	***	***	***	***	***

MTS reduction capability in H9c2 cells after treatment with imatinib (Figure 20 A, B) showed the bi-phasic characteristic found in NRVCM only after 48 and 72 h of incubation. Significant increases (listed in Table 11) were found at 30 µM imatinib, after 24, 48 and 72 h, at 20 and 10 µM after 48 and 72 h, at 5 µM after 48 h and at 1 and 0.1 µM after 72 h. The lowest effect concentration, which caused significant decreases in the MTS reduction capability, was 50 µM.

Doxorubicin had a time- and dose-dependent effect on MTS reduction capability in H9c2 cells (Figure 20 C, D). Increased incubation times led to the lowest effective doxorubicin concentration. Significant effects occurred at concentrations above 20 µM (6 h), 5 µM (24 h), 1 µM (48 h) and 0.1 µM (72 h).

The responses of imatinib and doxorubicin were similar to that found in NRVCM. In both systems doxorubicin was more potent than imatinib. The H9c2 cell model was less sensitive as compared to NRVCM.

5.1.2.3 Caspase 3/7 Activation in NRVCM and H9c2 by Imatinib Treatment

It was reported that imatinib induced the mitochondrial release of cyt c in NRVCM [Kerkelä *et al.* 2006]. As caspase 3/7 activation is a down-stream event of the mitochondrial cyt c release it thus represents a more relevant marker for the execution of apoptosis. Therefore, the caspase 3/7 activity was measured.

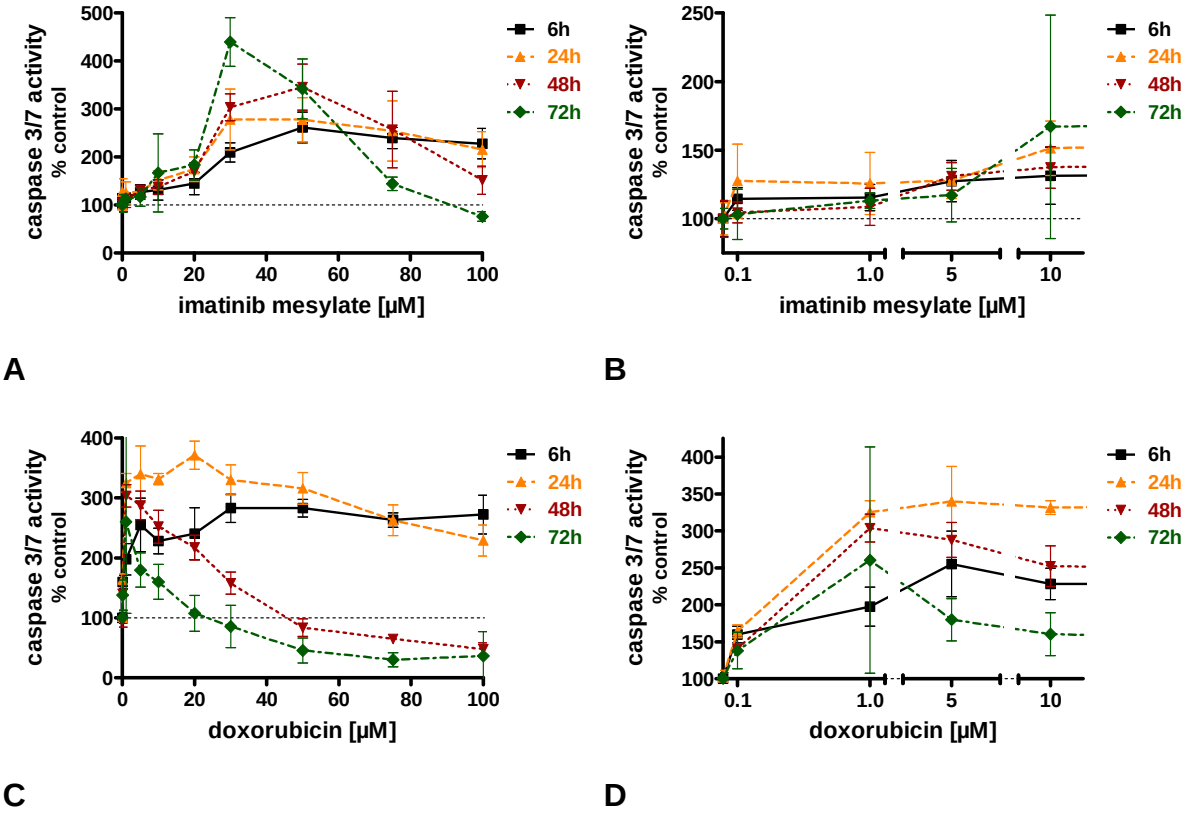

Figure 21 Caspase 3/7 activity in NRVCM. A. Imatinib concentrations ranging from 0.1 – 100 µM. **B.** Detailed view into 0.1 – 10 µM. **C.** Doxorubicin concentrations ranging from 0.1 – 100 µM. **D.** Detailed view into 0.1 – 10 µM. All data were normalised to 100 %, represented by compound-free incubation. Mean ± SD of 2-4 independent experiments.

Table 12 Table of significances of caspase activity after imatinib (IM) or doxorubicin (DX) treatment in NRVCM at the concentrations and time points indicated. Level of significance: * P < 0.05, ** P < 0.001, *** P < 0.0001.

		0.1 µM	1 µM	5 µM	10 µM	20 µM	30 µM	50 µM	75 µM	100 µM
IM	6h	ns	ns	ns	ns	**	***	***	***	***
	24 h	ns	ns	ns	*	***	***	***	***	***
	48 h	ns	ns	ns	ns	**	***	***	***	ns
	72 h	ns	ns	ns	*	**	***	***	ns	ns
DX	6h	ns	**	***	***	***	***	***	***	***
	24 h	***	***	***	***	***	***	***	***	***
	48 h	***	***	***	***	***	***	ns	*	***
	72 h	ns	***	*	ns	ns	ns	ns	ns	ns

In Figure 21 the time- and dose-response curves of caspase 3/7 activity induced by imatinib (A, B) or doxorubicin (C, D) treatment are displayed. Imatinib emerged bell-shaped curves in the caspase 3/7 activity assay (Figure 21 A, B) with the

maximum at 30 µM (24, 72 h) and 50 µM (6, 48 h). No significant differences compared to the controls were found (Table 12) up to 10 µM (24, 72 h) and 20 µM (6, 48 h) imatinib, respectively. Concentrations of up to 30 µM imatinib induced a time-dependent increase of caspase 3/7 activity which was highest elevated after 72 h. Increased imatinib concentrations did not result in a proportional increase of the caspase 3/7 activity. The curves faded into a plateau between 30 and 50 µM after a maximum effect (~5-fold of the control level) after 72 h at 30 µM imatinib treatment. Further increased concentrations of imatinib above 50 µM led to decreased caspase 3/7 activity. Decreases in the caspase 3/7 activity were steeper the longer the incubations were.

Doxorubicin treatment (Figure 21 C, D) induced a statistically significant increase of caspase 3/7 starting at the lowest concentration (0.1 µM). Maximum caspase 3/7 activation was reached between 1 and 5 µM doxorubicin, depending on the incubation time. Decreases were observed at concentrations higher than 5 µM. Contrary to imatinib treatment, the curves of the caspase 3/7 activity induced by doxorubicin decreased steeper, having more significant effects at lower concentrations and at earlier time-points. For levels of significance please refer to Table 12.

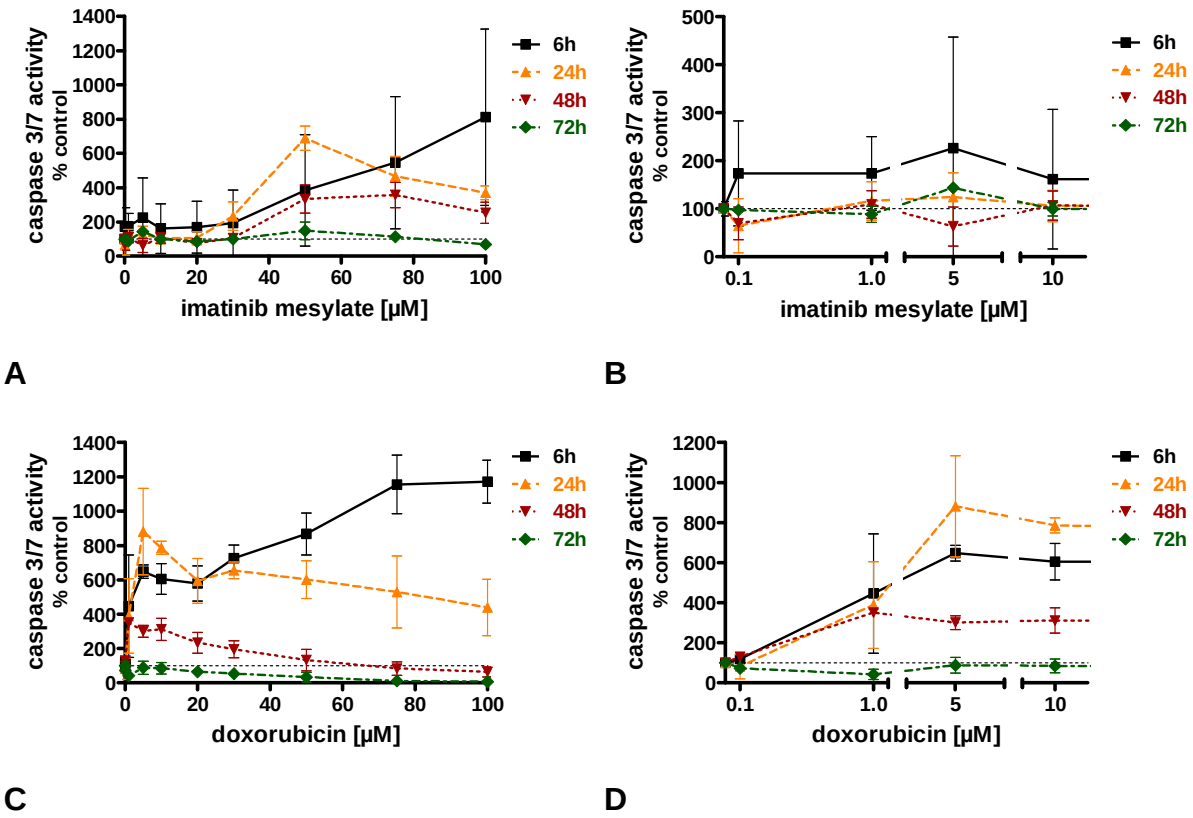

Figure 22 Caspase activity in H9c2 induced by imatinib and doxorubicin. A. Imatinib concentrations ranging from 0.1 – 100 µM. **B.** Detailed view into 0.1 – 10 µM. **C.** Doxorubicin concentrations ranging from 0.1 – 100 µM. **D.** Detailed view into 0.1 – 10 µM. All data were normalised to 100 %, represented by compound-free incubation. Mean ± SD of 2-4 independent experiments.

Table 13 Table of significances of caspase activity after imatinib (IM) or doxorubicin (DX) treatment in H9c2 at the concentrations and time points indicated. Level of significance: * P < 0.05, ** P < 0.001, *** P < 0.0001.

		0.1 µM	1 µM	5 µM	10 µM	20 µM	30 µM	50 µM	75 µM	100 µM
IM	**6h**	ns	ns	ns	ns	ns	ns	*	***	***
	24 h	ns	ns	ns	ns	ns	***	***	***	***
	48 h	ns	ns	ns	ns	ns	ns	***	***	***
	72 h	ns	ns	ns	ns	ns	ns	**	ns	ns
DX	**6h**	ns	***	***	***	***	***	***	***	***
	24 h	ns	**	***	***	***	***	***	***	***
	48 h	ns	***	***	***	***	***	ns	ns	ns
	72 h	ns	***	ns	ns	*	**	***	***	***

Caspase 3/7 activity in H9c2 (Figure 22 A, B) after 6 h imatinib treatment increased dose-dependently. Longer incubation times followed a bell-shaped pattern with decreases in the caspase 3/7 activity at concentrations above 30 µM. Statistically significant differences compared to the control started at concentrations of 50 µM for all time-points except after 24 h treatment (30 µM; see Table 13). The induction of caspase 3/7 activity was found to be dose- and time-dependent, though the strongest increase was found after 6 h; 72 h after

incubation an increase was found only after 50 µM imatinib. The observed plateaus induced in NRVCM were also found, though starting at later time-points. The increase of activity was generally possible to a higher amount in H9c2 as compared with NRVCM. In Figure 22 C, D the caspase 3/7 activity was shown after doxorubicin treatment. The activity started at longer time points than with imatinib treatment and decreased again with increasing concentrations. In contrast to imatinib, the 72 h curve crossed the 100 % indicating that necrosis may have started. Significant differences compared with the particular control are listed in Table 13. The higher cytotoxicity of doxorubicin as against imatinib was confirmed again. In addition, the sensitivity of NRVCM was shown to be higher than that of H9c2 cells.

In contrast, doxorubicin (Figure 22 C, D) induced statistically significant increases at concentrations starting from 1 µM at all time-points observed. The strongest effect was found after 6 h incubation and concentrations above 50 µM doxorubicin. Except for 6 h incubation, the caspase 3/7 activity peaks at 5 µM doxorubicin, fading into a slight (24 h) or steeper (48 h) decrease. 72 h of incubation emerged no increases of caspase 3/7 activity. Instead, concentrations above 20 µM caused significant decreases compared to the control.

5.1.2.4 LDH release of NRVCM 24 h after Imatinib Treatment

The cellular effect of imatinib was determined by the release of the lactate dehydrogenase enzyme (LDH) into the supernatant. LDH is released when the cells' membranes are damaged.

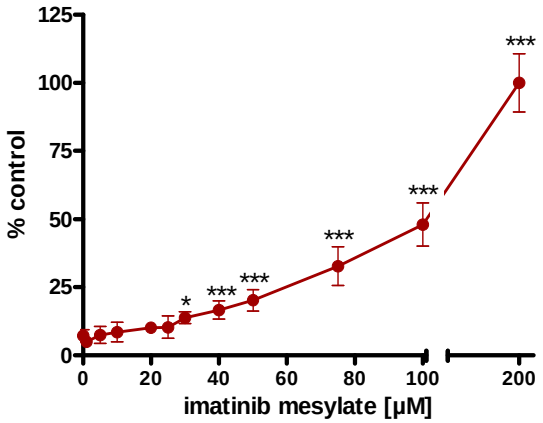

Figure 23 LDH release in imatinib-treated NRVCM after 24 h. All data were normalised to 100 %, represented by compound-free incubation. Mean ± SD of 6 independent experiments. Level of significance: * $P < 0.05$, *** $P < 0.0001$.

After 24 h treatment the membrane integrity was measured by LDH release from the cells (Figure 23). A clear, linear concentration-response was seen at

concentrations ranging from 1 to 200 µM imatinib. Concentrations starting from 30 µM were significantly different compared with the control.

5.1.3 Discussion

NRVCM were isolated from neonatal rats since cardiomyocytes are much easier to cultivate as compared to cells from adult animals. The cell culture conditions for this study were very similar to that used by Kerkelä and colleagues [Kerkelä *et al.* 2006]. However, there are minor deviations between both laboratories. Instead of using 2-4 day old rats for the preparation of NRVCM, rats were used directly at the day of birth or one day later. The selection of younger animals is based on unpublished observation (Brigitte Greiner, personal communication) that NRVCM yield a better quality when derived from freshly born pups. Compared to Kerkelä and co-workers, the medium for this study was DMEM:F12 and free of phenol red. The lack of phenol red was chosen since it is known that muscle cells react sensitively to this dye and may cause some toxicity by itself which could overlap with the effect of the test compound (Brigitte Greiner, Marianne Schwald, Novartis Pharma, personal communication). To suppress the growth of fibroblasts and to make the culture more specific to cardiomyocytes, horse serum was added in addition to fetal calf serum. The concentrations of sera were fixed in the present study (2 % horse serum, 2 % fetal calf serum) while the concentration of fetal bovine serum was reported to be 2-5 % in the medium the group around Kerkelä have used. The antibiotics used by Kerkelä were standard (penicillin/streptomycin). For this study primocin, a new kind of antibiotic, was used which also acts on mycoplasma. Primary cells are known to have a higher risk to be contaminated by mycoplasma as compared with cell lines.
The mentioned above difference in terms of culture conditions are considered to be minor and can not used to explain any significant discrepancy in terms of obtained results.

For the work of Kerkelä and co-workers, capsules of imatinib were purchased, dissolved in distilled water and repeatedly centrifuged to yield highly purified material.

The cell line H9c2 derived from embryonic rat hearts was used to compare the results gained in NRVCM. Experiments with H9c2 cells were performed in addition to NRVCM; however, also in H9c2 cells imatinib was not tested. Since H92c is an established cell line and not a primary culture, there was no need to add antibiotics, which potentially could cause some difficulties by interacting with the test compounds.

ATP contents were measured as a marker of cellular energy homeostasis. A significant drop indicates impaired energy supply or dying cells. The cellular ATP content of NRVCM was reported to be decreased to ~35 % [Kerkelä *et al.* 2006] at 5 µM imatinib. In the current study, 5 µM imatinib showed an increase of ATP content under the same conditions. The results obtained in this study were recently confirmed; the IC_{50} of the ATP content in H9c2 cells is reported to be 30.5 ± 1.5 µM (this study: 36.4 ± 1 µM) [Will *et al.* 2008].

Caspase 3/7 activity was investigated as a marker of apoptosis and determined by a luciferase-based chemiluminescence assay. In that assay, activated caspase 3/7 cleave and thereby release a substrate for luciferase, subsequently leading to the emission of light in the presence of ATP.
In the Kerkelä paper, apoptosis was measured with the activity of caspase 3/7 and the cleavage of caspase 3. The activity of caspase 3 was reported to be increased fold and caspase 3/7 activity was increased by approximately 1.15 at 5 µM 26 h after imatinib treatment. In the current study caspase 3/7 activity was determined along a broad concentration range. It was found that there was a significant time- and concentration-dependency after treatment with imatinib as well as with the reference compound doxorubicin. In addition, the concentration-dependencies followed a bi-phasic response.
In addition to caspase 3/7 activity Kerkelä determined the number of TUNEL positive stained cells. At 5 µM and 24 h treatment of imatinib, the number of TUNEL positive cells increased ~8-fold. A pronounced release of cyt c to the cytosole was also reported at 5 µM imatinib. [Kerkelä *et al.* 2006]
Kerkelä and colleagues have observed at 5 µM imatinib after 24 h in NRVCM a ~1.5-fold increase of caspase 3/7 activity. In the current study, the caspase 3/7 activity was significantly increased at 10 µM (1.5-fold) and at 20 µM (1.75-fold). The dose-response curve followed a bell-shape characteristic with a maximum effect at 30 µM with concentration-dependent decrease of caspase 3/7 activity at higher concentrations of imatinib. Bell-shaped characteristics have often been described by apoptosis-inducing compounds. Considering the concentrations of imatinib and the time-points at which increased caspase 3/7 activities were observed, it is apparent that caspase 3/7 activity and cellular ATP contents were paralleled.
ATP is an important cellular factor for the shift from apoptosis to necrosis. During apoptosis, high concentrations of ATP are needed since a lot of active reconstructions occur within the cell. Once ATP has dropped, cells undergo necrosis. This switch may be also suggested in the case of imatinib. At higher concentrations and later time points of treatment, caspase 3/7 activity dropped in parallel to the ATP levels.

LDH release, which is a marker of cell membrane damage, had similar cytotoxic threshold concentrations as ATP. LDH release is, in comparison to the MTS reduction, ATP content and caspase 3/7 activity, a later marker of cytotoxicity.

The MTS reduction assay is a tetrazolium-based assay which is used to determine the percentage of viable cells. Tetrazolium salt reduction is generally assumed to be intracellular and related to energy metabolism. However, it was found that most reduction appears to be non-mitochondrial. Several tetrazolium salts were shown to be reduced extracellular by electron transport over the plasma membrane. [Berridge MV 1996]. A closely related tetrazolium salt, MTT (2-(4,5-dimethyl-2-thiazolyl)-3,5-diphenyl-2H-tetrazolium bromide) [Berridge *et al.* 2005]), is suggested to be readily taken up be the plasma membrane and to be reduced intracellularly mainly by NAD(P)H-oxidoreductases [Berridge *et al.* 2005]. MTS is an inner salt (positive charge on the core counterbalanced by a negative negatively charged sulfonate group on one phenole ring) having a weakly acidic carboxymethoxy group on a second phenyl ring. Hence, MTS is not expected to readily enter the cell via the membrane potential because of its lipophilic properties [Berridge *et al.* 2005]. MTS is used with 1-methoxy 5-methyl-phenazinium methyl sulphate (mPMS), an intermediate electron carrier, which mediates tetrazolium salt reduction at the cell surface. There, or at a site in the plasma membrane which is readily accessible, mPMS picks up electrons to form a radical intermediate that then reduces the dye [Berridge *et al.* 2005]. The intracellular reduction of MTS may be mainly addressed to NADH, similar to MTT [Berridge *et al.* 1993].
The suggested direct mitochondrial toxicity was investigated recently in H9c2 cells and revealed IC_{50}s of the oxidative phosphorylation complexes well above clinical c_{max} values (above 190 µM). Neither impact on oxygen consumption nor mitochondrial swelling was induced by imatinib treatment [Will *et al.* 2008]. Hence, the suggestion of mitochondria as a chief target of imatinib could not be confirmed.
The differences found with the MTS assay in the cell types used may be explained by the membranes. Considering that the isolation of NRVCM is a long procedure it may be concluded that these cells' membranes might be different (e.g. more sensitive and thinner) to those of a cell line. In addition, the cell line is derived from embryonic hearts whereas NRVCM derive from neonatal, non-proliferating hearts and MTS reduction is reported to be different depending on which cell type used [Berridge MV 1998].
The reference compound doxorubicin drops at 1 µM the ATP content after 14 h to 58 % of the control in neonatal rat cardiomyocytes [Jeyaseelan *et al.* 1997]. This data is similar to the observed drop in this study after 24 h to an ATP amount of about 60 %. In H9c2 cells the IC_{50} determined 16 h after doxorubicin treatment is reported to be 5.6 ± 1.3 µM [Menna *et al.* 2007], another group showed a

reduction to about 55 % viability 24 h after incubation with 20 µM doxorubicin [Hannon *et al.* 1991]. Both results are obtained with a MTT assay which is tetrazolium salt based like MTS but only partly reduced by the same enzymes [Berridge *et al.* 2005]. With an IC_{50} of 29 µM 24 h after treatment and a reduction to about 68 % after 20 µM treatment the result obtained in this work are less toxic than those reported. However, comparing data points show that the results are in the same range. The effects found with doxorubicin appear to be in the range which was reported. Therefore, the assays can be assumed to have worked properly as well as the cell culture quality to be comparable.

Both doxorubicin and imatinib have shown that NRVCM are more sensitive to drug-induced effects as compared to H9c2.

The calculated IC_{50}s and EC_{50}s are listed in Table 14.

Table 14 IC_{50}s and EC_{50}s [µM] of the cell viability in NRVCM and H9c2 after incubation of imatinib for the time points indicated. Caspase activity is represented by EC_{50} [µM]. n.a.: not applicable**.**

	time	ATP		MTS		LDH	CAS	
IM	**[h]**	***NRVCM***	***H9c2***	***NRVCM***	***H9c2***	***NRVCM***	***NRVCM***	***H9c2***
	6	38.3 ± 1	n.a.	71.9 ± 1	59.1 ± 1	-	25.5 ± 1	108.4 ± 4
	24	33.5 ± 1	36.4 ± 1	26.6 ± 1	76.8 ± 1	197.1 ± 1	n .a.	n.a.
	48	39.7 ± 1	39 ± 1	24.4 ± 1	48.9 ± 1	-	n.a.	n.a.
	72	31.6 ± 1	37.7 ± 1	24 ± 1	43.7 ± 1	-	n.a.	n.a.
DX	6	n.a.	n.a.	42.3 ± 2	214.2 ± 1	-	1.4 ± 9	n.a.
	24	27.8 ± 1	57.2 ± 1	7.7 ± 1	29.3 ± 1	-	n.a.	n.a.
	48	15 ± 1	28.3 ± 1	0.3 ± 1	24.3 ± 1	-	31.9 ± 1	38. 6 ± 1
	72	0.03 ± 6	0.58 ± 8	0.39 ± 1	18.3 ± 1	-	20.2 ± 1	45.3 ± 1

As expected, primary NRVCM were found to be more sensitive to either treatment than the cell line H9c2 which was reflected in significant differences of the concentrations as well as the IC_{50}s/EC_{50}s. The cytotoxicity induced by doxorubicin was more profound as compared with imatinib, which was seen easily in the levels of significance that occurred at earlier time points and with lower concentrations when treated with doxorubicin as compared with imatinib.

The concentrations of imatinib investigated in the present study ranged from 10-100 µM. Effective threshold concentrations were observed between 30 and 50 µM imatinib. In comparison to pharmacoceutical concentrations (c-Abl kinase activity inhibition (IC_{50} = 0.025 µM) (Jürgen Mestan, Novartis, internal communication; [Druker *et al.* 1996]) the specific tyrosine kinase inhibition is highly exceeded already at 10 µM imatinib. Concentrations exceeding 10 µM affect also other tyrosine kinases [Buchdunger *et al.* 2002]. This indicates the unspecific nature of the observed cytotoxic effects (see chapter 5.7.3).

The deviations of the current effective threshold concentrations of imatinib compared to that of Kerkelä and colleagues are not known. One obvious

difference compared to Kerkelä is that all the experiments were performed with the extracts of the Glivec tablets, which are different to the current conditions. Here the pure active compound was used instead. It can only be speculated that during the extraction from the tablet an error has occurred which led to different data and finally to misleading interpretation of these data.

In summary, the concentration- and time-dependent testing of imatinib in NRVCM and H9c2 cells allowed the determination of the threshold concentration in terms of cytotoxicity, apoptosis and mitochondrial toxicity. The results could be qualitatively reproduced but not quantitatively. There are huge deviations in the effective imatinib concentrations as compared to the studies of Kerkelä and co-workers.

5.2 Evaluation of Imatinib-Induced Endoplasmatic Reticulum Stress in NRVCM

5.2.1 Background

ER stress can be modulated via different pathways, for example PERK and IRE1. The PERK-arm acts via phosphorylation of eIF2α and results in inhibition of protein synthesis and thus counteracts ER stress. In addition, anti-apoptotic proteins are up-regulated during ER stress. The other arm investigated is IRE1. This arm includes activation and splicing of XBP-1, leading to JNK-activation and subsequently to apoptosis. Both proteins also induce CHOP, an ubiquitously expressed protein though at very low levels, that accumulates in the nucleus under ER stress [Ron *et al.* 1992]. CHOP was revealed to be one of the highest inducible proteins upon ER stress [Matsumoto *et al.* 1996]. The induction of CHOP in ER stress is suggested to be mainly caused by the PERK/eIF2α signalling pathway [Harding *et al.* 2000; Scheuner *et al.* 2001]. CHOP finally mediates ER stress-induced apoptosis.

In the present experiments imatinib-induced ER-stress in NRVCM was investigated by the markers eIF2α, XBP1 and CHOP after 24 h treatment with concentrations ranging from 10 – 50 µM imatinib.

5.2.2 Results

5.2.2.1 EIF2α Protein Levels

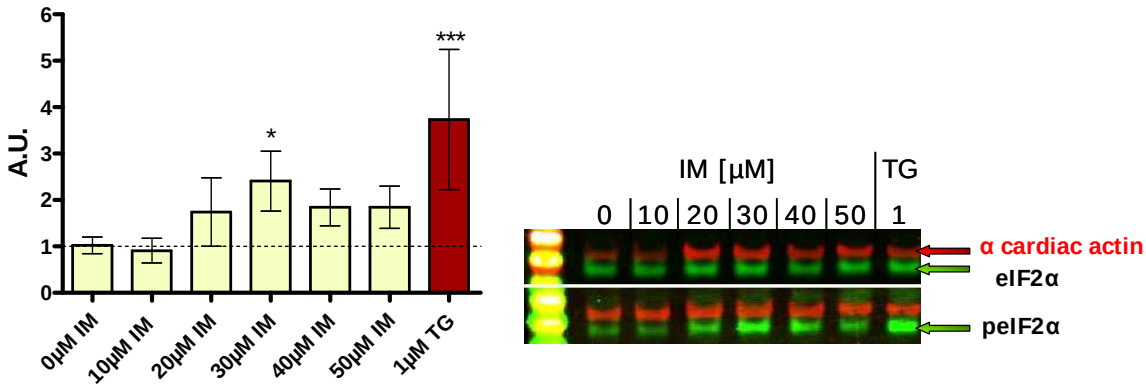

A **B**

Figure 24 Induction of eIF2α protein expression in NRVCM 24 h after imatinib treatment. A. Expression of eIF2α protein. **B.** A representative blot of eIF2α and p eIF2α, each sample is normalised to α cardiac actin of each sample, then the ratio of normalised data peIF2α/ eIF2α is calculated. The data is finally displayed as fold change of the compound-free sample. Mean ± SD of triplicates. Level of significance: * $P < 0.05$; *** $P < 0.001$.

The investigation of eIF2α showed no significant differences in the phosphorylation status after 24 h except for 30 µM imatinib (IM) treatment as displayed in Figure 24. The positive control thapsigargin (TG), an inhibitor of the ER Ca^{2+} ATPase causing Ca^{2+} depletion of the ER, was shown to induce this protein significantly to about 4-fold.

5.2.2.2 XBP1 mRNA and protein levels

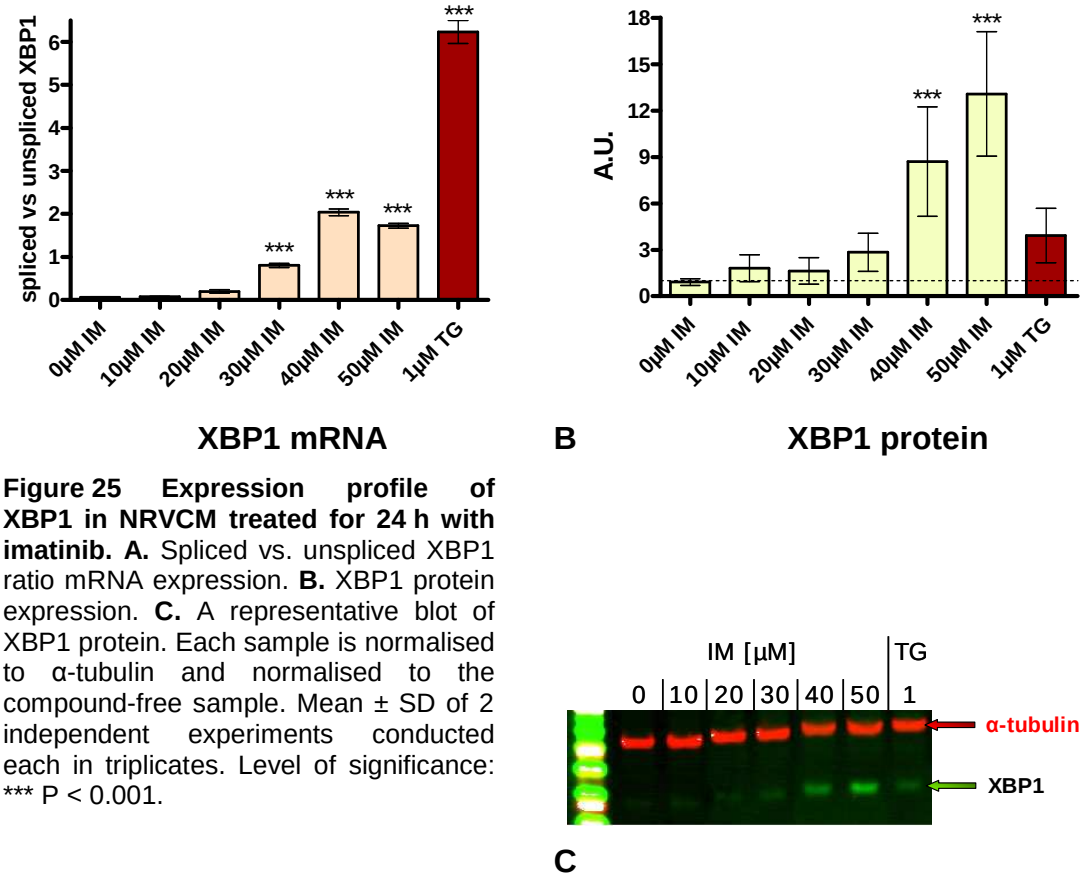

Figure 25 Expression profile of XBP1 in NRVCM treated for 24 h with imatinib. A. Spliced vs. unspliced XBP1 ratio mRNA expression. **B.** XBP1 protein expression. **C.** A representative blot of XBP1 protein. Each sample is normalised to α-tubulin and normalised to the compound-free sample. Mean ± SD of 2 independent experiments conducted each in triplicates. Level of significance: *** P < 0.001.

In NRVCM, the spliced vs. unspliced mRNA ratio of XBP1 after 24 h of treatment with imatinib increased significantly at concentrations of 30 µM imatinib and above (Figure 25 A). The positive control thapsigargin increased the XBP1 mRNA expression significantly to 99-fold compared to control whereas the induction by 30 µM imatinib was increased 13-fold, with 40 µM 33 and with 50 µM 28-fold.

Under the same conditions the protein levels of XBP1 were determined (Figure 25). Significant increases induced by imatinib treatment were observed with a maximum effect of 14-fold at 50 µM compared to the control. The positive control thapsigargin was elevated to about 4-fold.

5.2.2.3 CHOP mRNA and Protein Levels

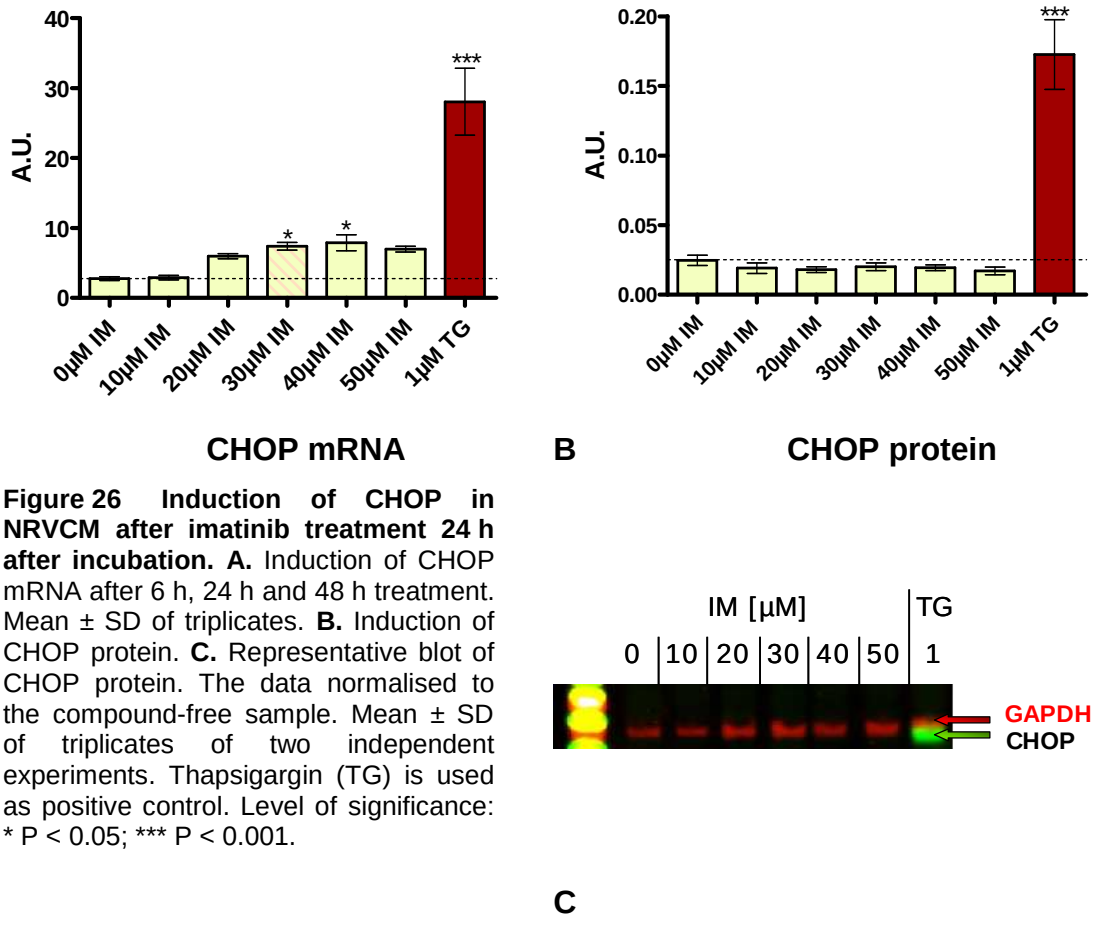

Figure 26 Induction of CHOP in NRVCM after imatinib treatment 24 h after incubation. A. Induction of CHOP mRNA after 6 h, 24 h and 48 h treatment. Mean ± SD of triplicates. **B.** Induction of CHOP protein. **C.** Representative blot of CHOP protein. The data normalised to the compound-free sample. Mean ± SD of triplicates of two independent experiments. Thapsigargin (TG) is used as positive control. Level of significance: * $P < 0.05$; *** $P < 0.001$.

CHOP mRNA expression is shown in Figure 26 A. As already seen with XBP1 spliced vs. unspliced mRNA, a slight elevation of the mRNA level was observed at concentrations above 20 µM. Significant increases were found with 30 and 40 µM of imatinib treatment with a maximum increase by 2.8-fold. The positive control, thapsigargin, was significantly elevated by 10-fold as compared to the control.

The protein levels of CHOP 24 h after imatinib-treatment (Figure 26 B) had not changed when compared to the control. The positive control Thapsigargin caused significant CHOP protein elevation, demonstrating that the assay has worked.

5.2.3 Discussion

The ER plays key roles in protein biosynthesis, modification, folding, and trafficking, and it is also the major pool for calcium storage. Perturbation of ER homeostasis leads to an ER stress response that can initially protect against cellular damage, but can eventually trigger cell death if ER dysfunction is severe or prolonged [Boyce *et al.* 2006].

The positive control thapsigargin inhibits the calcium influx into the ER [Kitamura *et al.* 2003]. As the ER needs high luminal calcium concentrations for proper folding, the function of ER is perturbed which leads to ER stress [Kuznetsov *et al.* 1993; Di Jeso *et al.* 2003; Oyadomari *et al.* 2004]. Thapsigargin showed significant increases compared to the control at eIF2α protein levels, in the XBP1 spliced vs. unspliced ratio and in mRNA and protein levels of CHOP in NRVCM 24 h after treatment. In XBP1 protein levels thapsigargin did not induce significant differences compared to the control. This finding was unexpected but is reported in the literature. IRE1 (and XBP1 as a downstream target) was shown to be activated in the beginning of the unfolded protein response (UPR) and decayed after eight hours of the activation of ER stress. The termination of its activity is important for the induction of cell death [Lin *et al.* 2007]. The increases in the spliced transcript levels are different to those obtained in the protein levels, thus, a different way of action of imatinib as opposed to thapsigargin may be suggested.
Imatinib treatment caused significant increases in all markers at concentrations at or above 30 µM. However, no concentration induced an increase of the protein levels of CHOP. CHOP protein was induced by the positive control but not with imatinib even though upstream proteins were elevated or spliced as well as CHOP mRNA. This excludes the possibility that the turn-over of CHOP mRNA was longer than 24 h and later time points could reveal an increase. Maybe the cells have a threshold for induction of CHOP protein which finally triggers apoptosis. Possible mechanisms could include the translation of CHOP mRNA only after a certain amount or a fast degradation of CHOP which is not relevant if a huge pool of CHOP mRNA is available (compare to [Batulan *et al.* 2003]).

Kerkelä and co-workers [Kerkelä *et al.* 2006] reported that 5 µM imatinib induced phosphorylation of eIF2α significantly in NRVCM 6 and 24 h after incubation. More profound increases were reported in the hearts of imatinib-treated mice. The membranes displayed seem to show a stronger phosphorylation status than after 24 h, however, a graph displaying the analysed data is missing. In addition, the experimenters have chosen mice to investigate the effects *in vivo*. The choice of another animal model than rats which were the donors of NRVCM was not explained.
The induction of ER stress by imatinib is discussed controversially in the literature. Imatinib has been proposed to induce ER stress in murine myeloid progenitor [Pattacini *et al.* 2004]. Others mainly address the intrinsic pathway to the induction of imatinib-induced toxicity in CML cells [Du *et al.* 2006], which can also be activated when ER stress is triggered. However, these

investigations were made in tumour cells. The UPR may be a characteristic of cancer cells and not of normal cells, since XBP1 was shown to be required *in vivo* for tumourigenesis. As all functions of XBP1 are downstream of the UPR, the UPR is essential for tumour growth [Koong *et al.* 2006].

5.3 Evaluation of the Specificity of Imatinib-Induced Toxicity

5.3.1 Background

Kerkelä and colleagues concluded that the toxic effects of imatinib were specific to cardiac cells since they have found cyt c release induced by imatinib in NRVCM but not in primary fibroblasts isolated from neonatal rat hearts. Neither the data nor the tested concentrations were shown in the paper. In addition, cytotoxicity was induced at unphysiologically high concentrations of imatinib. Thus, rat fibroblasts derived from heart, lung and skin (Figure 27) were investigated under the same conditions as NRVCM after treatment with imatinib and markers of cytotoxicity, apoptosis and ER stress were determined.

5.3.2 Results

5.3.2.1 Cytotoxic and Apoptotic Markers in Fibroblasts

Imatinib was investigated for cytotoxicity and apoptosis in rat fibroblasts derived from heart, lung and skin. The concentrations tested ranged from 1 – 100 µM with an incubation time of 24 h. Markers for cytotoxicity were ATP content, MTS reduction and LDH release. Apoptosis was monitored with the ADP/ATP ratio and caspase 3/7 activation.

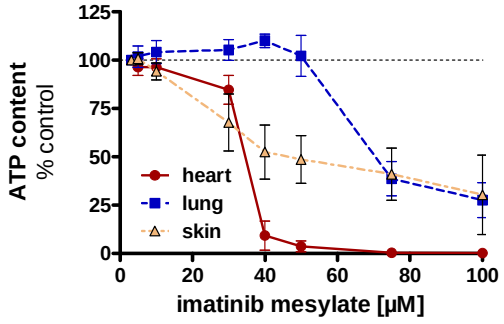

A

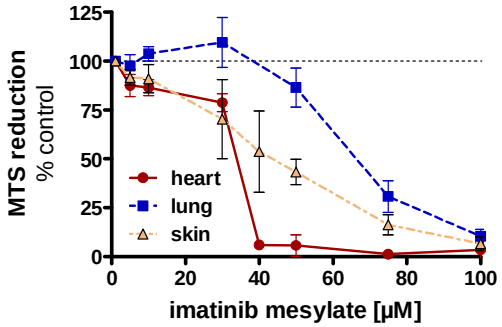

B

Figure 27 Cytotoxicity tests in different kinds of fibroblasts 24 h after imatinib treatment. A. ATP content. **B.** MTS reduction capability. **C:** LDH leakage. **D.** ADP/ATP ratio. **E.** Caspase 3/7 activity. All data are normalised to 100 %, represented by compound-free incubation. Mean ± SD of 3 independent experiments conducted in triplicates.

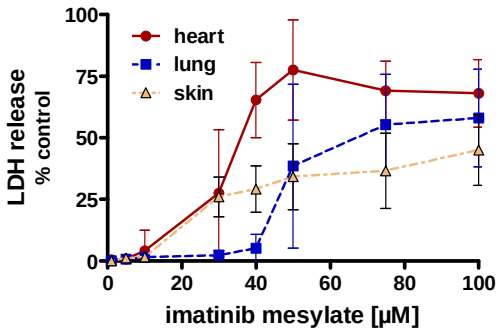

C

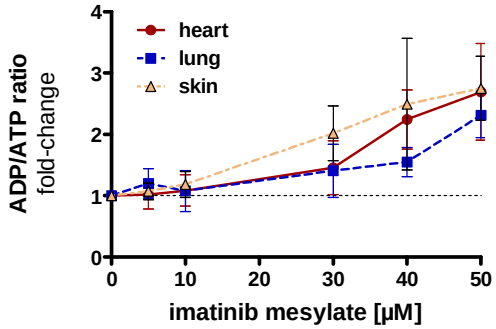

D

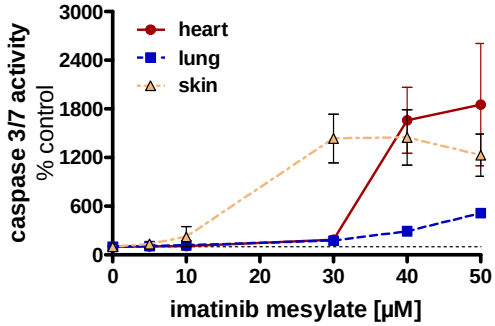

E

Table 15 Table of significance levels of ATP content, MTS reduction, ADP/ATP ratio, caspase 3/7 activity and LDH release after imatinib (IM) treatment in different types of fibroblasts for 24 h. nd: not determined. Levels of significance: ns: not significant, * P < 0.05, ** P < 0.001, *** P < 0.0001.

imatinib		5 µM	10 µM	30 µM	40 µM	50 µM	75 µM	100 µM
ATP	**heart**	ns	ns	***	***	***	***	***
	lung	ns	ns	ns	ns	ns	***	***
	skin	ns	ns	***	***	***	***	***
MTS	**heart**	**	***	***	***	***	***	***
	lung	ns	ns	ns	nd	ns	***	***
	skin	ns	ns	*	***	***	***	***
LDH	**heart**	ns	ns	*	***	***	***	***
	lung	ns	ns	ns	ns	***	***	***
	skin	ns	ns	**	***	***	***	***
ADP/ATP	**heart**	ns	ns	ns	***	***	nd	nd
	lung	ns	ns	ns	ns	**	nd	nd
	skin	ns	ns	ns	*	**	nd	nd
CAS	**heart**	ns	ns	ns	***	***	nd	nd
	lung	ns	ns	*	***	***	nd	nd
	skin	ns	ns	***	***	***	nd	nd

Table 16 IC_{50}s [µM] of the cell viability in different kinds of fibroblasts after 24 h incubation of imatinib. Caspase activity is represented by EC_{50} [µM]. n.a.: not applicable

	ATP	MTS	LDH	ADP/ATP	CAS
heart	34.2 ± 1	33.5 ± 1	31.5 ± 1	36.6 ± 1	35.6 ± 1
lung	65.4 ± 1	63.5 ± 1	47.6 ± 1	n.a.	n.a.
skin	32.3 ± 1	49.5 ± 1	28.3 ± 1	34.2 ± 3	n.a.

MTS and ATP contents after treatment with imatinib in the different fibroblasts were very similar. Imatinib caused a dose-dependent decrease of ATP content and MTS reduction in all types of fibroblast cells investigated (see Figure 27 A, B and Table 15). In both assays the least sensitive fibroblast type was derived from lung causing statistically significant effects at 75 µM. Cardiac fibroblast cells proved to be most sensitive to imatinib induced toxicity, with statistically significant effects above 30 µM and 5 µM for ATP and MTS, respectively (Table 15, Table 16). The threshold of toxicity was comparable in cardiac and dermal fibroblasts, having less effect at higher concentrations of imatinib. However, the dose-response curves were less steep in dermal fibroblasts, having fewer effects at higher imatinib concentrations.

The markers for apoptosis are shown in Figure 27 D and E. Both assays were found to show similar curves. The ADP/ATP ratio showed no significant differences up to 30 µM of imatinib. An increased ratio at concentrations above 10 µM was observed, which is regarded as induction of apoptosis. The caspase 3/7 activity (Figure 27 E) measured under the same conditions indicated that apoptosis was increased above 30 µM imatinib as compared to the controls. Dermal fibroblasts were the most sensitive cells in terms of imatinib-induced caspase activation. Threshold concentrations at which significant effects on

ADP/ATP and caspase-3/7 activities were observed were 30 µM in dermal, 40 µM in cardiac and 50 µM imatinib in pulmonary fibroblasts.
The results found after ATP and MTS determination were confirmed by the LDH releases. Significant differences compared to the controls were found at concentrations above 30 µM imatinib for cardiac and dermal, 75 µM in pulmonary fibroblasts. Threshold concentrations at which significant increases were observed was 40 µM imatinib in heart and skin fibroblasts, and 50 µM imatinib in the lung model.

5.3.2.2 ER stress Induced by Imatinib Treatment in Fibroblasts

Molecular ER stress markers were tested after imatinib treatment in different fibroblast cells, treated under the same conditions as in NRVCM.

5.3.2.2.1 EIF2α activation

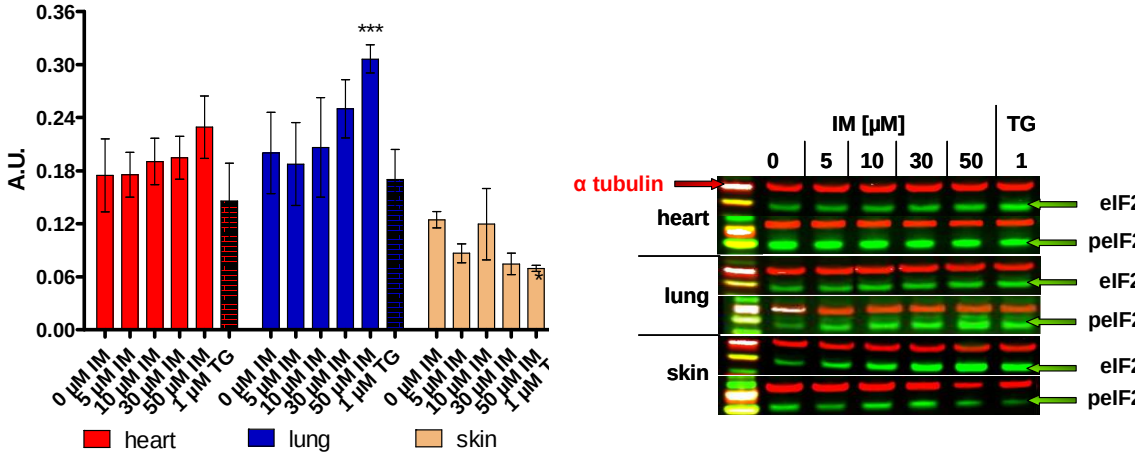

A **eIF2α protein** **B**

Figure 28 Expression of eIF2α in different kinds of fibroblasts 24 h after imatinib incubation. A. Graph of peIF2α/eIF2α protein in cardiac, pulmonary and dermal fibroblasts. **B.** Representative blots of (un)phosphorylated eIF2α protein, normalised to α-tubulin and phosphorylated form is divided by the unphosphorylated form. Mean ± SD from 3 independent experiments in duplicate. Level of significance: * $P < 0.05$; *** $P < 0.001$.

The protein amount of eIF2α (Figure 28 A) was investigated 24 h after increasing concentrations of imatinib. The positive control thapsigargin showed no or decreasing effects on the protein level of eIF2α. Treatment with imatinib revealed no clear dose-response effect; significant differences compared to the particular control were only found at 50 µM in pulmonary fibroblasts.

5.3.2.2.2 Ratio of spliced vs. unspliced XBP-1 mRNA

The results obtained for XBP-1 mRNA expression in fibroblast cells after 24 h of imatinib treatment are shown in Figure 29.

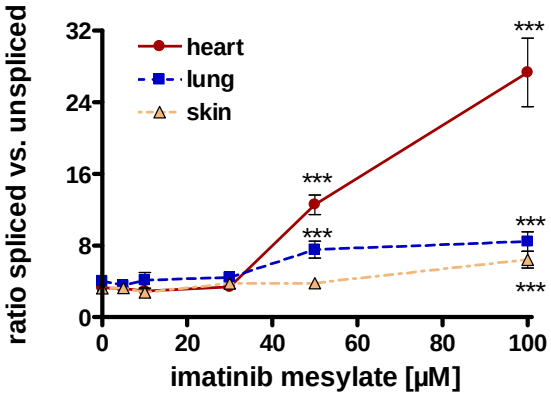

XBP1 spliced vs. unspliced mRNA

Figure 29 mRNA expression profile of XBP-1 spliced vs. unspliced after 24 h imatinib treatment in different kinds of fibroblasts. All mRNA is normalised to 18S and normalised to the control. Mean ± SD of triplicates. Level of significance: *** P < 0.001.

In all types of fibroblasts investigated, no increases of the ratio of spliced to unspliced XBP-1 were observed up to a concentration of 30 µM of imatinib (Figure 29). Significant increases of the induction of spliced XBP1 were found in cardiac and pulmonary fibroblasts at concentrations starting from 50 µM imatinib. However, the dose-response curve was less steep in pulmonary fibroblasts, more similar to dermal fibroblasts which were least sensitive to imatinib treatment showing significant differences only at 100 µM.

5.3.2.2.3 CHOP Expression

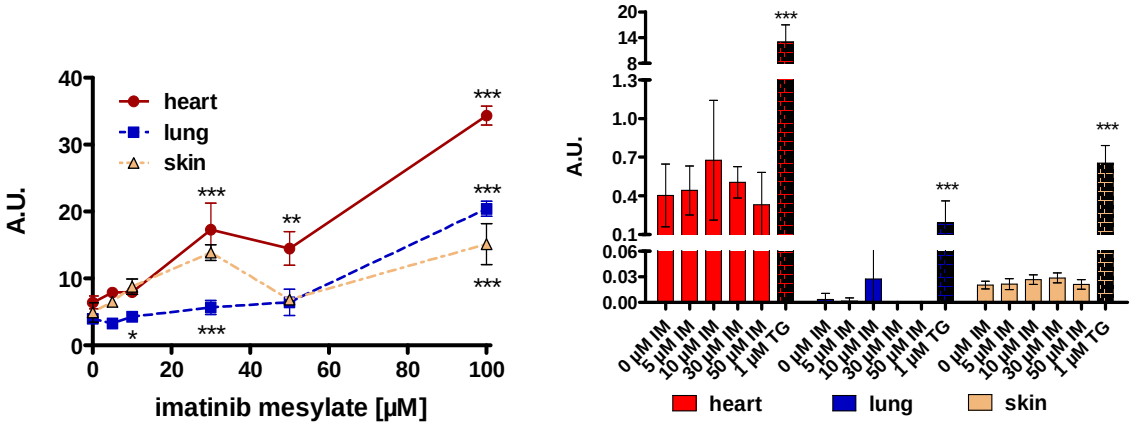

Figure 30 CHOP expression profile 24 h after imatinib treatment in different kinds of fibroblasts. A. mRNA expression. All mRNA is normalised to 18S. Mean ± SD of triplicates. **B.** Protein expression. **C.** A representative blot of CHOP protein. Samples are normalised to GAPDH and then normalised to the control. Mean ± SD two independent experiments of duplicates. Level of significance: *** P < 0.001, ** P < 0.01, * P < 0.05.

The mRNA expression of CHOP (Figure 30 A) shows a dose-dependent increase of CHOP mRNA expression in all fibroblasts investigated. Significant increases were found above 30 µM in cardiac and at 100 µM in dermal and pulmonary fibroblasts.

The cellular level of CHOP protein (Figure 30 B) was investigated in parallel. The basal control level of the CHOP protein was found to vary between the different types of fibroblasts, in contrast to the mRNA levels which were found to be at a comparable range. None of the investigated concentrations (up to 50 µM) of imatinib in either cell model did induce an increase of CHOP protein levels. The positive control thapsigargin was clearly elevated under the same conditions.

5.3.3 Discussion

The specificity of the imatinib-induced effects occurring in cardiomyocytes was not yet clear. And presently there is no data comparing the effect in fibroblasts from other organs than the heart. The specificity of imatinib-induced toxicity was investigated because it was reported that imatinib induces apoptosis in NRVCM and not in primary cardiac fibroblast cells. Since no data or tested concentrations were provided [Kerkelä *et al.* 2006], experiments for specificity were conducted in rat fibroblasts derived from different organs under the same conditions like NRVCM.

The data showed that cardiac and dermal fibroblasts had similar IC_{50}s and threshold concentrations of cytotoxicity as revealed by ATP content, MTS reduction and LDH release. Pulmonary fibroblasts were the least sensitive cell type. When compared to NRVCM and H9c2 cells (see Table 15 and Table 16) the fibroblast cell types were in the same range as NRVCM and H9c2 in the ATP assay, with the exception of pulmonary fibroblasts which were least sensitive.

In the MTS assay, NRVCM revealed to be most sensitive to imatinib-induced toxicity, followed by cardiac fibroblasts. Dermal fibroblasts were less sensitive, pulmonary fibroblasts and H9c2 cells were found to be least sensitive.

Similar results were found in the caspase assay. Thus, imatinib-induced toxicity was not found to be specific to cardiac myoblasts which is in conflict with the report from Kerkelä, saying that cytotoxic effects were triggered by imatinib in NRVCM but not in fibroblasts. One suggestion of that finding was that cardiomyocytes contracting in cell culture may have a significantly greater dependence on oxidative phosphorylation for ATP production and/or the greater ATP consumption.

The protein levels of phosphorylated eIF2α showed a statistically significant increase only after 50 µM imatinib treatment in pulmonary fibroblasts. Dermal fibroblasts were found to be decreased. In NRVCM the levels were increased above 20 µM imatinib.

The ratio of spliced vs. unspliced XBP1 was found to be higher in fibroblast cells as compared with NRVCM. Except for dermal fibroblasts, statistically significant increases were found above 30 µM. The final induction of the CHOP transcript was found to be strongest in cardiac and dermal fibroblasts. Though statistically significant differences were found at transcript levels, imatinib induced neither in NRVCM nor in any fibroblast type investigated an increase of CHOP protein.

The results of Kerkelä and co-workers, showing elevated ER stress markers after 5 µM and 10 µM imatinib, were not confirmed. With the investigation of

dose-dependent induction of ER stress markers in this study, ER stress markers such as eIF2α, spliced XBP1 and CHOP mRNA were found to be significantly elevated at concentrations above 30 µM.

The hypothesis of Kerkelä [Kerkelä *et al.* 2006] saying imatinib triggers ER stress could be confirmed from a qualitative point of view – however, not quantitatively. All ER stress effects occurred at cytotoxic concentrations and to a similar or higher extend in fibroblasts as well as in NRVCM. Thus, the specificity of imatinib-induced cellular effects was not proven and appears to be the result of unspecific cytotoxicity.

The investigations of cytotoxicity and ER stress in both NRVCM and different kinds of fibroblasts support the suggestion that imatinib induces apoptotic pathways not specifically in cardiomyocytes.

5.4 Evaluation of the Reversibility of Imatinib-Induced Effects in H9c2 cells

5.4.1 Background

Reversibility of impaired mitochondrial functions is a known property of some mitochondrial toxic agents. CCCP (carbonyl cyanide m-chlorophenylhydrazone) and Cytochalasin B (CB) were used as reference compounds affecting the mitochondrial function [Rampal *et al.* 1980; Cooper 1987; Haidle *et al.* 2004]. Cellular functional impairments of both compounds have been studied in the literature by oxygen consumption as well as by decreased pH values, due to increased glycolytic activity.

The role of reversibility in the imatinib-induced cytotoxicity has not been investigated. Online monitoring using the Bionas technology was applied to evaluate the reversibility of imatinib-induced effects, as well as on mitochondrial functions. NRVCM did not attach to the surface of the chips; therefore H9c2 cells were used for this investigation.

In the present study cells were attached over night before being inserted into the units of the Bionas device. During 8 h the cells were adapted to the experimental conditions by perfusion with control medium, marked by a grey column on the left side (Figure 31). After the adaption phase, the cells were perfused with the incubation medium for total 24 h, indicated in the graph by white colour field. At the beginning of the incubation period with the test compound, each electrode served as its own control (100 %) and all measurements were normalised to these values. In order to investigate the reversibility of the effects, an additional phase of 6 h medium perfusion free of test compounds was added (marked with a grey column on the right side). After each experiment, cells were lysed by Triton X-100, which served as a quality control measurement.

Since NRVCM did not attach to the glass surface of the Bionas chips, H9c2 were used. For this study, concentrations of 0, 10, 30 and 50 µM imatinib were investigated over 24 h and after a 6 h recovery period. The reference compounds were incubated under the same conditions, at a concentration of 10 µM (CCCP) and 2 µM (CB), respectively.

5.4.2 Results

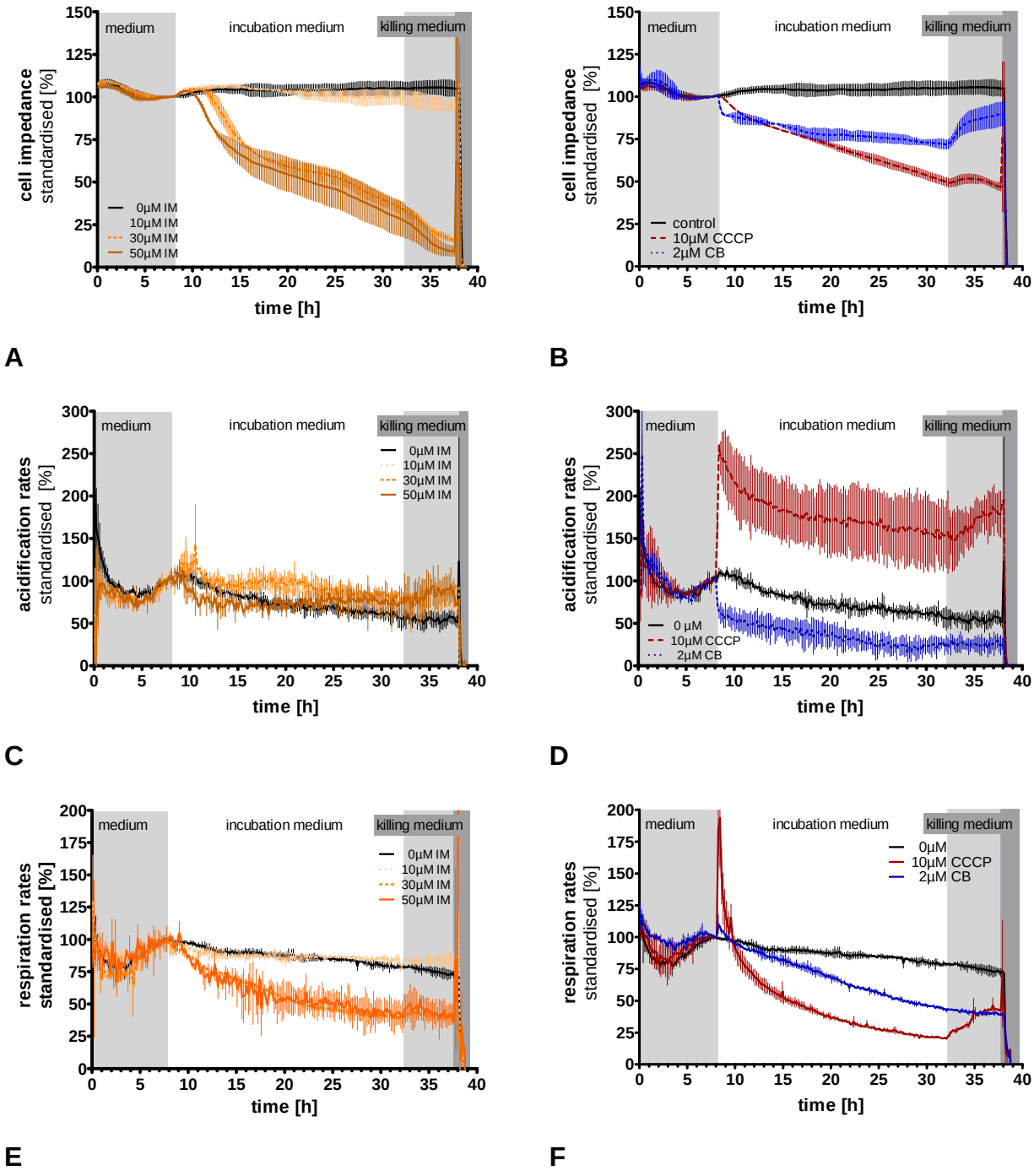

Figure 31 Online cell measurement during 24 h of imatinib incubation on H9c2. A. Standardised cell impedance of imatinib-treated cells. **B.** Standardised cell impedance acidification rates of positive controls. **C.** Standardised acidification rates of imatinib-treated cells. **D.** Standardised cell impedance of positive controls. **E.** Standardised respiration rates of imatinib-treated cells. **F.** Standardised respiration rates of positive controls. All electrodes were normalised to the value shortly before the incubation medium is added to the cells. A single chip without any compounds was used as control. Light grey marks time incubated with running medium, dark grey marks killing medium. Mean ± SD of two independent experiments.

Table 17 Table of significances of acidification rates, cell impedance and respiration rates after compound treatment in H9c2 cells for 24 h. Only the time of incubation was considered for calculation. Level of significance: * P < 0.05, ** P < 0.001, *** P < 0.0001.

	10 µM IM	30 µM IM	50 µM IM	10 µM CCCP	2 µM CB
respiration	ns	***	***	***	***
cell impedance	ns	***	***	***	***
acidification	***	***	***	***	***

The reference compounds were tested first to evaluate the specificity and sensitivity of the online monitoring system.

CCCP decreased significantly the impedance by 50 % during 24 h in comparison to the untreated control (Figure 31 A, B); this level remained constant during the recovery phase. The effect of CB was less pronounced, reaching a 25 % decrease of the impedance after 24 h incubation. During the recovery phase of CB, the impedance level increased nearly to the control level.

Acidification (Figure 31 C, D) was determined in parallel in the same cells. The positive control CCCP caused an immediate increase of acidification compared to controls. During the recovery phase acidification was still elevated and did not reach the level of control cells. Perfusions with CB immediately resulted in decreased acidifications, reaching about 50 % of the control level. Recovery did not occur.

Changes in oxygen consumption during 24 h treatment are shown in Figure 31 E, F. The positive control CCCP peaked when perfusion of the cells started. This peak was emerged by a rapid increase of oxygen consumption in about half an hour which declined towards the control level after 2 h. After 24 h of incubation, oxygen consumption was decreased by up to 25 % of the control values. During the recovery phase the oxygen consumption was regained to about 50 % of the control values. CB caused a constant decrease of the oxygen consumption during 24 h, without further changes during the recovery phase.

Incubation with imatinib had no effect at 10 µM; however, 30 and 50 µM imatinib caused nearly a total (75 %) decrease after 24 h of incubation. This effect decreased further during the recovery phase. The onset of the decreased impedance after imatinib treatment was dose-dependently delayed. While the lag time for the onset at 30 µM was after 4 h of incubation, the lag time at 50 µM was about 2 h. Imatinib treatment caused statistically significantly different values compared to control on the acidification; these differences were very small and thus might not be relevant. Imatinib had no effect at 10 µM on oxygen consumption, however 50 % decrease of the oxygen consumption was reached with 30 and 50 µM after 24 h of incubation and again, recovery was not observed.

5.4.3 Discussion

In general, online monitoring of cellular functions has a huge advantage compared to endpoint measurements. It allows to determine the onset of specific effects in a defined interval of observation and to evaluate recovery of cellular effects. The beginning and the course of the toxicity can be also observed over a specific time window as well as its reversibility. The Bionas approach is automated and works without assistance once started; repeated compound addition could be easily investigated if wanted. In addition, the current model mimics the *in vivo* situation because cells are perfused in a dynamic system. While cell cultures are static systems and kinetics can only be determined by several individual experiments. The current model offers the opportunity to monitor in a non-invasive way various cellular functions in one experiment and the same cells.

Beside all advantages of such a system, the planned measurement of the beating rate was not possible. NRVCM did not attach on the chip surface despite of different coatings. The surface of the chips is glass-like and NRVCM were known not to attach on glass sildes.

For experimental settings, the flow of the medium had to be adjusted to be slow; therefore it took about one hour until the medium had reached the chip. Before and after each experiment the tubes had to be washed and disinfected which took about half an hour each. Thus, this system is not adequate for high throughput. However, with this technology three parameters over the complete time can be measured during the whole time on the same cells; several incubations, more cells and more time for doing the endpoint measurement were thereby circumvented. The use of antibiotics is mandatory since the system is half-open.

In the current evaluation of the Bionas method, the reference compounds CCCP and CB were applied in H9c2 cells. CCCP is a known uncoupler of the respiratory chain by disturbing the mitochondrial proton gradient [Heytler 1963]. Cytochalasin B is a fungal metabolite which inhibits monosaccharide transport [Rampal *et al.* 1980]. Many cytochalasins are known to inhibit actin polymerisation, causing inhibition of cell division leading and induction of apoptosis [Cooper 1987; Haidle *et al.* 2004].

Both compounds reduced the impedance in the time period of 24 h, suggesting a reduction of attached cells. While there was no reversibility observed with CCCP after the 6 h recovery period, the CB treatment showed significant recovery. Considering the molecular mechanism of action, CB is affecting actin polymerisation, which did not lead to complete detachment of the cells. By interfering with the cellular cytoskeleton, CB could lead to slight surface

changes which could be measured by decreased impedance. This would explain the reversible effect which is also described in the literature [Yahara *et al.* 1982]. The effect of CCCP was also supposed to be reversible [Legros *et al.* 2002]. However, the concentration used in the current experiments most probably was too high. The reduction of the impedance may have also been induced by rounding up the cells which was also reported previously [Schliwa 1982; Yahara *et al.* 1982]. It is very likely that the reversibility is impossible if a certain threshold concentration is exceeded.

The effects induced by CB in terms of acidification and oxygen consumption were according to the expectations, since CB inhibits glucose cellular uptake. This causes a general reduction of the cellular energy metabolism by affecting the basic glycolytic rates which was accompanied by decreased oxygen consumption.

The effects of CCCP on acidification and oxygen consumption are also known effects. CCCP equilibrates the proton gradient and decreases the internal pH by transporting the protons back into the matrix so that electron transfer proceeds without generating ATP. This leads to a Ca^{2+} efflux from mitochondria and subsequent inhibition of NADH dehydrogenase inhibition. As a result, NADH levels are decreased and cause the inhibition of the respiratory chain. After prolonged incubation with CCCP, the activation of the respiratory chain was strongly inhibited as described in the literature and to a similar degree. Lower concentrations of CCP (e.g., 1 µM) elevated the respiratory activation without a subsequent inhibition. [Gabai 1993] The observed elevation of acidification, which was observed with CCCP exposure, results directly from the inhibition of the respiratory chain. The ATP production has to switch from oxidative phosphorylation to the catabolism of glucose. The increased breakdown of glucose emerges metabolites such as lactic acid which subsequently acidify the medium [Sole *et al.* 2000].

The continuous decrease over time might be the result of decreased cell numbers on the chips, due to cytotoxicity. In the literature a maximum increase of cellular oxygen consumption was found at 6-8 µM CCCP, to a two-fold extend, like it was found in this study. Higher concentrations are reported to decrease the cell viability and the oxygen consumption significantly [Wittenberg *et al.* 1985; Shen *et al.* 2003; Petit *et al.* 2005]. It is interesting to note that cells when incubated with CCCP had about 25 % recovery in terms of oxygen consumption.

Adding up the results of the reference compounds used, the Bionas system seems to be sensitive to evaluate the effects in all targeted parameters. The results from imatinib experiments confirm in principle the effects obtained for the

cytotoxic endpoint measurements under static conditions. Equally to the endpoint measurements, imatinib's toxic concentrations were found at concentrations starting from 30 and 50 µM. Additional information given by the Bionas experiments was that the onset of toxicity occurred 2 and 4 h after perfusion. Although there were statistically significant differences observed in the acidification rates after imatinib treatment in comparison to the control, the biological relevance of these effects is questionable. Considering the effects of the reference compounds, the effects induced by imatinib appear negligible and not relevant. This is supported indirectly by the literature: The effect of imatinib on Bcr-Abl positive cells, to decrease the glucose uptake (to 65 – 77%) from the media at relevant therapeutic concentrations (0.1 – 1.0 mol/L), was not found in Bcr-Abl negative cells [Gottschalk *et al.* 2004]. In addition, the main metabolism in cardiomyocytes was found to be β-oxidation of fatty acids [Stanley, 1997 941 /id] (~60-90%), only 10-40 % derive from the oxidation of pyruvate (emerged approximately half from glycolysis and half from lactate oxidation) [Stanley *et al.* 2005]. Therefore no changes in glycolysis may be expected.

The decreases of oxygen consumption observed after imatinib treatment might be directly the result of reduced cell numbers on the chips.

It has been suggested very recently in the literature that mitochondrial toxicity is not a primary event in imatinib's cytotoxic pathway. In these studies, imatinib inhibited the oxidative phosphorylation complexes at concentrations well above clinical c_{max} values (> 190, 300 µM) and no mitochondrial swelling was observed [Will *et al.* 2008]. These concentrations are much higher than the concentrations found to induce cytotoxicity and apoptosis in the Kerkelä report.

Summarising the results of the current investigations with imatinib and the data in the literature, it can be suggested that imatinib's toxicity is not reversible; in addition, it has neither specific effects on mitochondrial functions, nor on oxygen consumption, nor on acidification rates. The observed decreased impedance is very likely the result of unspecific cytotoxicity. This would also explain the lack of reversibility of imatinib-induced effects in any investigated parameter.

5.5 Evaluation of Imatinib-Induced Reactive Oxygen Species Formation in NRVCM

5.5.1 Background

C-Abl is involved during oxidative stress in both pro-oxidative as well as in anti-oxidative cellular events [Kumar *et al.* 2001; Mann 2006]

Imatinib-mediated ROS formation under the current experimental conditions in NRVCM is not known and has not been investigated yet. Therefore, ROS formation in response to imatinib treatment was determined directly and by co-incubation with antioxidants to evaluate potential cytoprotective effects.

5.5.2 Results

5.5.2.1 Formation of Reactive Oxygen Species by Direct Measurement in NRVCM

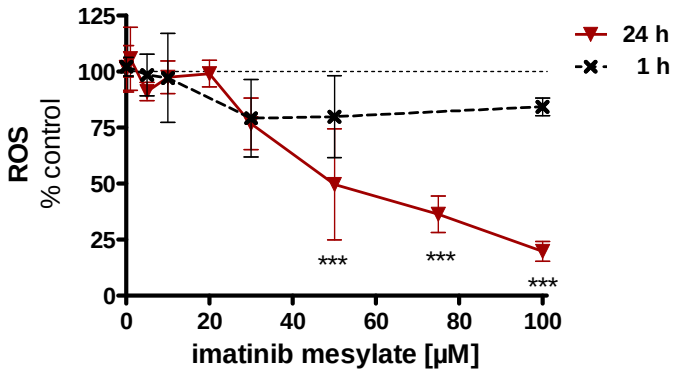

Figure 32 ROS generation in imatinib treated NRVCM. DCF assay. Each data point represents the mean ± SD of 3 independent experiments. Level of significance: *** P < 0.0001.

2'-7'-Dichlorofluorescin diacetate (H_2DCFDA) becomes cleaved and trapped in the cells. In the presence of ROS, the fluorescent DCF (2′,7′-dichlorofluorescein) is formed. H_2DCFDA and different concentrations of imatinib were co-incubated with NRVCM for 1 and 24 h. The fluorescence signal observed at the end of the incubation is proportional to the amount of ROS formed.

The results are depicted in Figure 32. After one hour of incubation imatinib decreased the intensity of fluorescence only slightly compared with the control at the highest concentration. After 24 h of incubation this effect became more profound. The fluorescence intensity decreased with increased imatinib concentrations starting to become statistically significant at concentrations above 50 µM.

5.5.2.2 Effect of Antioxidants on imatinib-induced toxicity in NRVCM

The toxicity of 50 µM imatinib was evaluated after 24 h in the presence of various antioxidants, possessing different ways of action (reducing agent dithiothreitol (DTT), glutathione antioxidant precursor N-acetylcysteine (NAC), antioxidant TPGS (d-α-tocopheryl polyethylene glycol 1000 succinate) d the spin trap reagent α-phenyl-tert-butyl nitrone (PBN)). Prior to co-incubation, NRVCM were incubated for 4.5 h with antioxidants. Each concentration tested was incubated alone and in co-incubation with imatinib; ATP content, MTS reduction and caspase 3/7 activity were investigated. In all experiments significant changes were induced by 50 µM imatinib as reported in the previous chapters.

The results found after 50 µM imatinib treatment are comparable to those found in the cytotoxicity assays. The results are shown as floating bars including the mean and the standard deviation. Figure 33 summarises the investigations with the strong reducing agent **dithiothreitol** (DTT) at concentrations ranging from 16 µM to 4 mM.

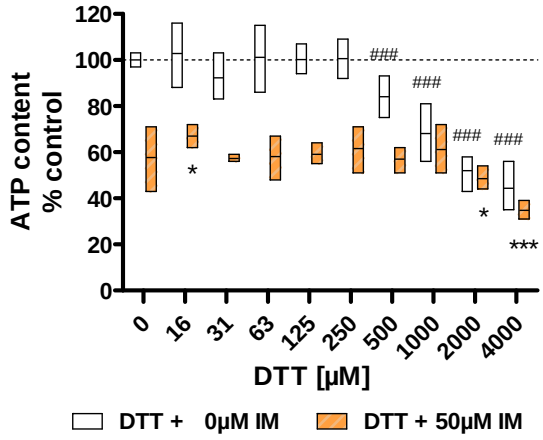

A

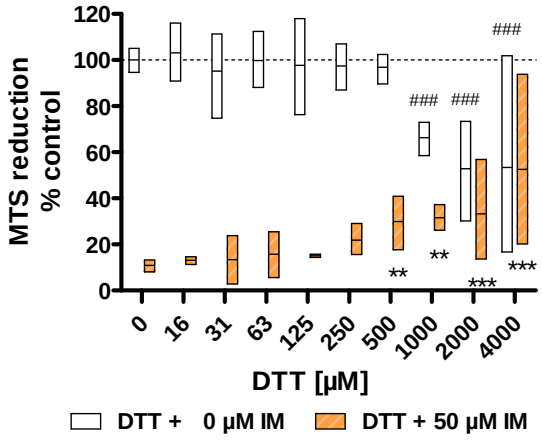

B

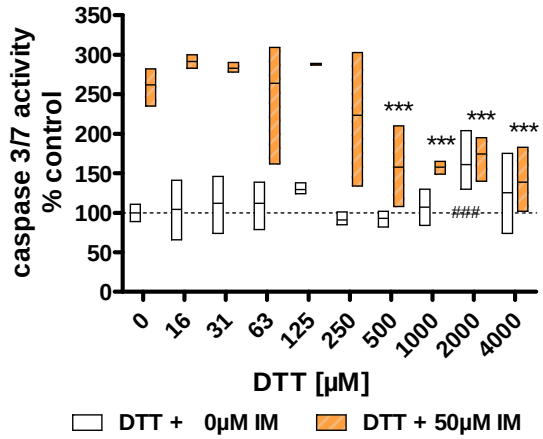

C

Figure 33 Modulation of imatinib induced toxicity 24 h after treatment by different concentrations of the reactive oxygen scavenger DTT. NRVCM incubated with DTT are displayed as floating bars the line indicating the mean. DTT co-incubated is shown as bars. **A.** ATP content. **B.** MTS reduction. **C.** Caspase 3/7 activity. All data are normalised to 100 %, represented by compound-free incubation. Mean ± SD of 4 independent experiments in duplicates. Significance levels, # for DTT, * for co-incubation: ** P < 0.001, *** P < 0.0001.

DTT itself caused decreases the cellular ATP levels. At concentrations above 500 µM (Figure 33 A) DTT decreased the ATP content statistically significantly. DTT had no effect of imatinib-induced ATP depletion up to concentrations of 1000 µM. Concentrations above 1000 µM DTT co-incubated with imatinib caused decreased ATP levels comparable to those found with DTT alone.

The capability of DTT to decrease MTS reduction (Figure 33 B) was significantly affected at concentrations starting from 1 mM. Imatinib caused about 90 % decrease of MTS-reduction. DTT increased the imatinib-induced changes in the MTS reduction capability. At concentrations above 500 µM, DTT was effective in amelioration of the imatinib-induced changes in the MTS reduction capability.

Similar results were found in the caspase 3/7 assay (Figure 33 C). DTT had no effect on caspase 3/7 activation except for 2000 µM. Concentrations above 2000 µM DTT caused significant increases of the caspase 3/7 activity; co-incubation with imatinib showed decreased activities at concentrations higher than 500 µM DTT.

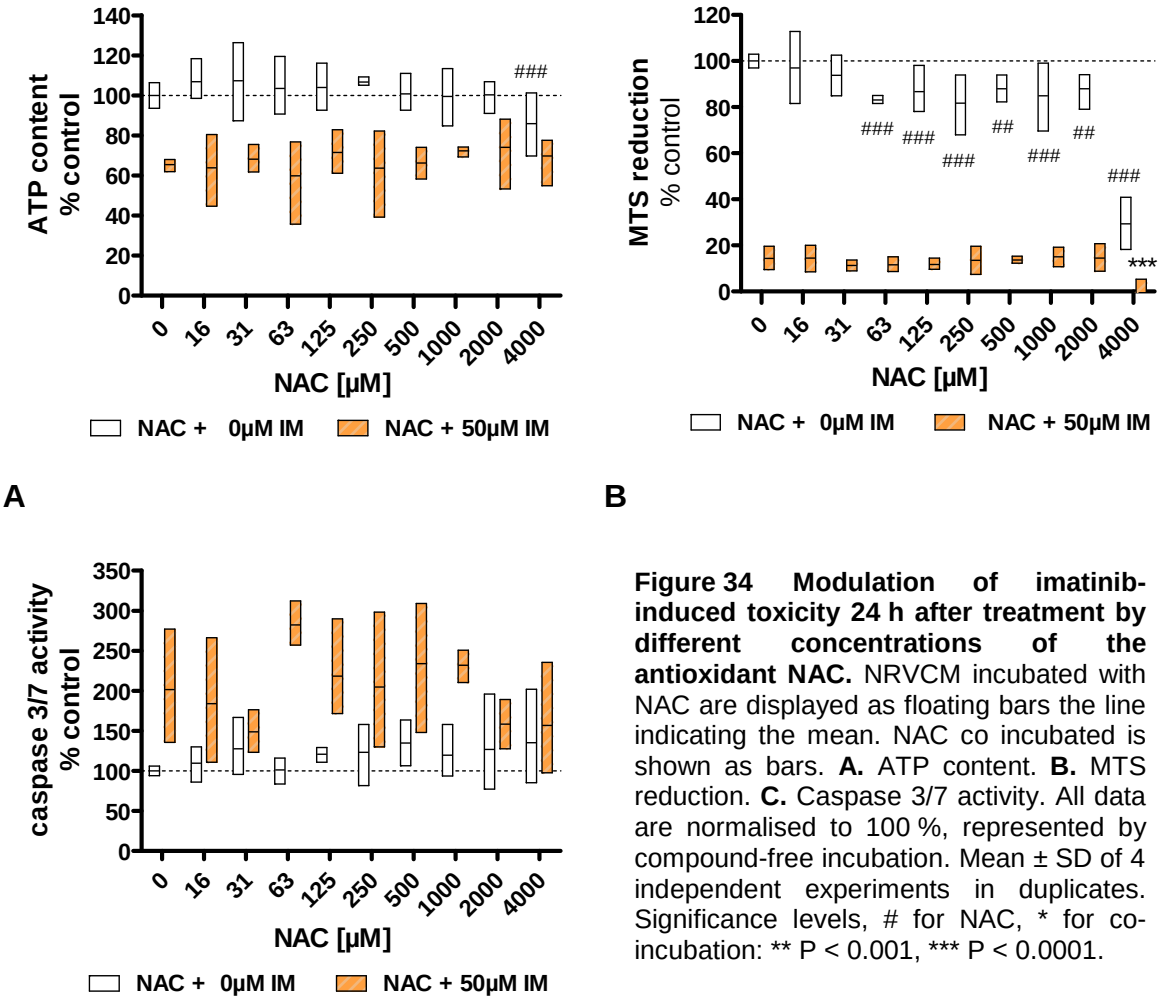

Figure 34 Modulation of imatinib-induced toxicity 24 h after treatment by different concentrations of the antioxidant NAC. NRVCM incubated with NAC are displayed as floating bars the line indicating the mean. NAC co incubated is shown as bars. **A.** ATP content. **B.** MTS reduction. **C.** Caspase 3/7 activity. All data are normalised to 100 %, represented by compound-free incubation. Mean ± SD of 4 independent experiments in duplicates. Significance levels, # for NAC, * for co-incubation: ** P < 0.001, *** P < 0.0001.

The effect of **N-acetyl cysteine** (NAC) in NRVCM incubated with imatinib is shown in Figure 34. In the ATP assay (Figure 34 A), the highest concentration (4 mM NAC) lead to significant decrease of ATP; co-incubation of NAC with imatinib revealed no changes in the ATP content.

NAC induced significant decreases of the MTS reduction potential (Figure 34 B) at concentrations starting from 63 µM. Co-incubation with imatinib caused a significant decrease of the reduction potential at 4 mM of NAC.

NAC had neither an effect on the caspase 3/7 activity assay (Figure 34 C) nor did it change the imatinib-induced increased activities.

A derivative of the extremely effective antioxidant α-tocopherol is **D-α-tocopheryl polyethylene glycol 1000 succinate** (TPGS). It is cleaved within the cell by esterases into its active radical scavenging form, α–tocopherol. It was used at concentrations ranging from 6 µM to 1.5 mM. The data obtained after incubation with imatinib are displayed in Figure 35.

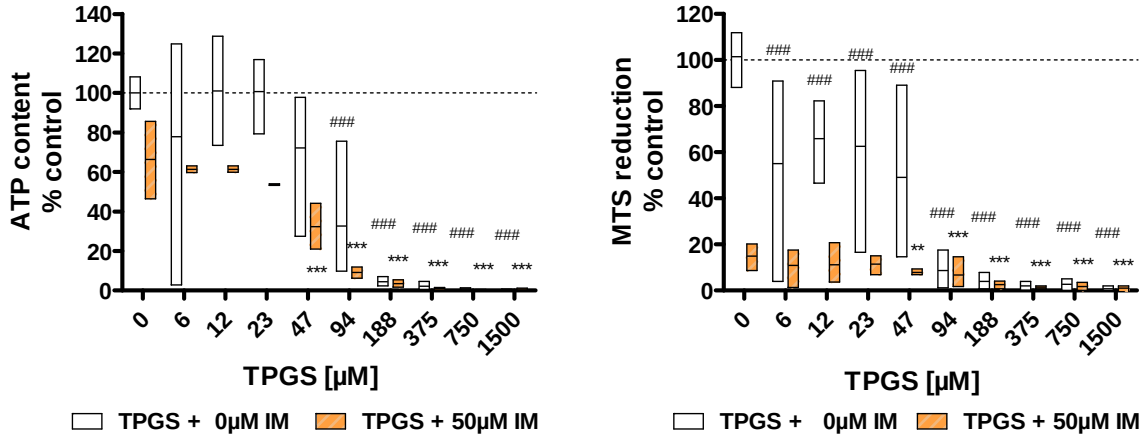

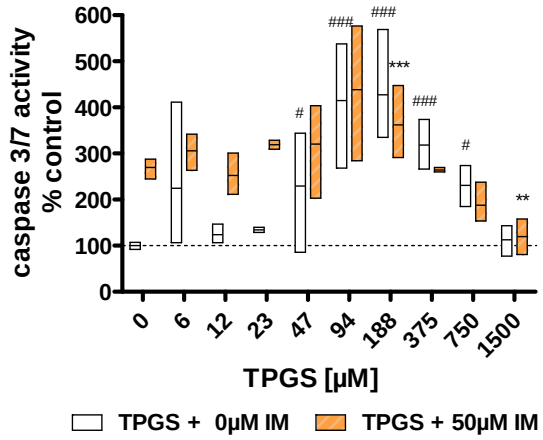

Figure 35 Modulation of imatinib induced toxicity 24 h after treatment by different concentrations of the tocopherol derivative TPGS. NRVCM incubated with TPGS are displayed as floating bars the line indicating the mean. TPGS co incubated is shown as bars. **A.** ATP content. **B.** MTS reduction. **C.** Caspase 3/7 activity. All data are normalised to 100 %, represented by compound-free incubation. Mean ± SD of 4 independent experiments in duplicates. Significance levels, # for DTT, * for co-incubation: * P < 0.05, ** P < 0.001, *** P < 0.0001.

TPGS showed a significant dose-dependent decline in the ATP content at concentrations starting from 94 µM (Figure 35 A). The ATP depletion was further decreased at cytotoxic TPGS concentrations above 47 µM.

In the MTS assay all concentrations of TPGS induced significant decreases of the MTS reduction capability. Similar to the results found in the ATP assay, TPGS was decreasing MTS reduction capability dependent on the concentration (Figure 35 B).

Similar to the other assays, the caspase 3/7 activity was increased at concentrations starting from 47 µM TPGS (Figure 35 C). The maximum effect was observed at 188 µM TPGS, higher concentrations of TPGS resulted in

decreased caspase 3/7 activity. The effect of TPGS co-incubated with imatinib was paralleled at concentrations above 47 µM.

The effect of the spin trap reagent, **α-phenyl-tert-butyl nitrone** (PBN) was also investigated and the results are shown in Figure 36.

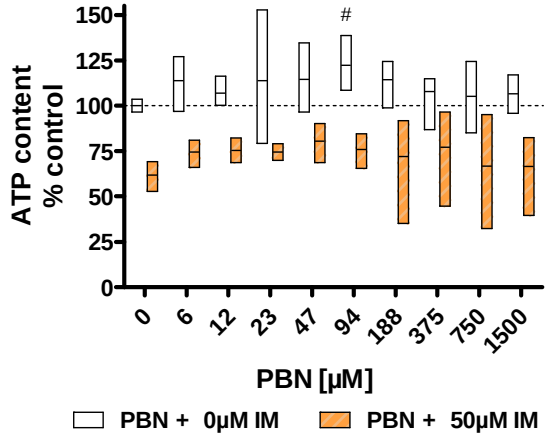

A

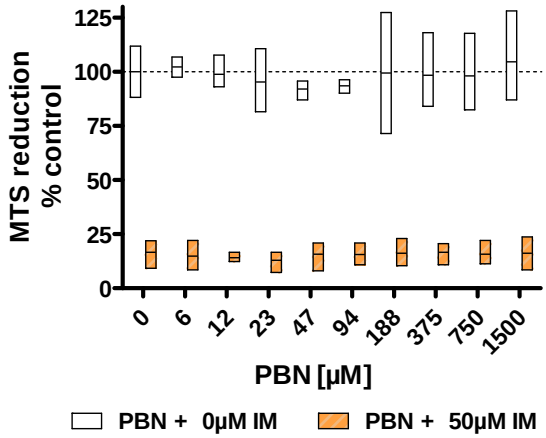

B

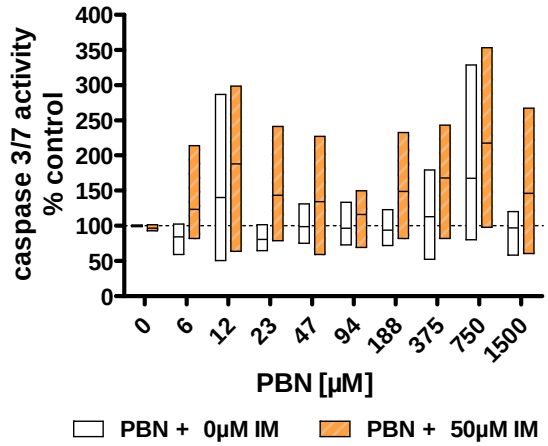

C

Figure 36 Modulation of imatinib induced toxicity 24 h after treatment by different concentrations of the RNS scavenging PBN. NRVCM incubated with PBN are displayed as floating bars the line indicating the mean. PBN co incubated is shown as bars. **A.** ATP content. **B.** MTS reduction. **C.** Caspase 3/7 activity. All data are normalised to 100 %, represented by compound-free incubation. Mean ± SD of 4 independent experiments in duplicates. Significance level # $P < 0.05$.

PBN had no effect on imatinib-induced changes, in none of the assays investigated (see Figure 36).

5.5.3 Discussion

Oxidative reactions are important events in the initiation and progression of cardiac disease either by injurious levels of reactive oxygen species (ROS) emerged from reperfusion and inflammation or by ROS as mediators of signal transduction. Hypertrophy, apoptosis and contractile failure are induced by stress predisposing directly or indirectly cardiac failure [Bolli 1988; Aikawa *et al.* 1997; Griendling *et al.* 2000; Aikawa *et al.* 2001]. The cell counterbalances these events but if these are impaired, the susceptibility to environmental stress

and leads to cardiomyocytes dysfunction and heart failure is enhanced [Hirota *et al.* 1999; Fujio *et al.* 2000]. The heart bears considerably less protective mechanisms (glutathione, superoxide dismutase or catalase) than other metabolic organs like liver or kidney [Sarvazyan 1996].
C-Abl also plays an important role in the oxidative stress. According to Mann [Mann 2006], the translocation of c-Abl from the cytosol to mitochondria is mediated by ROS. In mitochondria, c-Abl interacts with catalase to finally degrade the ROS. By this mechanism, c-Abl activates catalase and thereby stabilises the mitochondrial function. During excessive oxidative stress, c-Abl dissociates and thus inactivates mitochondrial catalase, causing mitochondrial collapse, increased ROS levels and triggers ER stress.
Activation of c-Abl in response to oxidative stress was described in human leukaemia cells to cause apoptosis [Kumar *et al.* 2001].

Investigations with the strong reducing agent DTT showed an apparent protective effect against the imatinib-induced toxicity, as measured by MTS reduction capability and caspase 3/7 activity at concentrations up to 500 µM DTT. However, in the ATP assay this concentration of DTT indicated that the effective DTT concentration caused a significantly decreased ATP level which is correlated to cytotoxicity. A decrease of cell number could therefore mimic an apparent protection by DTT.

NAC is known to stimulate GSH synthesis, to enhance glutathione-S-transferase activity, to promote detoxification and to act directly on oxidant radicals [De Vries *et al.* 1993]. In cell based assays, the uptake of cysteine from the medium is promoted by NAC [Issels *et al.* 1988]. In the current experiments NAC did not show any protective effects against the imatinib cytotoxicity as measured by different parameters in NRVCM.

Other well-known non-enzymatic antioxidants include vitamins E (tocopherols) [McCall *et al.* 1999]; α-tocopherol is extremely effective. Its antioxidant activity, however, is very low if added to cellular systems into the cell culture medium. Therefore, a more hydrophilic derivate is the choice for cell-based assays: TPGS is the D-α-tocopheryl polyethylene glycol 1000 succinate. This derivative of vitamin E is highly stable compared to naturally occurring vitamin Es. It has amphiphilic attitudes with a hydrophilic polar head group (tocopheryol succinate) as well as a lipophilic alkyl tail (polyethylene glycol) [Eastman 2005]. Its antioxidative properties are exerted within the cell where the intact molecule is hydrolysed [Traber *et al.* 1988; Youk *et al.* 2005].
The uptake of TPGS into the cell is time-dependent, three hours after incubation of TPGS, 50 % of the total amount is transformed into α-tocopherol. The

efficacy of TPGS as an antioxidant is considered to be due to a gradual release of α-tocopherol by esterase activity [Carini *et al.* 1990].
NRVCM revealed to be sensitive to TPGS. TPGS is often used as an enhancer of absorption and bioavailability of certain drugs [Sokol *et al.* 1991; Bittner *et al.* 2002; Mu *et al.* 2003]. In addition, TPGS activates the bioavailability of some compounds by inhibiting the multidrug transporter permeability-glycoprotein (P-gp). P-gp is located in the membrane and functions as an ATP-dependent drug efflux pump. This protein reduces the cytotoxicity by lowering the intracellular concentration of the drug [Gottesman *et al.* 1988; Gottesman 1993; Dintaman *et al.* 1999]. In human tumours this protein has been shown to be over-expressed resulting in drug resistance and failure of chemotherapy [Gottesman 1993; Druker *et al.* 2001; Bogman *et al.* 2005]. The IC_{50} of P-gp inhibition by TPGS was determined with 3.6 µM (0.0006 % w/v) [Bogman *et al.* 2003].
All concentrations of TPGS used in the present study were above the IC_{50} of the P-gp inhibition. Therefore, the concentrations chosen were overlapping with antioxidant effects. The increasing toxicity with imatinib is most probably caused by the inhibition of P-gp by TPGS. Imatinib is suggested to be a substrate for P-gp and to inhibit it with a IC_{50} of 18.3 µM [Hamada *et al.* 2003]. Another drug transporter, ABCG2, is inhibited by imatinib but imatinib is not a substrate of ABCG2 [Jordanides *et al.* 2006]. According to these findings and the increase/start in toxicity above 20 µM it may be concluded that the toxicity was caused due to the increased inhibition of P-gp causing an accumulation of imatinib in the cells.

Spin trapping nitrones such as α-phenyl-*N-tert*-butylnitrone (PBN) have been traditionally used to trap and stabilize free radicals for detection by electron paramagnetic resonance (EPR) spectroscopy. Same as classical antioxidants their therapeutical effect has been demonstrated in free radical mediated diseases. Therapeutic interventions with PBN have been demonstrated to decrease free reactive oxygen species (ROS) as well as reactive nitrogen species (RNS). In rat heart models PBN was found to have protective effects in myocardial impairment. [Paracchini *et al.* 1993] De Atley and colleagues have used 100 µM PBN successfully for investigations in cardiomyocytes during 24 h of incubation, which is in the range of the concentrations tested in the current investigations and found some reasonable protective effects [DeAtley *et al.* 1999].
With PBN no significant modulation of the imatinib-induced toxicity was observed. These results suggest that neither ROS nor reactive nitrogen species play a role in imatinib-induced toxicity in NRVCM.

Determining ROS directly and indirectly via antioxidants acting with different mechanisms has led to the same results. These results confirmed the results by Lasfer and colleagues [Lasfer *et al.* 2006] who did not observe imatinib-induced ROS formation. As CHOP was reported to increase the production of ROS [McCullough *et al.* 2001] and CHOP protein levels were not found to be increased after imatinib treatment in the present study, the involvement of ROS may be excluded in imatinib-induced toxicity.

Imatinib did not have direct effects on ROS formation. This was shown by direct measurement of ROS as shown by the fluorescence label DCF. By means of various antioxidants with distinct mechanisms of action, the imatinib–induced effects on the cellular endpoints, ATP levels, MTS reduction capability and caspase 3/7 activity were evaluated. There was no effect found by none of the investigated antioxidants, in comparison to the effects induced by imatinib alone.

5.6 Gene Silencing of c-Abl by RNAi

5.6.1 Background

The results of Kerkelä and co-workers with NRVCM suggest that imatinib triggered apoptosis by a mechanism of ER stress and collapsed mitochondrial membrane potential, mediated by c-Abl. One of the key experiments performed by Kerkelä and co-workers was the specific gene transfer of c-Abl by means of retroviral gene transfer of an imatinib-resistant mutant c-Abl into NRVCM. It appeared that the mutant c-Abl form rescued NRVCM from imatinib-induced cell death. Since the low proliferation of cardiomyocytes would preclude efficient retroviral-mediated gene transfection of c-Abl into NRVCM, the proliferation rate of NRVCM used in this study was determined. The results suggest that NRVCM proliferation rates (7 % during 24 h) were too low to achieve the >90 % efficiency of retroviral-mediated gene transfer reported by Kerkelä and co-workers.

In this study instead of retroviral gene transfer the specific siRNA approach was used to knock-down the c-Abl gene and protein. Cytotoxicity was evaluated under both c-Abl-silenced and unsilenced conditions.

5.6.1.1 RNA interference

Much of the knowledge about protein functions was gained by specific gene silencing. In 1998 Fire and Mello pointed the term RNA interference (RNAi) after having discovered that injection of double stranded (dsRNA) into the nematode *Caenorhabditis elegans* led to specific silencing of genes which were homologous to the sequence of the injected dsRNA [Elbashir *et al.* 2001]. RNAi is a form of post transcriptional gene silencing in which the mRNA is degraded by complementary dsRNA in tandem with protein complexes. The principle itself is ancient as it is a vital part of the immune response to foreign genetic material from viruses in plants, worms, flies or vertebrates [Putral *et al.* 2006]. This break through of Fire and Mello led to a lot of investigations in many other organisms.

In 2001 Elbashir and colleagues discovered the success for application of siRNA (short interfering RNA, see Figure 37) in mammalian cells [Elbashir *et al.* 2001]. SiRNA directed gene silencing helps to understand and determine the function of specific genes that are expressed in a cell-type or specific

Figure 37 Structure of siRNA. SiRNAs consist of 19-27 nts with characteristic 2-nt unpaired overhangs, 5'-phosphate and 3'-hydroxyl groups.

pathway of interest [Dykxhoorn *et al.* 2003]. Besides the use as a mechanistic tool, there is also potential to use siRNA for therapy for instance in infectious diseases, genetic disorders and cancer [Putral *et al.* 2006].

5.6.1.2 Mechanism of siRNA

The RNAi mechanism (illustrated in Figure 38) is restricted to the cytoplasm in mammals [Hutvagner *et al.* 2002; Zeng *et al.* 2002; Kawasaki *et al.* 2003]. Long dsRNA is cleaved by the highly conserved Dicer family of RNase III enzymes into small interfering RNAs (also known as short interfering RNA: *siRNA*) [Bernstein *et al.* 2001; Billy *et al.* 2001; Ketting *et al.* 2001].

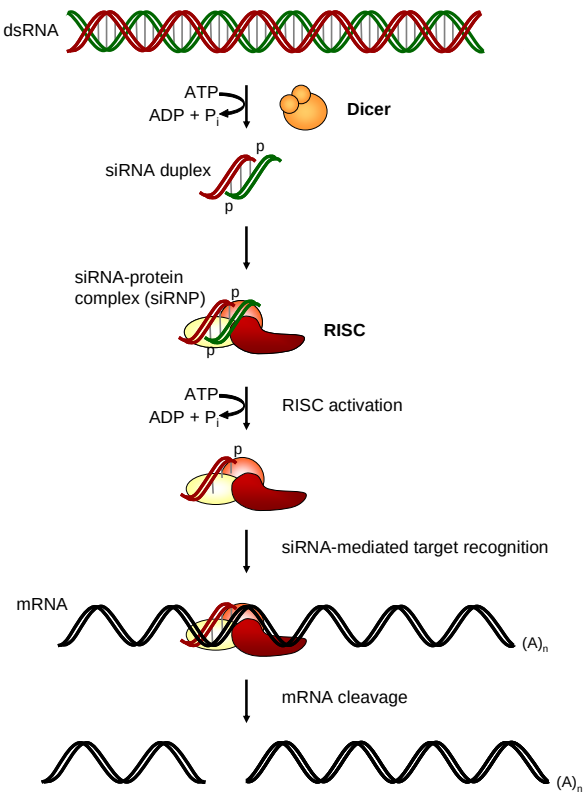

Figure 38 siRNA-mediated post-transcriptional gene silencing mechanism. The siRNA pathway to RNA interference. The RNAse-III-like enzyme Dicer processes long dsRNA into siRNAs which are then unwound and separated in the siRNP (siRNA-protein complex). Thus, a single strand is incorporated into the RNA-induced silencing complex (RISC) and guided to a complementary sequence of an available mRNA. The target mRNA will then be cut at the centre of the newly formed duplex between target RNA and the small antisense RNA. (adapted from [Dykxhoorn *et al.* 2003])

21-23-nt dsRNA duplexes with symmetric 2-3-nt 3' overhangs and 5'-phosphate and 3'-hydroxyl groups are the characteristics of *siRNA* (Figure 37). It represents an RNase-III-like enzymatic cleavage pattern and is therefore a substrate for the highly conserved Dicer family of RNase III enzymes mediating dsRNA cleavage [Paddison *et al.* 2002; Dykxhoorn *et al.* 2003].

If siRNA is not phosphorylated at the 5' end, an endogenous kinase [Schwarz *et al.* 2002] rapidly phosphorylates it in order to get the siRNA entered into a multiprotein RNA-inducing silencing complex (RISC) [Paddison *et al.* 2002].. RISC is a catalytic complex responsible for RNA cleavage [Hutvagner *et al.* 2002; Schwarz *et al.* 2003] to which Dicer is associated without participating in its catalytic activity. Both strands can be included in RISC and both can

successfully induce RNAi [Martinez *et al.* 2002]. However, other studies showed that the tightly bound strand to the 5' end is degraded while the other strand is incorporated in RISC leading to RNAi [Schwarz *et al.* 2003]. The strand binds to its homologous target mRNA for endonucleolytic cleavage by the antisense strand. The cleavage occurs at a single site in the centre of the duplex region of the target mRNA and the guide siRNA, 10 nt from the 5' end of the siRNA [Elbashir *et al.* 2001]. The cutting of the mRNA is often referred to as slicer function probably executed by a member of the argonaute protein family that is likely to act as an endonuclease [Bernstein *et al.* 2001]. The RNAi pathway works well in mammals but up to now no naturally occurring siRNAs have been found in mammals yet [Dykxhoorn *et al.* 2003].

5.6.1.3 Potential Issues of siRNA as a Mechanistic Tool

The cell has developed a defence system to recognise and eliminate foreign DNA and RNA, which can initiate the induction of interferons and inflammatory cytokines [Sioud 2005]. Dependent of the design of the siRNA, the response varies.

After application of dsRNA longer than 30nt a non-sequence-specific interferon response is triggered [Elbashir *et al.* 2001]. Interferon leads to degradation of mRNA via indirect activation of RNase L. Additionally, the protein kinase PERK is activated. This phosphorylates the translation initiation factor eIF2α which then inhibits mRNA translation. By means of chemically synthesised siRNAs the unspecific interferon and cytokine response can be circumvented [Elbashir *et al.* 2001].

Immune responses are activated by pathogen components [Kawai *et al.* 2006]. There are two types of microbial nucleic acid sensors. Transmembrane toll-like receptors (TRLs), which are located in the plasma membrane as well as in endosomes, are one of them. The others are represented by cytoplasmic pattern-recognition receptors, protein kinase (PKR) and retinoic acid-inducible gene 1 (RIG1) being the main proteins. RIG1 contains a helicase domain which recognises dsRNA and activates its two caspase recruitment domains. It triggers by downstream signalling interferon and inflammatory cytokine production [Yoneyama *et al.* 2004]. Interferon responses induced by siRNAs are believed to be sequence specific effects initiated in endosomes rather than in the cytoplasm [Sioud 2005]. However, it was shown that the cytoplasmic sensing of siRNAs is more dependent on the end structure than on the sequence [Marques *et al.* 2006]. If siRNAs bear immunostimulatory motifs, RL7 and TRL8 are activated by gene expression of NF-κB, IRF-3 and IRF-7 transcription factors. In addition, TRLs also use siRNA modifications to

discriminate between self and non-self siRNA. In the cytoplasm TRL7 and TRL8 are not present and siRNA therefore cannot be recognised. This mechanism was developed during evolution to protect against self destruction of body own RNA.
Especially lipid-delivered siRNAs bear the risk of triggering the interferon response. Lipid-delivered siRNAs are packed in TRL7 and TRL8 bearing endosomes triggering the immune response. In contrast to the lipid-delivered siRNAs, electroporation is very likely not leading to unspecific interferon response, since the delivered siRNA directly enters into the cytoplasm [Sioud 2005]. This is explained by the fact that these siRNAs do not need to be processed by Dicer [Robbins *et al.* 2006].

The applied siRNA concentration has to be regarded very critically concerning unspecific effects. A siRNA can affect non-specifically more than 1000 genes as well as its protein products being involved in various cellular functions. The critical threshold for siRNA in general is between 25 and 50 nM. While 50 nM siRNA is leading to modest unspecific gene expression, 25 nM are clearly less effective. These effects are transient throughout the course of siRNA treatment. [Persengiev *et al.* 2004]

5.6.1.4 Selection of siRNA

The selection of the most efficient siRNA was performed in the H9c2 cell line using electroporation for delivery and RT-PCR for monitoring the silencing efficiency for c-Abl. Screening is necessary since different siRNA sequences display widely varying efficacy [Holen *et al.* 2002; Scherer *et al.* 2003; Scherer *et al.* 2004]. Basically two different strategies for efficient silencing can be chosen, the separate testing and the testing of several candidates in a pool. In the first case, the siRNAs are tested separately and the most efficient one is chosen for further experiments. In the second case, a pool of *in vitro* transcribed siRNAs can be used, resulting in several siRNAs for gene silencing similar to Dicer cleavage which yields several different siRNA [Zhang *et al.* 2002]. However, this cost effective and efficient method bears some problems: the PERK is activated by any residual dsRNA that results in unspecific translational inhibition via the phosphorylation of eIF2α [Williams 1999] and the off-target effect risk is increased with a pool of siRNA [Jackson *et al.* 2003]. The competition of siRNAs in a pool may also decrease the efficacy compared to one selected siRNA. With one siRNA the possibility is given to verify the observed phenotype by the means of another siRNA targeting the same gene [Amarzguioui *et al.* 2005].

H9c2 cells were used for the screening of 14 small interfering RNAs (siRNAs) for their silencing efficiency. The electroporation was conducted at 400 nM with the amaxa technology and cells were harvested 24 h after transfection. Real-time PCR was used as a sensitive and fast detection method. As a control a siRNA had to be chosen which has no target in the genome of the rat. This control is also called “mismatch” and in this study it was specific to the green fluorescent protein (GFP). Thereby the siRNA machinery is triggered but no gene silencing is possible. This control is always set to 100 % of the investigated transcript or protein. The effects found with siRNAs specific for this gene or protein are always normalised to that control.

In order to evaluate the function of a protein by silencing it, the time window with the most efficient silencing activity has to be found. Each cell type, each protein and each siRNA has its own kinetics which has to be evaluated before the experiments. Therefore, mRNA and protein levels were investigated at several time points after transfection. Since the experiments of Kerkelä and co-workers had to be repeated, the time of incubation (24 h) was given. Hence, NRVCM were analysed over a period of 72 h, with both siRNAs both concentrations selected.

5.6.2 Results

5.6.2.1 Selection of the siRNA

Out of the 14 siRNAs tested in H9c2 cells, the siRNAs with the highest silencing efficiency were identified. The screened siRNAs revealed c-Abl_4Q and c-Abl_10_S to be the most effective (Figure 39) in comparison with GFP.

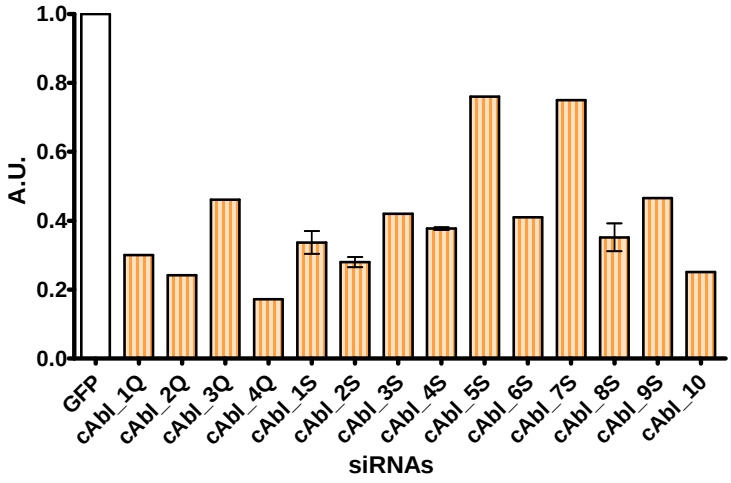

Figure 39 mRNA expression of c-Abl 24 h after nucleofection of several siRNA directed against different regions in the c-Abl gene in H9c2. Fold change of c-Abl after normalisation to 18S. Mean ± SD of mono- to duplicates.

Table 18 Silencing efficiencies of several siRNA oligos as determined by RT-PCR 24 h post nucleofection. The most efficient siRNAs are 10S and 4Q, both highlighted in red.

c-Abl oligo	1S	2S	3S	4S	5S	6S	7S	8S	9S	*10S*	1Q	2Q	3Q	*4Q*
silencing efficiency [%]	66	72	58	62	24	59	25	65	54	***75***	70	76	54	***83***

The silencing efficiencies of the tested siRNAs are listed in Table 18. In the screening most of the siRNAs tested decreased c-Abl transcripts to at least 50%. Two siRNA with silencing efficiencies of c-Abl of 83 and 75%, respectively, were selected for further experiments in NRVCM.

5.6.2.2 Transfection of NRVCM

The electroporation method used in H9c2 cells caused too much damage to the fragile NRVCM. Therefore the method of chemical transfection with lipofectamine 2000 was chosen and conducted with the most efficient working siRNAs found in H9c2 cells.

5.6.2.2.1 Optimisation of transfection in NRVCM

Transfection conditions of NRVCM were optimised using lipofectamine. Hence, several lipofectamine 2000 (subsequently referred to as lipo) concentrations with two different concentrations of siRNA were tested three days after plating.

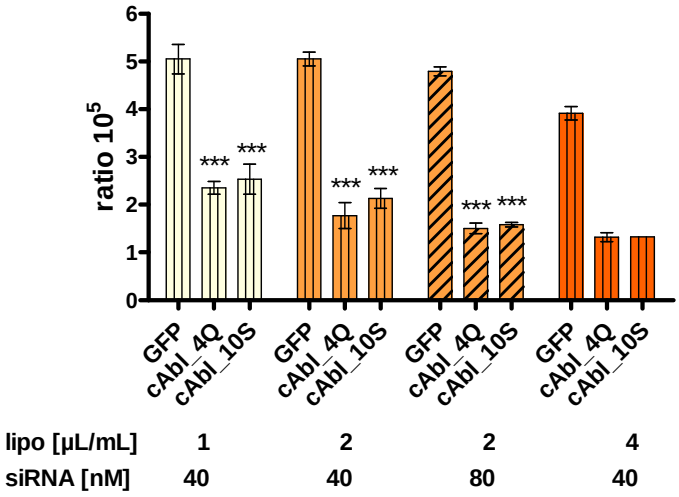

Figure 40 Optimisation of lipofection in NRVCM. Three different lipo concentrations are tested with 40 and 80 nM siRNA 24 h post transfection. Mean ± SD of quadruplicates. Significance level: *** P < 0.0001.

Table 19 Silencing efficiencies of lipofected NRVCM.

	1 µL/mL lipo	2 µL/mL lipo		4 µL/mL lipo
	40 nM siRNA	*40 nM siRNA*	*80 nM siRNA*	*40 nM siRNA*
c-Abl_4Q	53%	65%	69%	66%
c-Abl_10S	50%	58%	67%	66%

Figure 40 displays the c-Abl mRNA level in NRVCM after incubation of different lipo/siRNA-cocktails according to the range of the manufacturer's recommendations. With this experiment the most efficient silencing cocktail with the tested siRNA was selected without impairing the viability of the cells. The amount of c-Abl for each condition tested was down-regulated to at least 50 % (Table 19).

1 µL/mL lipo had the lowest efficacy while higher lipo and siRNA concentrations of lipo led to better efficacy in silencing. However, with the highest lipo concentration of 4 µL the GFP-control was decreased indicating loss of cells,

maybe due to lipo-induced toxicity. The c-Abl gene expressions in GFP-transfected NRVCM indicated that the amount of c-Abl mRNA decreased with increased lipo- as well as siRNA concentrations. Therefore, 1 µL/mL and 2 µL/mL lipo with 40 nM siRNA reached the same level of c-Abl gene expression and were both considered as non-toxic. 2 µL/mL lipo with 80 nM siRNA further decreased the c-Abl mRNA amount only marginally. This effect was more prominent with 4 µL/mL lipo.
Therefore, the lipo cocktail was chosen with 2 µL/mL mixed with 40 and 80 nM, respectively.

5.6.2.3 Induction of Interferon Response

2', 5'-Oligoadenylate synthetase 1 (OAS1) and interferon-inducible double-stranded RNA activated protein kinase (Prkr or eIF2α) were investigated as they are reported to be increased when the interferon response is triggered (Figure 41). These proteins are expressed during viral infection and are involved in its elimination [Samuel 2001].

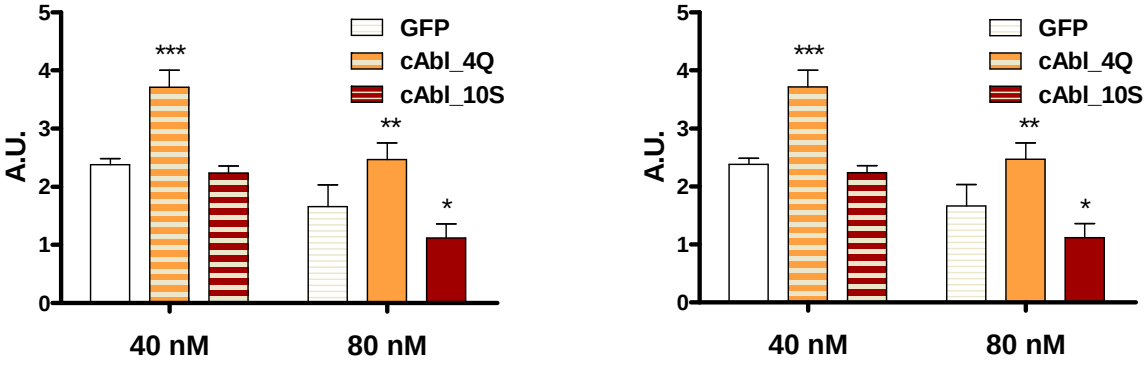

A **OAS1 mRNA** **B** **eIF2α mRNA**

Figure 41 Gene expression of IFN response markers in NRVCM 24 h after silencing. A. OAS1 mRNA after silencing with 40 nM and 80 nM siRNA. **B.** EIF2**α** after silencing with 40 nM and 80 nM siRNA. Results are normalised to the GFP amount of its concentration. Mean ± SD of triplicates. Significance levels: * P < 0.05, ** P < 0.001, *** P < 0.0001 compared to 0 µM IM, GFP.

In addition to non-specific effects, especially lipid-delivered siRNAs bear the risk of triggering the interferon response [Sioud 2005]. Therefore the selected siRNAs (c-Abl_4Q and c-Abl_10S) were tested on NRVCM with the optimised transfection method. Two genes were investigated that are reported to be increased when the interferon response is triggered (Figure 41). 2', 5'-Oligoadenylate synthetase 1 (OAS1) and interferon-inducible double-stranded RNA activated protein kinase (Prkr or eIF2α).
Interferon response-related genes were significantly increased after c-Abl_4Q siRNA at both concentrations as compared to the GFP-siRNA silenced. No

increases were found after transfection with 40 nM c-Abl_10S, whereas 80 nM of c-Abl_10S resulted in a significant decrease of the OAS1 transcript.

5.6.2.4 Silencing kinetics of the c-Abl transcripts in NRVCM

Both siRNAs assayed, c-Abl_4Q as well as c-Abl_10s at the concentrations of 40 nM, followed a similar time course of c-Abl gene expression: 16 h post transfection, c-Abl mRNA was decreased to about 75%. Between 24 h and 36 h c-Abl mRNA reached the lowest level of about 40%, with the tendency to increase to 60 % after 72 h (Figure 42 A, B).

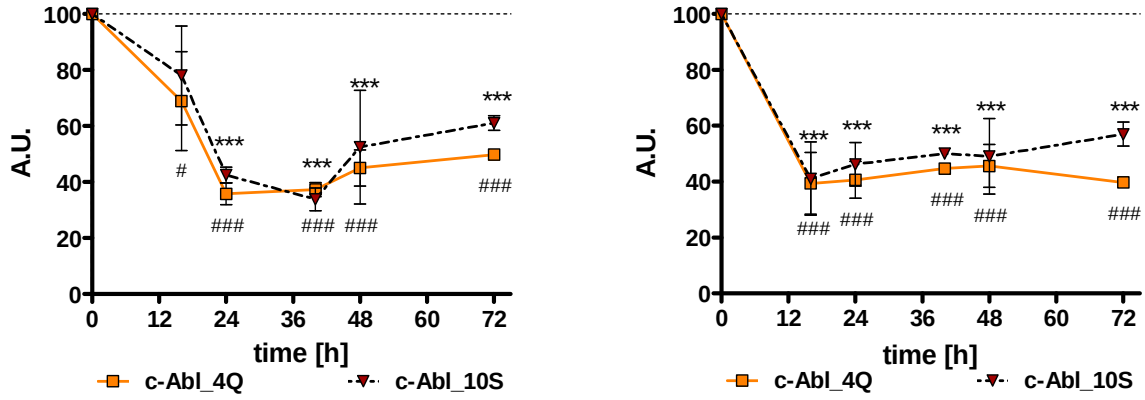

Figure 42 Gene expression of c-Abl after silencing in NRVCM. A. 40 nM siRNA in NRVCM. **B.** 80 nM siRNA in NRVCM. Each sample is normalised to 18S. Mean ± SD of 1-5 independent experiments in triplicates. Significance levels: * P < 0.05, ** P < 0.001, *** P < 0.0001; # c-Abl_4Q, * c-Abl_10S.

Table 20 Table of conducted experiments of gene silencing investigations in NRVCM.

n	16	24 h	40 h	48 h	72 h
40 nM	2	2	1	3	1
80nM	2	5	1	4	1

For both siRNAs the concentration of 80 nM was the most effective. Already 16 h post transfection the mRNA levels were decreased to about 40 %. Up to 72 h both curves slowly increased to 40 % and 60 %, respectively.

The results of this experiment demonstrated that both siRNAs are following the same kinetics over 72 h and showed very similar silencing efficacies. Silencing efficiencies of mRNA were found to be similar in both concentrations tested, with 80 nM causing an earlier and more stable response. After successful silencing the mRNA of the gene, the protein level had to be investigated.

5.6.2.5 Silencing kinetics of the of c-Abl protein in NRVCM

Depending on the specific function and the amount of the protein which is needed in a particular cell type, the translation time may vary in general between 24 and 48 h [McManus *et al.* 2002]. For the present studies the period of observation was extended up to 72 h post transfection, in order not to miss relevant changes of the protein levels.

The goal of the following experiments was to determine the time window where the selected siRNA oligos had the greatest silencing efficacy of the c-Abl protein. In Figure 42 the protein levels of c-Abl after silencing with two siRNAs are shown.

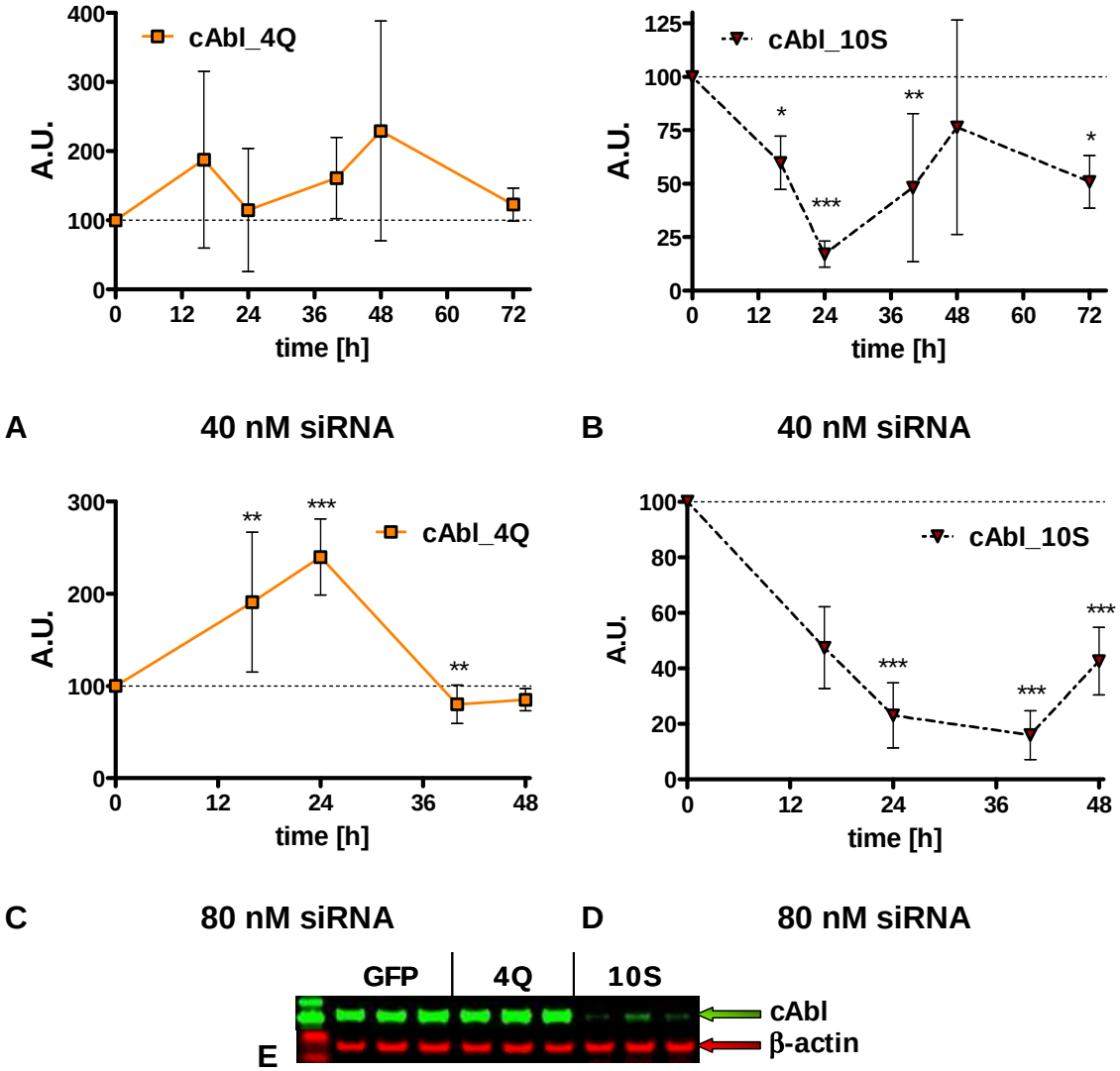

Figure 43 Protein expression of c-Abl after silencing c-Abl. A. 40 nM siRNA c-Abl_4Q. **B.** 40 nM siRNA c-Abl_10S. **C.** 80 nM siRNA c-Abl_4Q. **D.** 80 nM siRNA c-Abl_10S. E. Representative blot of silenced c-Abl protein. Significance levels: * $P < 0.05$, ** $P < 0.001$, *** $P < 0.0001$; # c-Abl_4Q.

Table 21 Silencing efficiencies of c-Abl mRNA and protein in NRVCM. All values given are % c-Abl gene expression and protein normalised to β-actin. n.t.: not tested

	c-Abl_4Q								c-Abl_10S							
	mRNA				protein				mRNA				protein			
[h]	**40nM**	n	**80nM**	n	**40nM**	n	**80nM**	n	**40nM**	n	**80nM**	n	**40nM**	n	**80nM**	n
16	69 ± 18	2	39 ± 11	2	188 ± 128	2	191 ± 76	3	78 ± 18	2	41 ± 13	2	60 ± 12	2	47 ± 15	3
24	*36 ± 4*	2	*41 ± 7*	5	115 ± 89	2	240 ± 41	4	42 ± 3	2	46 ± 8	5	*17 ± 6*	2	36 ± 21	4
40	*37 ± 3*	1	45 ± 1	1	161 ± 59	2	80 ± 21	2	*34 ± 4*	1	50 ± 1	1	48 ± 35	2	*16 ± 9*	-
48	45 ± 6	3	46 ± 8	4	229 ± 159	2	85 ± 12	3	52 ± 20	3	49 ± 14	4	76 ± 50	2	43 ± 12	2
72	50 ± 1	1	40 ± 1	1	123 ± 24	2	n.t.		61 ± 3	1	57 ± 4	1	51 ± 12	2	n.t.	3

Table 22 Achieved silencing efficiencies [%] of the used siRNAs in NRVCM at concentrations of 40 and 80 nM in mRNA and protein. The time frame is 24 h, starting at time = 0 h, 24 h and 48 h and the silencing efficiency was calculated by area under the curve (AUC).

	c-Abl_4Q				c-Abl_10S			
	mRNA		protein		mRNA		protein	
time frame	40 nM	80 nM	40 nM	80 nM	40 nM	80 nM	40 nM	80 nM
0-24	26	40	-47	-69	21	39	34	37
24-48	***62***	56	-57	-34	***60***	52	***58***	***73***
48-72	54	56	-81	n.t.	47	48	37	n.t.

Although both selected oligos had similar silencing efficiencies in terms of the c-Abl mRNA expression, significant differences were observed concerning protein expression. Instead of the expected c-Abl silencing, the c-Abl_4Q-siRNA increased its protein level at 40 and 80 nM siRNA concentrations and at all time points of investigation (Figure 43 A, C). The c-Abl_10S siRNA was more effective (Figure 43 B, D). At siRNA oligo concentrations of 40 nM, a statistically significant decrease of c-Abl proteins was observed during 24 h, with a maximum effect of about 80 %. The decrease of the c-Abl protein expression remained stable during 72 h with reaching a statistical significant decrease of about 50 % c-Abl protein at the end of the experiment. During 40 and 48 h the results exhibited huge deviations which are reflected by the high standard deviations. The variations in the experiments with 80 nM siRNA were lower compared to the experiments with 40 nM. Both experiments confirm nearly similar kinetics. In the experiment with 80 nM siRNA, the time window with the highest silencing efficacy of the c-Abl protein was between 24 and 48 h. This is the time window which was chosen for further evaluations of the IM cytotoxicity in combination with specific gene silencing. The silencing efficiencies from all experiments are listed in Table 21 and Table 22, the most efficient time points are highlighted in red and italic.

5.6.3 Discussion

For the establishment of the RNAi method in the laboratory special measurements had to be conducted and several control experiments had to be performed.

The selection of the correct housekeeping gene was important for the normalisation of the obtained PCR data of mRNA expression, since a variability depending of the treatment conditions form one experiment to another may be caused. A common and widely used house-keeping gene is Glyceraldehyde-3-Phosphate Dehydrogenase (GAPDH). However, during the last years more and more investigators have reported about variations in its gene expression [Bustin 2000]. This and most of the other genes corresponding to basic cellular functions exhibited varying gene expressions during proliferation and differentiation [Barbu *et al.* 1989].

The present c-Abl mRNA expression data were normalised by the house-keeping gene 18S which is the small subunit of ribosomes and has several advantages compared to other house-keeping genes used in several studies. 18S has no introns, the likelihood for contamination by genomic DNA is lowered which reduces variations [Rawer 2005]. In addition, ribosomal genes are transcribed by distinct polymerases [Paule *et al.* 2000]. The 18S gene did not show many deviations depending on the treatment with a test compound and allowed to normalise the results on a very reproducible basis.

The control for siRNA experiments has to trigger the siRNA machinery without affecting any gene in the investigated species. Therefore the siRNA targeting green fluorescent protein (GFP) was chosen.

The preferred method for transfection was electroporation with the amaxa technology. This method is fast but causes also a lot of stress to the cells. Unfortunately, this method worked only in the cell line. The electroporation of NRVCM probably resulted not in efficient viability because of the isolation procedure. Therefore, NRVCM were transfected with lipofectamine. Lipofectamine 2000 has advantages above other reagents. This includes highest silencing efficiency (around 70%) and a long half-life of the siRNA when packed into the reagent (only 20 % siRNA was found degraded after 6 days). [Zhelev *et al.* 2004]

The optimisation of the siRNA:lipo ratio was optimised with the most efficient silencing siRNAs, 4Q and 10S, as revealed with electroporation in H9c2 cells. Out of the tested ratios, 2 µL/mL lipo with 40 nM and 80 nM were chosen for further experiments. Higher concentrations than 80 nM of siRNA were not tested, since they theoretically could induce non-specific effects like interferon response [Persengiev *et al.* 2004].

C-Abl_10S-siRNA-mediated silencing of c-Abl was not associated with non-specific interferon responses in NRVCM. Neither the interferon-induced, double-stranded RNA-activated protein kinase (PRKR) gene nor the 2',5'-oligoadenylate synthetase 1 (OAS-1) gene was affected by the treatment of 40 and 80 nM c-Abl siRNA (Figure 41). These data support the specific siRNA-mediated targeting of c-Abl mRNA in NRVCM. Opposite to c-Abl_10S siRNA, the c-Abl_4Q siRNA caused elevated levels of interferon response relevant transcripts. The observed increases were statistically significantly higher than that of the control; however the biological meaning is not clear. It is not clear, whether the slight increase indicates an unspecific response. In the literature unspecific OAS-1 or PRKR elevations of a factor between 10- and 1000-fold of the control are considered being relevant unspecific signals.

The mRNA and protein silencing efficiency was investigated over a period of 72 h after transfection with 40 and 80 nM of the selected c-Abl siRNA. Both 40 nM and 80 nM c-Abl siRNA caused a statistically significant reduction of the c-Abl mRNA expression level. After 16 h of transfection, 80 nM siRNA reached a decrease of about 55 % c-Abl mRNA, while 40 nM reached about 25 %.

It was the goal of the kinetic experiments to evaluate the time window when the c-Abl transfected cells lead to the most efficient decrease of the c-Abl transcripts and c-Abl proteins. One method to estimate the c-Abl expression over a time interval of 72 h is to calculate the area under the time-expression curve (AUC). The AUC value with the lowest expression values were selected to investigate imatinib in c-Abl silenced cells.

The AUC time-expression calculations revealed that the most effective silencing was achieved between 24-48 h post transfection. For both 40 and 80 nM c-Abl siRNA, the silencing efficiency was about 52-62 % (calculated by AUC from the mRNA concentration curve during 24-48 h) as determined by mRNA expression level. Between 24 and 48 h after treatment of NRVCM with the c-Abl_10S siRNA, c-Abl protein expression was decreased by 58 and 73 %, respectively (calculated by AUC from the protein concentration curve during 24-48 h) for 40 nM and 80 nM concentrations of c-Abl siRNA. A maximum of 76 % decrease of c-Abl protein expression was achieved at 40 h post-transfection.

The increase of the c-Abl protein after transfection with c-Abl_4Q was an unexpected result and cannot be explained. Comparing the targets of the two siRNA used revealed that c-Abl_10S targets c-Abl mRNA towards the 3' portion while Abl_4Q is directed more to the centre of the c-Abl gene. Novina and Sharp's unpublished observations indicate that targeting the gene towards the 3' terminus results in more effective siRNA [Dykxhoorn *et al.* 2003] which is supporting the higher efficiency of c-Abl_10S.

5.7 Influence of c-Abl silencing on Imatinib-mediated Impaired Cellular Function on NRVCM

5.7.1 Background

A range of important cellular functions were evaluated after the specific siRNA-mediated knock-down of the c-Abl gene to investigate the role of c-Abl in imatinib-induced toxicity. Between 24 and 48 h after treatment of NRVCM with a c-Abl-specific siRNA, c-Abl mRNA levels were decreased by 52-62 % and protein levels were decreased by up to 70 % (see Table 21). During this time frame, as well as before and afterwards, cytotoxicity and apoptosis assays were performed. As imatinib was found to be cytotoxic at concentrations above 20 µM in NRVCM, concentrations of 30 and 50 µM imatinib were tested after transfection with the two chosen siRNAs against c-Abl. The treatment with imatinib was conducted during the last 24 h of the given time frames.

5.7.2 Results

5.7.2.1 Cytotoxicity and apoptosis assays in c-Abl-silenced NRVCM

The cellular effects mediated by imatinib were measured in c-Abl silenced and un-silenced GFP transfected NRVCM. By comparing the effects of imatinib under both conditions it is possible to conclude on the role of c-Abl silencing in the toxicity mechanism.

Each assay was performed with transfection of the vehicle lipo alone, the siRNA directed against GFP and two siRNAs directed against c-Abl, c-Abl_4Q and c-Abl_10S. The last 24 h of transfection were incubated with imatinib. All values are normalised to GFP with 0 µM imatinib of each siRNA concentration (represented by the dashed line). For calculation of significance levels values of each time points are compared with the particular GFP siRNA control.

The cytotoxicity assays conducted (overview of all time points and the two siRNA concentrations are shown in Figure 44 (ATP), Figure 45 (MTS) and Figure 46 (Caspase 3/7 activity)) generally revealed no significant differences compared to the particular GFP control. However, after incubation with 30 µM imatinib on 40 nM c-Abl_10S-silenced cells a significant change was observed.

Comparing to the cytotoxicity data gained from normal NRVCM the results showed that silenced and unsilenced cells react similarly.

Few significant differences were found at 30 µM imatinib treatment and with lower cAbl_10S siRNA concentration in the ATP assay. Silencing by means of the cAbl_10S siRNA slightly increased the imatinib-mediated effects.

5.7.2.2 ATP content in silenced NRVCM

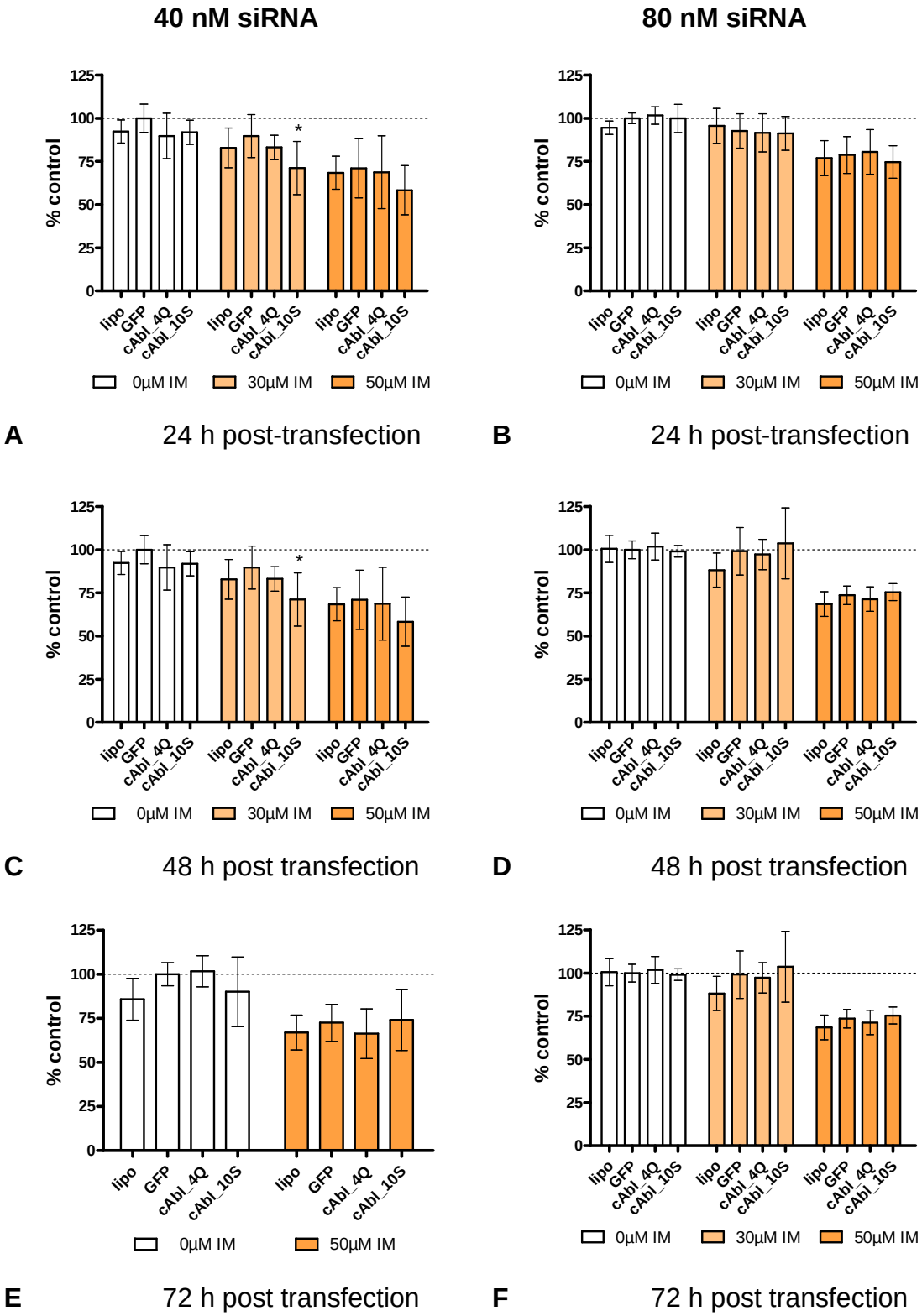

Figure 44 ATP content in silenced NRVCM 24 h after imatinib treatment. A 40nM siRNA for 24 h. **B.** 80nM siRNA for 48 h. **C.** 40nM siRNA for 48 h. **D.** 80 nM siRNA for 48 h. **E.** 40nM siRNA for 72 h. **F.** 80 nM siRNA for 72 h. Mean ± SD of 3 independent experiments. Level of significance: * $P < 0.05$.

The ATP levels reached after imatinib treatment of transfected cells were the same as found in untransfected NRVCM. The decreased, imatinib-induced ATP content was not statistically significantly changed at either time frame after transfection of c-Abl. Except for c-Abl_10S-transfected NRVCM and 30 µM imatinib treatment 24 and 48 h after transfection (Figure 44**).**

Generally, all concentrations of (0/30 and 50 µM) imatinib showed the same ATP level independent from the transfection was chosen.

5.7.2.3 MTS reduction in silenced NRVCM

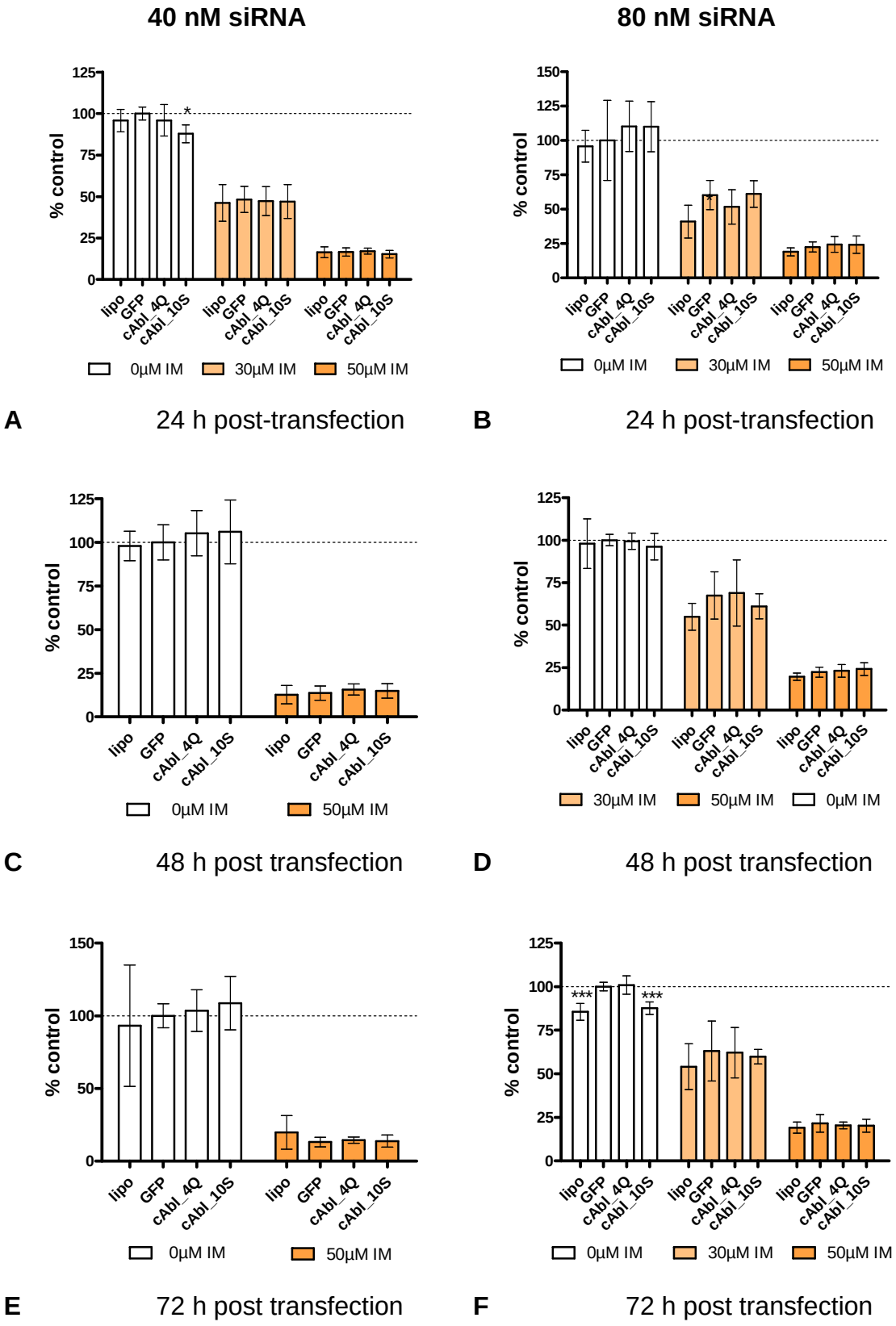

Figure 45 MTS reduction in silenced NRVCM 24 h after imatinib treatment. A. 40nM siRNA for 24 h. **B.** 80nM siRNA for 48 h. **C.** 40nM siRNA for 48 h. **D.** 80 nM siRNA for 48 h. **E.** 40nM siRNA for 72 h. **F.** 80 nM siRNA for 72 h. Mean ± SD of 3 independent experiments. Level of significance: * P < 0.05; ** P < 0.01; *** P < 0.001.

MTS reduction of c-Abl-transfected cells after different post transfection times is shown in Figure 45. 30 and 50 µM imatinib caused dose-dependent decreases of the MTS reduction capability. No significant differences were found with either siRNA tested in all assays, except for 72 h after transfection at 80 nM c-Abl_10S-siRNA. However, the difference was found to be similar to that of the lipo reagent alone and was thus found to be not relevant.

Silencing of c-Abl had no effect on the imatinib-inhibited MTS-reduction capability.

5.7.2.4 Caspase 3/7 activity in silenced NRVCM

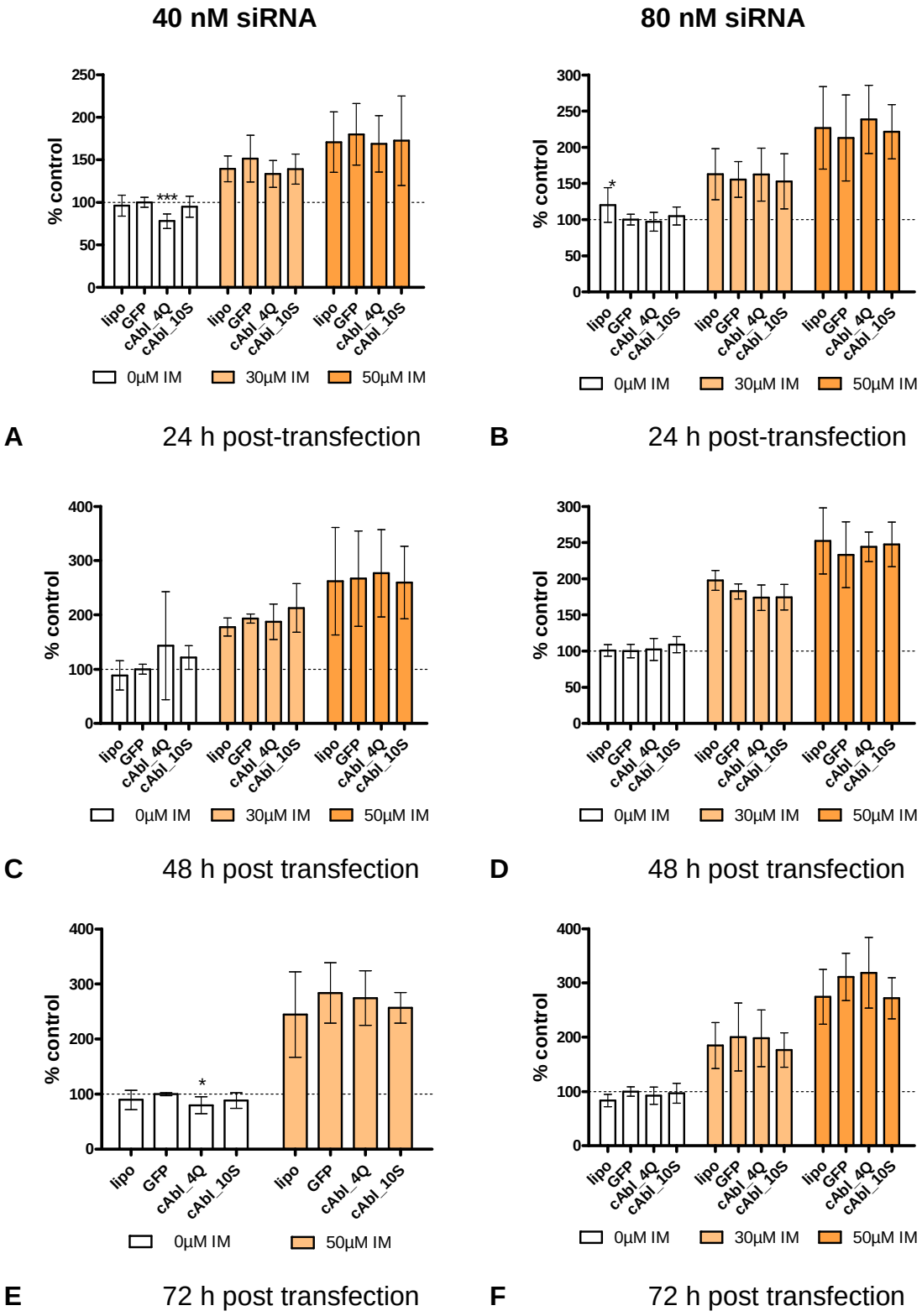

Figure 46 Caspase 3/7 activity in silenced NRVCM 24 h after imatinib treatment. A. 40nM siRNA for 24 h. **B.** 80nM siRNA for 48 h. **C.** 40nM siRNA for 48 h. **D.** 80 nM siRNA for 48 h. **E.** 40nM siRNA for 72 h. **F.** 80 nM siRNA for 72 h. Mean ± SD of 3 independent experiments. Level of significance: * P < 0.05.

The caspase 3/7 activity was found to be increased dose-dependently after imatinib treatment in GFP-transfected cells. In c-Abl treated NRVCM imatinib caused nearly the same response as in GFP transfected cells.
C-Abl silenced NRVCM did not rescue the cells from imatinib-induced caspase-3/7 activation in none of the investigated time intervals.

5.7.2.5 ER Stress in c-Abl-silenced NRVCM

The influence of c-Abl in ER stress was investigated after c-Abl silencing. The mRNA expressions are shown in **Figure** 47**.**

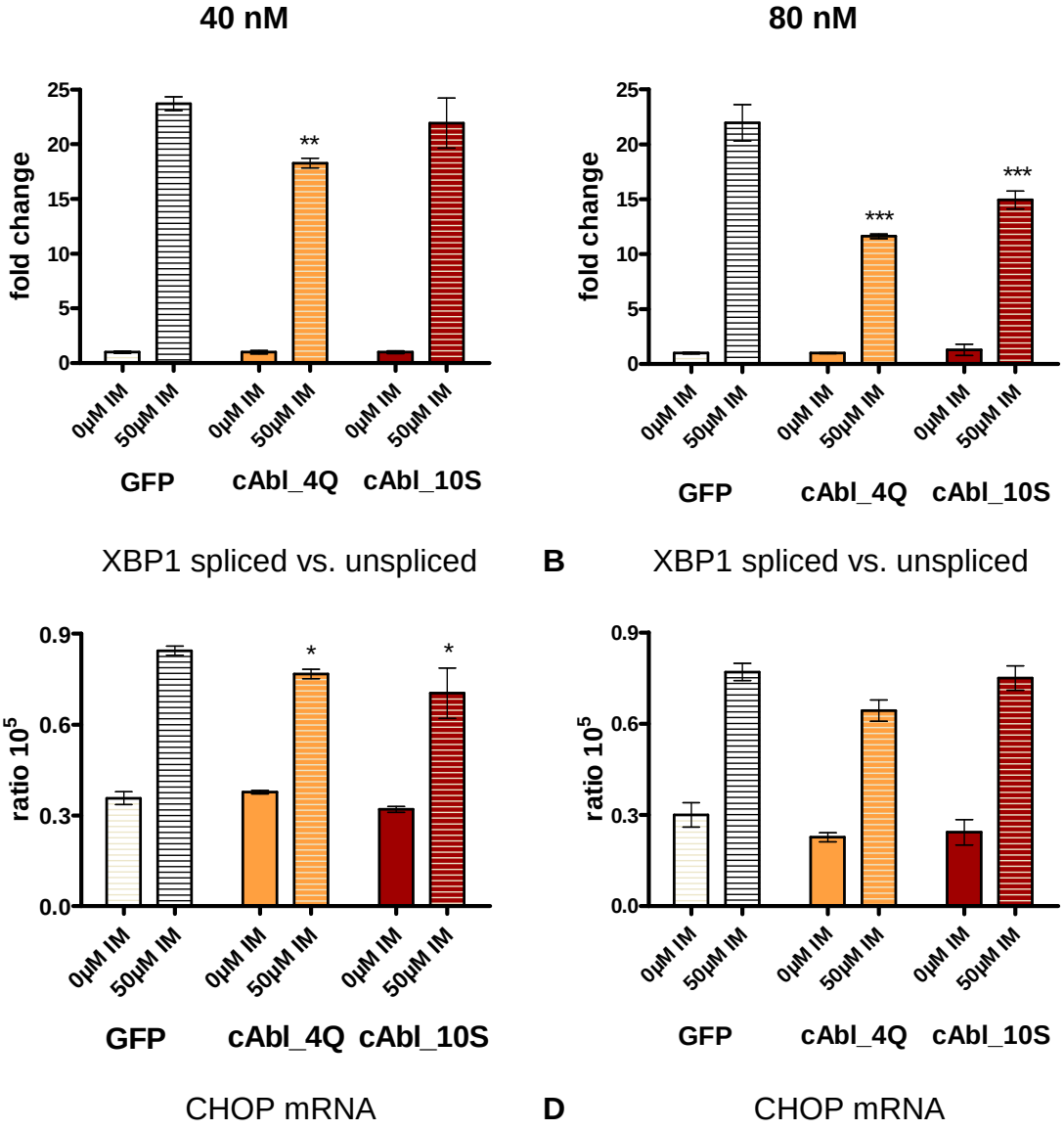

Figure 47 Gene expression of ER stress-related genes on c-Abl silenced NRVCM 24 h after incubation. A. Fold change of XBP1 spliced vs. unspliced transfected with 40 nM. **B.** Fold change of XBP1 spliced vs. unspliced transfected with 80 nM. **C.** Ratio of CHOP transfected with 40 nM. **D.** Ratio of CHOP transfected with 80 nM. Mean ± SD of triplicates. Level of significance: * P < 0.05, ** P < 0.001, *** P < 0.0001.

In all experiments 50 µM imatinib treatment caused a significant increase of the spliced versus unspliced XBP1 variant (Figure 47 A, B). Using 40 nM siRNA only small differences inter siRNA was observed. With 80 nM siRNA both c-Abl silenced and imatinib-treated cells showed a lower expression of this ER stress marker compared to GFP-treated cells.

The induced gene expression by XBP1, CHOP, was also investigated and the results are shown in (Figure 47 C, and D). CHOP was expressed to a higher level at all conditions when treated with imatinib. A marginal decrease of CHOP

expression after imatinib treatment was observed after transfection with 80 nM siRNA.

XBP1 spliced mRNA was highly elevated after a treatment with a high concentration of imatinib. Silencing the cells with c-Abl directed siRNA causes significant reduction. Significant changes in CHOP were only observed with 40 nM. As CHOP protein was shown to be not induced in imatinib-treated cells though XBP1 as well as CHOP mRNA was elevated.

It is not clear whether the slight statistically reduced XBP1 mRNA in c-Abl transfected cells has a biological relevance. Since this investigation was only a single experiment, though with three replicates, the biological relevance remains questionable. It appears possible that the inter-experimental variability is larger than the observed differences under the described conditions. In this case the observed differences would be in the frame of the normal inter-experimental conditions and not relevant.

5.7.2.6 Effect of Imatinib on Spontaneous Contractions in c-Abl silenced NRVCM

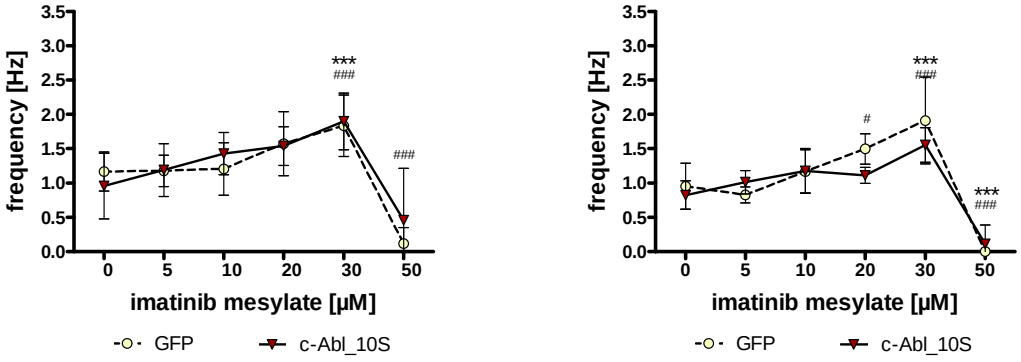

Figure 48 Beating rate of NRVCM after silencing c-Abl with 80 nM c-Abl_10S siRNA and 24 h imatinib treatment. A. 24 h post transfection. **B.** 48 h post transfection. Mean ± SD of 2-3 independent experiments. Level of significance of compared to particular 0 µM IM control: * P < 0.05, *** P < 0.0001; * cAbl_10S, # GFP.

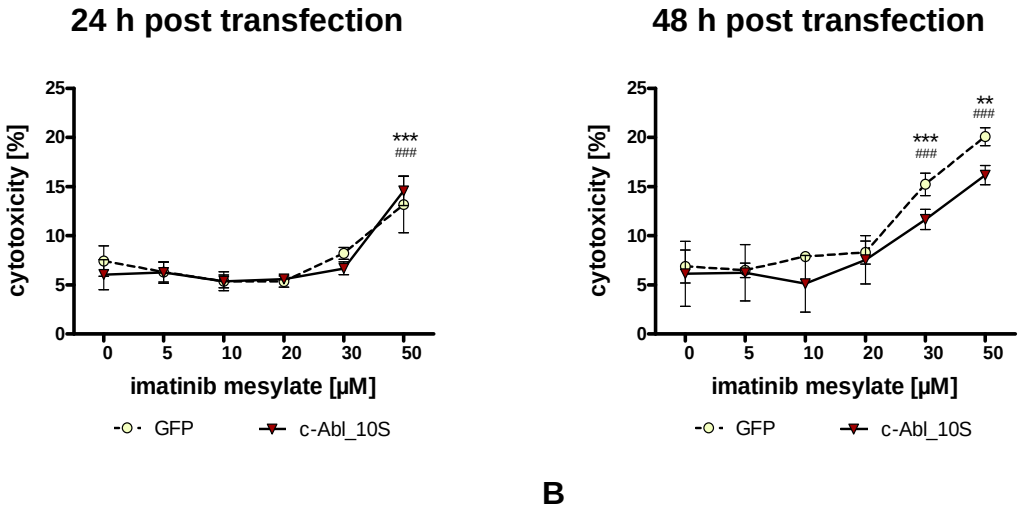

Figure 49 Cytotoxicity (LDH release) of NRVCM after silencing c-Abl with 80 nM c-Abl_10S siRNA and treatment for 24 h with imatinib. A. 24 h post transfection. **B.** 48 h post transfection. Mean ± SD of 2-3 independent experiments. Level of significance of compared to particular 0 µM IM control: * P < 0.05, *** P < 0.0001; * cAbl_10S, # GFP.

Imatinib treatment of spontaneously beating NRVCM had an effect on cardiac functionality (Figure 48). Imatinib treatment caused a dose-dependent increase of the beating frequencies. Significant changes compared to the control were monitored after 24 h treatment after 24 h and 48 h silencing above 30 µM. No changes were observed comparing GFP and cAbl_10S-silenced cells. The drop at 50 µM is very likely the result of unspecific cytotoxicity (Figure 49). 24 h post transfection imatinib was cytotoxic as determined by LDH release at the concentration of 30 µM imatinib. 48 h post transfection statistically significant increased LDH-releases compared to control were observed at 30 and 50 µM.

imatinib. There was no statistical significant difference between imatinib-induced LDH-releases between GFP- and c-Abl transfected NRVCM.

5.7.3 Discussion

The key experiment of the Kerkelä paper is the retroviral gene transfer of an imatinib-resistant mutant c-Abl into NRVCM which appeared to reduce imatinib-induced cell death. Since the retroviral gene transfer is very unlikely to happen in non-dividing cardiomycoytes [Romano 2006] by 90 % transfection efficiency, RNAi was applied to explore the specific gene knock down.

Currently no heart specific functional data are available, which could link the knock-down of c-Abl with its functionality, for instance like influencing the spontaneous beating rates. Also it is unknown whether imatinib changes the functionality of the cardiomyocytes in c-Abl knock-down cells.

The evaluation of saving cells from imatinib-induced toxicity by silencing c-Abl was investigated with doses of 30 and 50 µM imatinib. Here 50 µM imatinib had the strongest effect, whereas 30 µM had an intermediate effect. Up to 10 µM imatinib induced no relevant effects. The selection of an intermediate toxic imatinib concentration was important since it might be possible that a threshold concentration of imatinib exists which potentially cannot be rescued by c-Abl silencing. These results, however, demonstrated that there was a difference between the concentrations of imatinib and the potential rescuing effect of c-Abl-mediated silencing.

Under the current condition c-Abl had no effect on the imatinib-induced cytotoxicity. This result is in agreement with Zhelev and co-workers. They reported that silencing of c-Abl in normal lymphocytes have to effect on imatinib-induced toxicity [Zhelev *et al.* 2004].

c-Abl silencing did not alter cytotoxicity, apoptosis or ER stress markers in NRVCM during a period of 72 h following transfection. In the time window from 24 to 48 h, where knock-down of c-Abl protein expression was most efficient, the cytotoxicity of imatinib (at concentrations of 30 and 50 µM) was evaluated in both GFP siRNA-transfected and c-Abl siRNA-transfected cells (40 and 80 nM). There was no statistically significant difference between GFP siRNA- and c-Abl siRNA-transfected cells in terms of imatinib-induced changes in MTS reduction, ATP content and caspase 3-/7 activities effects. These results suggest that a 73 % reduction of c-Abl protein expression during 24 h did not rescue cardiomyocytes from the imatinib-induced cytotoxicity. Since 73 % of the protein content is decreased, there is still 27 % of c-Abl protein left in the cells. This amount of conserved c-Abl protein theoretically might be sufficient to maintain

important c-Abl-mediated functions and may cover a potential protective effect on the imatinib-induced cytotoxicity.

In order to explore this possibility further studies concerning the c-Abl activity have to be performed. Assays on c-Abl activity after silencing should be performed in the time window with the lowest protein quantity. In the case of healthy cardiomyocytes a sensitive c-Abl kinase activity assay is not available. This also excluded the possibility to determine c-Abl activity in c-Abl silenced cells. In cardiomyocytes c-Abl is tightly regulated and bound to proteins to suppress its kinase activity [Welch *et al.* 1993; Yoshida *et al.* 2005]. Besides other proteins inhibiting the c-Abl kinase activity c-Abl itself bears an intra-molecular mechanism of inhibition [Pluk *et al.* 2002]. C-Abl is reported to be mostly inactive in cells [Davis *et al.* 1985; Pendergast *et al.* 1991]. Though c-Abl can be activated by PDGF [Plattner *et al.* 1999; Plattner *et al.* 2003; Vittal *et al.* 2007] or by ionising radiation among other stimuli, only c-Abl in a specific compartment is activated [Plattner *et al.* 1999] and / or shuttling to different compartments in the cell is induced. The kinase activity half-life of activated c-Abl is with 7 ± 2.3 h much shorter than of the c-Abl protein (18 ± 4.8 h) [Echarri *et al.* 2001]. The peak of its activation has been determined to be 5 min after stimulation with PDGF-BB and remains elevated for at least 20 min [Plattner *et al.* 1999]. Even though results can be obtained, the artificial circumstances may lead to cellular responses which are artificial as well. C-Abl is a very complex protein, exogenous stimuli may change the subcellular localisation of c-Abl [Lewis *et al.* 1996] and therefore different pathways are likely to be triggered.
In comparison to low c-Abl activity in healthy somatic cells, c-Abl is highly expressed in oncogenic cells by the Bcr-Abl protein. Silencing c-Abl as part of the Bcr-Abl oncoprotein has been reported in the literature. Scherr and co-workers electroporated a CML-cell line, K562 harbouring constitutively active Bcr-Abl with siRNAs directed against the fusion region. After 24 h a reduction to 25-32% of mRNA and to 35-61% after 48 h with two different siRNAs was observed. Four days after electroporation the proliferation of the K562 cells is reported to be reduced by 75 %. The mRNA of electroporated cells with their proliferation dependent on Bcr-Abl, was silenced to 70 % and the protein to 55 %. The proliferation is decreased to the same extent as seen in cultures treated with 1 µM imatinib. In all experiments the level of Bcr as well as c-Abl is reported to remain unaffected by the siRNA-treatment. [Scherr *et al.* 2003]. More efficient silencing was obtained by repeated treatments with multiple siRNAs: Silencing K562 cells every second day over 6 days with a pool of three siRNA, each 60 nM, revealed a reduction of 82 % in the Bcr-Abl mRNA level and 64 % of the protein level. The decrease in Bcr-Abl activity accounts for

57 % and the proliferation is inhibited by 50 %. In comparison, imatinib used at the same conditions and at 180 nM decreased the proliferation to about the same extend (54 %) whereas Bcr-Abl activity is decreased by 73 %. Most important, the protein level of Bcr-Abl was only affected to a small extend (14 % decrease). [Zhelev *et al.* 2004]

These results indicate that the silencing efficiencies obtained in the present study were similar to those reported in the literature. It can be assumed that silencing threshold of the c-Abl protein, which had a cellular consequence by inhibiting proliferation can also be achieved in the time interval between 24 and 48 h of the present study.

The effect of 24 h imatinib treatment on the beating rate of both silenced and non-silenced NRVCM was investigated instead. siRNA-transfection was performed in parallel to imatinib treatment and 48 h after transfection with c-Abl siRNA. Incubation with increasing concentrations of imatinib resulted in a dose-dependent increase of the beating frequencies which was significant compared to the control above 30 µM. No differences were found between non-silenced and c-Abl-silenced cells. Co-incubation with imatinib did not alter the observed dose-dependent increases in beating frequencies as well as not on LDH-release. Hence, c-Abl has no effect on the imatinib-induced cytotoxicity as well on the cardiomyocytes-specific function to beat spontaneously.

Silencing experiments with 80 nM in GFP or c-Abl siRNA transfected cells did not significantly differ in terms of beating frequencies 24 h post transfection. These experiments confirm that c-Abl does not influence the normal cardiac cellular function of spontaneous contractions.

Specificity of a c-Abl-mediated mechanism of imatinib-induced toxicity was directly investigated in the previous chapter by means of the RNAi method. However, there is indirect evidence about the relevance of the possible involvement of c-Abl in the imatinib mediated mechanisms of cytotoxicity.

A possible explanation for increased ATP content and MTS reduction capability may be found: Cardiac cells produce ATP to about 95 % under no ischemic conditions by oxidative phosphorylation. The production of ATP in the healthy heart is exclusively linked to the rate of ATP hydrolysis keeping the ATP content constant in the heart (reviewed in [Stanley *et al.* 2005]). So if contraction is increased, an increase of all components in the system should be observed. This was found with the ATP content at concentrations to up to 20 µM where no significant increases in contraction were found.

These data might be improved by the patch clamp technique which monitors in addition the amplitude and the ion channels affected. Hence, a drug can be

shown to cause arrhythmia, furthermore if and which ion channel is changed. Also the reversibility of a toxic effect can be shown.

Under the current experimental condition the applied concentrations of imatinib in NRVCM do not specifically inhibit the c-Abl kinase activity since these concentrations are already close to saturation. This estimation is based on results in Ba/F3-Bcr-Abl murine haematopoietic cell model. These cells express high Bcr-Abl autophosphorylation activity and imatinib was found to inhibit the Bcr-Abl autophosphorylation with an IC_{50} of 0.25 µM, and nearly complete inhibition at a concentration of 1 µM (internal Novartis unpublished information). These results are in agreement with published literature to date [Druker *et al.* 1996; Druker *et al.* 2001; Azam *et al.* 2003]. Assuming similar effects of imatinib on c-Abl activity in cardiomyocytes as compared to Bcr-Abl activity in Ba/F3 cells, these results suggest saturated inhibition of c-Abl kinase activity would occur in the 10-50 µM concentration range. This implies that further increases in the dose of imatinib above 10 µM should not significantly increase c-Abl-mediated effects of imatinib in NRVCM. However, the clear dose-response relationship which was observed with imatinib for cytotoxicity, ER stress response and cell death signalling pathways in NRVCM is contradicting this hypothesis.

The comparison of the specific c-Abl inhibitory concentrations and the imatinib concentrations which were used in the current study further suggests that imatinib-induced ER stress response and cell death signalling are c-Abl-independent effects. They further confirm the results of the RNAi experiments.

5.7.4 Set-up of Stable Silencing in NRVCM

5.7.5 Background

In parallel to the RNAi experiments it was planned to set up the stable silencing of the c-Abl gene by means of the lentiviral vector. This method has several advantages compared to the siRNA method.

Silencing proteins with siRNAs are of transient nature, as observed in these experiments and reported in the literature [Paddison *et al.* 2002; Scherr *et al.* 2003; Zhelev *et al.* 2004]. To evaluate the impact of a certain protein better, another RNAi approach is helpful: Stable silencing with shRNAs. Though less efficient than siRNAs [Paddison *et al.* 2002], shRNAs are stably expressed within the cell after successful delivery into the cell. However, the cells express them by themselves, after transfection of the cell the quantity of shRNAs cannot be controlled and unlike siRNAs, the response does not occur immediately [Dykxhoorn *et al.* 2003]. In case that the effect of silencing c-Abl can only be observed after a longer exposition to RNAi, this approach was designated for this investigation. In contrast to Kerkelä and co-workers who have chosen a retrovirus-based transfection; in this work lentiviruses as vector were chosen. An advantage of lentiviruses over retroviruses is that they can also transfect non-dividing cells. Colleagues investigated the NRVCM for proliferation and have determined that only 7 % of NRVCM were dividing (Axel Vicart, Brigitte Greiner, unpublished data) 4h after plating. Also, in literature it is reported that cardiomyocytes discontinue proliferation after birth [Li *et al.* 1996; Liu *et al.* 1996; Chen *et al.* 2004]. This contradicts the results found by Kerkelä and colleagues that NRVCM were transduced to >90 % which is impossible as retroviruses can only transduce dividing cells [Romano 2006]. These experiments were started and transferred to another collaborator for following up in the laboratory.

5.7.6 Results

For endogenous expression of shRNAs the effective siRNAs in these experiments were designed first to result in a shRNAs after annealing. With the use of the BLOCK-iT™ RNAi Designer provided by Invitrogen the design of GFP and three of the siRNAs against c-Abl (4Q, 1S and 10S) were designed. As a positive control, the effective siRNA against Caspase 3 was chosen. By default a linker region is given, a G was additionally inserted if the sequence didn't start with a G. The loop was chosen to consist of 4 nucleotides, namely CGAA.

Table 23 List of designed shRNAs chosen for lentiviral transfection. Sense sequence coloured in green, loop region is centred, antisense sequence coloured in red and linker regions are located at the 5' ends.

siRNA		*shRNA sequence*
GFP	top	5'-CACCGCGGCAAGCTGACCCTGAAGTTCACGAA TGAACTTCAGGGTCAGCTTGCCG-3'
	bottom	3'-CGCCGTTCGACTGGGACTTCAAGTGCTT ACTTGAAGTCCCAGTCGAACGGCAAAA-5'
cas3	top	5'-CACCG*CAGCCACAATACAATACCTCACGAA TGAGGTATTGTATTGTGGCTG-3'
	bottom	3'-CGTCGGTGTTATGTTATGGAGTGCTT ACTCCATAACATAACACCGACAAAA-5'
4Q	top	5'-CACCGGACGGCAGCCTAAATGAACGAA TTCATTTAGGCTGCCGTCC-3'
	bottom	3'-CCTGCCGTCGGATTTACTTGCTT AAGTAAATCCGACGGCAGGAAAA-5'
1S	top	5'-CACCGTTGATCTCCTTCATCACTGCGCGAA CGCAGTGATGAAGGAGATCAA-3'
	bottom	3'-CAACTAGAGGAAGTAGTGACGCGCTT GAGTCACTACTTCCTCTAGTTCCCC-5'
10S	top	5'-CACCGTGATTATAACCTAAGACCCGGCGAA CCGGGTCTTAGGTTATAATCA-3'
	bottom	3'-CACTAATATTGGATTCTGGGCCGCTT GGCCCAGAATCCAATATTAGTAAAA-5'

According to the manufacturer's protocol the oligos were annealed and with the means of the BLOCK-iT™ kit the shRNAs were cloned into the pENTR™/U6 vector. This clone forms an expression clone together with the pLenti6/BLOCK-iT™-DEST vector after a LR recombination reaction.

After generation of the entry clone and the expression clone, the harvested colonies were amplified and DNA was purified to check for the correct sequence (work done by Solvias). All colonies of shRNA_10S failed to generate an expression clone.

For generation of lentiviral constructs these cDNAs were given to another work group within the group investigative Toxicology, Novartis.

6 CONCLUSION

In the current studies it was tried to reproduce the *in vitro* studies published by Kerkelä. It turned out that not all of the experiments could be repeated. Particularly in terms of quantitative observations huge differences exist between the two laboratories.

Based on the results of the study in hand, which are partially supported by other groups [Will *et al.* 2008], all effects occur simultaneously with the cytotoxicity of imatinib. This makes it very unlikely that c-Abl inhibition is leading to specific ER stress, followed by collapsed mitochondrial membrane potential leading to apoptosis. Time- and concentration-dependent monitoring of all effects showed that there was a huge overlap of the different cellular events at the same concentration. The results did not suggest a sequence of cellular events, which are triggered casually, one after the other. A specific imatinib-induced mitochondrial functional impairment which could be a trigger for subsequent cellular events was also investigated by other groups, which could not confirm mitochondria as being a specific target of imatinib [Will *et al.* 2008].

It is also very unlikely that the effects observed at these high imatinib concentrations are specifically mediated by c-Abl tyrosine kinase inhibition. Under the currently applied imatinib concentrations, the specific c-Abl tyrosine kinase activity is highly inhibited and overloaded, so that the observed dose-dependencies of various endpoints can not be explained.

The effects observed in NRVCM can also not to be considered as organ-specific for cardiomyocytes. Same effects were also found to the same or higher extend in fibroblasts from different origin.

The retroviral approach, which was used in the Kerkelä studies, is very unlikely to happen in cardiomyocytes due to the low proliferation rates. Alternatively, the direct role of c-Abl was evaluated by RNAi. It was demonstrated that the specific knock-down of the c-Abl gene and protein, below which a cellular relevant threshold of expression did not neither affect heart specific functions such as spontaneous contractions, nor led it to impaired mitochondrial functions or influence the general viability of cardiomyocytes to induce apoptosis. Silencing of c-Abl had also no protective effect against the imatinib cytotoxicity. Overall, these results do not support the observations of Kerkelä *in vitro*.

Currently it is not clear where the cause for the observed huge differences concerning the obtained results lies. The minor differences in terms of the cell culture conditions, which also exist, could not explain this huge difference. The conditions mentioned in the paper were not very well described. Changes were made in these studies at hand to improve the quality of the culture conditions.

Huge difference which might have also huge consequences, exist in terms of the application of the active ingredients imatinib. In this study the purified active ingredient imatinib was used, whereas Kerkelä have extracted imatinib from Glivec tablets. This could be a potential source for deviations.

All over it appears also questionable whether the described heart toxicity of Glivec does even exist in humans. The recent report [Kerkelä *et al.* 2006] has evoked replies of many scientists, saying that problem of cardiotoxicity with imatinib-medicated patients was not found in their studies. Criticism came up as several patients who developed congestive heart failure during the study had pre-existing cardiac conditions. Seven out of the ten patients monitored by Kerkelä had a history of hypertension, four diabetes and three coronary artery disease. Two of the three latter patients needed a coronary artery bypass grafting; one of them had a coronary stent in place. As no full case reports were provided, the risks of developing coronary disease cannot be quantified or placed in the appropriate context of the reported findings. [Hatfield *et al.* 2007]

Neither was information given about the total population size the patients were chosen from, nor about time of the decrease of left ventricular ejection – during imatinib medication or after its discontinuation. Cardiovascular disease is a common disease and its incidence should be compared to a population of similar age [Gambacorti *et al.* 2007]. The functionality of the heart during imatinib medication in 103 CML-patients was investigated. Four of them have developed cardiomyopathy or coronary artery disease but a substantial drop in the ejection fraction has not been found [Gambacorti *et al.* 2007]. Currently about 30000 patients have been treated by Glivec and no one case of cardiotoxicity has been clearly identified.

7 BIBLIOGRAPHY

A

Abelson, H. T., *et al.* (1970). "*Lymphosarcoma: Virus-induced Thymic-independent Disease in Mice*." Cancer Research 30(8): 2213-2222.

Acosta, D., *et al.* (1984). "*Cardiotoxicity of Tricyclic Antidepressants in Primary Cultures of Rat Myocardial-Cells*." Journal of Toxicology and Environmental Health 14(2-3): 137-143.

Aikawa, R., *et al.* (1997). "*Oxidative stress activates extracellular signal-regulated kinases through Src and ras in cultured cardiac myocytes of neonatal rats*." Journal of Clinical Investigation 100(7): 1813-1821.

Aikawa, R., *et al.* (2001). "*Reactive Oxygen Species in Mechanical Stress-Induced Cardiac Hypertrophy*." Biochemical and Biophysical Research Communications 289(4): 901-907.

Alnemri, E. S., *et al.* (1996). "*Human ICE/CED-3 protease nomenclature*." Cell 87(2): 171-171.

Amarzguioui, M., *et al.* (2005). "*Approaches for chemically synthesized siRNA and vector-mediated RNAi*." Febs Letters 579(26): 5974-5981.

Anonymous. (2009). "The History of Cancer." Cancer Reference Information Retrieved 01.02.2009, 2009, from http://www.cancer.org/docroot/CRI/content/CRI_2_6x_the_history_of_cancer_72.asp

Aouad, S. M., *et al.* (2004). "*Caspase-3 is a component of fas death-inducing signaling complex in lipid rafts and its activity is required for complete caspase-8 activation during Fas-mediated cell death*." Journal of Immunology 172(4): 2316-2323.

Ashkenazi, A., *et al.* (1998). "*Death receptors: Signaling and modulation*." Science 281(5381): 1305-1308.

Azam, M., *et al.* (2003). "*Mechanisms of autoinhibition and STI-571/imatinib resistance revealed by mutagenesis of BCR-ABL*." Cell 112(6): 831-843.

B

Bae, Y. S., *et al.* (1997). Epidermal Growth Factor (EGF)-induced Generation of Hydrogen Peroxide. Rolein EGF receptor-mediated tyrosine phosphorylation. **272:** 217-221.

Barbu, V., *et al.* (1989). "*Northern Blot Normalization with A 28S Ribosomal-Rna Oligonucleotide Probe*." Nucleic Acids Research 17(17): 7115-7115.

Barila, D., *et al.* (1998). "*An intramolecular SH3-domain interaction regulates c-Abl activity*." Nature Genetics 18(3): 280-282.

Baskaran, R., *et al.* (1997). "*Ataxia telangiectasia mutant protein activates c-Abl tyrosine kinase in response to ionizing radiation*." Nature 387(6632): 516-519.

Batulan, Z., *et al.* (2003). High Threshold for Induction of the Stress Response in Motor Neurons Is Associated with Failure to Activate HSF1. **23:** 5789-5798.

Beran, M., *et al.* (1998). "*Selective inhibition of cell proliferation and BCR-ABL phosphorylation in acute lymphoblastic leukemia cells expressing M-r 190,000 BCR-ABL protein by a tyrosine kinase inhibitor (CGP-57148) 1*." Clinical Cancer Research 4(7): 1661-1672.

Bernstein, E., *et al.* (2001). "*Role for a bidentate ribonuclease in the initiation step of RNA interference*." Nature 409(6818): 363-366.

Berridge, M. V., *et al.* (2005). "*Tetrazolium dyes as tools in cell biology: new insights into their cellular reduction*." Biotechnol Annu Rev 11: 127-52.

Berridge Mv, T. A. (1998). "*Trans-plasma membrane electron transport: A cellular assay for NADH- and NADPH-oxidase based on extracellular, superoxide-mediated reduction of the sulfonated tetrazolium salt WST-1* " Protoplasma 205, Numbers(1-4): 74-82.

Berridge Mv, T. A., Mccoy Kd, Wang R (1996). "*The biochemical and cellular basis of cell proliferation assays that use tetrazolium salts*." Biochemica 4: 14-19.

Berridge, M. V., *et al.* (1993). "*Characterization of the cellular reduction of 3-(4,5-dimethylthiazol-2-yl)-2,5-diphenyltetrazolium bromide (MTT): subcellular localization, substrate dependence, and involvement of mitochondrial electron transport in MTT reduction*." Arch Biochem Biophys 303(2): 474-82.

Bertolotti, A., *et al.* (2000). "*Dynamic interaction of BiP and ER stress transducers in the unfolded-protein response*." Nature Cell Biology 2(6): 326-332.

Billy, E., *et al.* (2001). "*Specific interference with gene expression induced by long, double-stranded RNA in mouse embryonal teratocarcinoma cell lines*." Proceedings of the National Academy of Sciences 98(25): 14428-14433.

Bittner, B., *et al.* (2002). "*Improvement of the bioavailability of colchicine in rats by co-administration of D-alpha-tocopherol polyethylene glycol 1000 succinate and a polyethoxylated derivative of 12-hydroxy-stearic acid*." Arzneimittel-Forschung-Drug Research 52(9): 684-688.

Blume-Jensen, P., *et al.* (2001). "*Oncogenic kinase signalling*." Nature 411: 355.

Bogman, K., *et al.* (2003). "*The role of surfactants in the reversal of active transport mediated by multidrug resistance proteins*." J Pharm Sci 92(6): 1250-61.

Bogman, K., *et al.* (2005). "*P-Glycoprotein and Surfactants: Effect on Intestinal Talinolol Absorption*." Clin Pharmacol Ther 77(1): 24-32.

Bolli, R. (1988). "*Oxygen-derived free radicals and postischemic myocardial dysfunction ("stunned myocardium")*." Journal of the American College of Cardiology 12(1): 239-249.

Boyce, M.*, et al.* (2006). "*Cellular response to endoplasmic reticulum stress: a matter of life or death*." Cell Death Differ 13(3): 363-373.

Brasher, B. B.*, et al.* (2001). "*Mutational analysis of the regulatory function of the c-Abl Src homology 3 domain*." Oncogene 20(53): 7744-7752.

Brodsky, J. L.*, et al.* (1999). "*The requirement for molecular chaperones during endoplasmic reticulum-associated protein degradation demonstrates that protein export and import are mechanistically distinct*." Journal of Biological Chemistry 274(6): 3453-3460.

Buchdunger, E.*, et al.* (2002). "*Pharmacology of imatinib (STI571)*." European Journal of Cancer 38: S28-S36.

Buchdunger, E.*, et al.* (1996). "*Inhibition of the abl protein-tyrosine kinase in vitro and in vivo by a 2-phenylaminopyrimidine derivative*." Cancer Research 56(1): 100-104.

Buday, L. (1999). "*Membrane-targeting of signalling molecules by SH2/SH3 domain-containing adaptor proteins*." Biochimica et Biophysica Acta-Reviews on Biomembranes 1422(2): 187-204.

Bustin, S. A. (2000). "*Absolute quantification of mRNA using real-time reverse transcription polymerase chain reaction assays*." Journal of Molecular Endocrinology 25(2): 169-193.

C

Cadenas, E. (1989). "*Biochemistry of Oxygen-Toxicity*." Annual Review of Biochemistry 58: 79-110.

Calfon, M.*, et al.* (2002). "*IRE1 couples endoplasmic reticulum load to secretory capacity by processing the XBP-1 mRNA*." Nature 415(6867): 92-96.

Carini, R.*, et al.* (1990). "*Comparative evaluation of the antioxidant activity of [alpha]-tocopherol, [alpha]-tocopherol polyethylene glycol 1000 succinate and [alpha]-tocopherol succinate in isolated hepatocytes and liver microsomal suspensions*." Biochemical Pharmacology 39(10): 1597-1601.

Carroll, M.*, et al.* (1997). "*CGP 57148, a tyrosine kinase inhibitor, inhibits the growth of cells expressing BCR-ABL, TEL-ABL, and TEL-PDGFR fusion proteins*." Blood 90(12): 4947-4952.

Chen, H. W.*, et al.* (2004). "*Dynamic changes of gene expression profiles during postnatal development of the heart in mice*." Heart 90(8): 927-934.

Chen, Q., *et al.* (1995). Participation of Reactive Oxygen Species in the Lysophosphatidic Acid-stimulated Mitogen-activated Protein Kinase Kinase Activation Pathway. **270:** 28499-28502.

Cohen, L., *et al.* (1995). "*Role of Kir, A Novel Ras-Like Protein, in Bcr/Abl-Leukemogenesis*." Journal of Cellular Biochemistry: 32-32.

Cooper, J. A. (1987). "*Effects of cytochalasin and phalloidin on actin*." The Journal of Cell Biology 105(4): 1473-1478.

Cortes, J., *et al.* (2004). Discontinuation of imatinib therapy after achieving a molecular response. **104:** 2204-2205.

Courtneidge, S. A. (2003). "*Cancer - Escape from inhibition*." Nature 422(6934): 827-828.

D

Davis, R. L., *et al.* (1985). "*Activation of the c-abl oncogene by viral transduction or chromosomal translocation generates altered c-abl proteins with similar in vitro kinase properties*." Mol.Cell Biol. 5: 204.

De Vries, N., *et al.* (1993). "*N-Acetyl-L-Cysteine*." Journal of Cellular Biochemistry: 270-277.

Deatley, S. M., *et al.* (1999). "*Antioxidants protect against reactive oxygen species associated with adriamycin-treated cardiomyocytes*." Cancer Letters 136(1): 41-46.

Deininger, M., *et al.* (2005). "*The development of imatinib as a therapeutic agent for chronic myeloid leukemia*." Blood 105(7): 2640-2653.

Deininger, M. W. N., *et al.* (1997). "*The tyrosine kinase inhibitor CGP57148B selectively inhibits the growth of BCR-ABL-positive cells*." Blood 90(9): 3691-3698.

Deininger, M. W. N., *et al.* (2000). "*The molecular biology of chronic myeloid leukemia*." Blood 96(10): 3343-3356.

Deininger, M. W. N., *et al.* (2000). "*BCR-ABL tyrosine kinase activity regulates the expression of multiple genes implicated in the pathogenesis of chronic myeloid leukemia*." Cancer Research 60(7): 2049-2055.

Delhalle, S., *et al.* (2003). "*An introduction to the molecular mechanisms of apoptosis*." Apoptosis: from Signaling Pathways to Therapeutic Tools 1010: 1-8.

Di Jeso, B., *et al.* (2003). Folding of thyroglobulin in the calnexin/calreticulin pathway and its alteration by loss of Ca2+ from the endoplasmic reticulum. **370:** 449-458.

Dintaman, J. M., *et al.* (1999). "*Inhibition of P-Glycoprotein by D-+Ý-Tocopheryl Polyethylene Glycol 1000 Succinate (TPGS)*." Pharmaceutical Research 16(10): 1550-1556.

Druker, B. J., *et al.* (2006). "*Five-year follow-up of patients receiving imatinib for chronic myeloid leukemia*." New England Journal of Medicine 355(23): 2408-2417.

Druker, B. J., *et al.* (2001). "*Activity of a specific inhibitor of the BCR-ABL tyrosine kinase in the blast crisis of chronic myeloid leukemia and acute lymphoblastic leukemia with the Philadelphia chromosome*." N.Engl.J.Med. 344: 1038.

Druker, B. J., *et al.* (2001). "*Efficacy and safety of a specific inhibitor of the BCR-ABL tyrosine kinase in chronic myeloid leukemia*." N.Engl.J.Med. 344: 1031.

Druker, B. J., *et al.* (1996). "*Effects of a selective inhibitor of the Abl tyrosine kinase on the growth of Bcr-Abl positive cells*." Nat.Med. 2: 561.

Du, Y., *et al.* (2006). "*Coordination of intrinsic, extrinsic, and endoplasmic reticulum-mediated apoptosis by imatinib mesylate combined with arsenic trioxide in chronic myeloid leukemia*." Blood 107(4): 1582-1590.

Dykxhoorn, D. M., *et al.* (2003). "*Killing the messenger: Short RNAs that silence gene expression*." Nature Reviews Molecular Cell Biology 4(6): 457-467.

E

Eastman (2005). Eastman Vitamin E TPGS NF - Applications and Properties, Eastman Chemical Company.

Echarri, A., *et al.* (2001). "*Activated c-Abl is degraded by the ubiquitin-dependent proteasome pathway*." Current Biology 11(22): 1759-1765.

El Jamali, A., *et al.* (2008). "*Novel redox-dependent regulation of NOX5 by the tyrosine kinase c-Abl*." Free Radical Biology and Medicine 44(5): 868-881.

Elbashir, S. M., *et al.* (2001). "*RNA interference is mediated by 21- and 22-nucleotide RNAs*." Genes and Development 15(2): 188-200.

Ellgaard, L., *et al.* (1999). "*Setting the standards: Quality control in the secretory pathway*." Science 286(5446): 1882-1888.

Estevez, M. D., *et al.* (2000). "*Effect of PSC 833, verapamil and amiodarone on adriamycin toxicity in cultured rat cardiomyocytes*." Toxicology in Vitro 14(1): 17-23.

Eufic. (1998, 2008/06/15/). "Diet, Lifestyle and Life Expectancy (EUFIC)." EUFIC REVIEW 11/1998, 2008, from http://www.eufic.org/article/en/page/RARCHIVE/expid/review-diet-lifestyle-life-expectancy/

F

Fariss, M. W., *et al.* (2005). "*ROLE of MITOCHONDRIA in TOXIC OXIDATIVE STRESS*." Molecular Interventions 5(2): 94-111.

Flynn, D. C. (2001). "*Adaptor proteins*." Oncogene 20(44): 6270-6272.

Fujio, Y., *et al.* (2000). "*Akt promotes survival of cardiomyocytes in vitro and protects against ischemia-reperfusion injury in mouse heart*." Circulation 101(6): 660-667.

G

Gabai, V. L. (1993). "*Inhibition of uncoupled respiration in tumor cells. A possible role of mitochondrial Ca2+ efflux*." FEBS Lett 329(1-2): 67-71.

Gambacorti-Passerini, C., *et al.* (1997). "*Inhibition of the ABL kinase activity blocks the proliferation of BCR/ABL(+) leukemic cells and induces apoptosis*." Blood Cells Molecules and Diseases 23(19): 380-394.

Gambacorti, C., *et al.* (2007). "*In reply to 'Cardiotoxicity of the cancer therapeutic agent imatinib mesylate'*." Nat Med 13(1): 13-14.

Gething, M. J., *et al.* (1992). "*Protein folding in the cell*." Nature 355(6355): 33-45.

Gewirtz, D. A. (1999). "*A critical evaluation of the mechanisms of action proposed for the antitumor effects of the anthracycline antibiotics Adriamycin and daunorubicin*." Biochemical Pharmacology 57(7): 727-741.

Gong, J. G., *et al.* (1999). "*The tyrosine kinase c-Abl regulates p73 in apoptotic response to cisplatin-induced DNA damage*." Nature 399(6738): 806-809.

Gottesman, M. M. (1993). "*How Cancer-Cells Evade Chemotherapy - 16th Richard-And-Hinda-Rosenthal-Foundation Award Lecture*." Cancer Research 53(4): 747-754.

Gottesman, M. M., *et al.* (1988). "*The Multidrug Transporter, A Double-Edged Sword*." Journal of Biological Chemistry 263(25): 12163-12166.

Gottschalk, S., *et al.* (2004). Imatinib (STI571)-Mediated Changes in Glucose Metabolism in Human Leukemia BCR-ABL-Positive Cells. **10:** 6661-6668.

Green, D. R., *et al.* (2004). "*The pathophysiology of mitochondrial cell death*." Science 305(5684): 626-629.

Greene, R. F., *et al.* (1983). "*Plasma Pharmacokinetics of Adriamycin and Adriamycinol - Implications for the Design of Invitro Experiments and Treatment Protocols*." Cancer Research 43(7): 3417-3421.

Gregor Malich, B. M., Chris Winder (1997). "*The sensitivity and specificity of the MTS tetrazolium assay for detecting the in vitro cytotoxicity of 20 chemicals using human cell lines*." Toxicology 124(3): 179-192.

Griendling, K. K., *et al.* (2000). "*NAD(P)H Oxidase : Role in Cardiovascular Biology and Disease*." Circulation Research 86(5): 494-501.

Gross, A. W., *et al.* (1999). "*Bcr-Abl with an SH3 deletion retains the ability to induce a myeloproliferative disease in mice, yet c-Abl activated by an SH3 deletion induces only lymphoid malignancy*." Molecular and Cellular Biology 19(10): 6918-6928.

Gschwind, H.-P.*, et al.* (2005). Metabolism and disposition of imatinib mesylate in healthy volunteers. **33:** 1503-1512.

H

Ha, H. C.*, et al.* (1999). "*Poly(ADP-ribose) polymerase is a mediator of necrotic cell death by ATP depletion*." Proceedings of the National Academy of Sciences of the United States of America 96(24): 13978-13982.

Haidle, A. M.*, et al.* (2004). "*An enantioselective, modular, and general route to the cytochalasins: Synthesis of L-696,474 and cytochalasin B 1*." Proceedings of the National Academy of Sciences of the United States of America 101(33): 12048-12053.

Hamada, A.*, et al.* (2003). "*Interaction of Imatinib Mesilate with Human P-Glycoprotein*." Journal of Pharmacology and Experimental Therapeutics 307(2): 824-828.

Han, X.*, et al.* (2008). "*Protective effects of naringenin-7-O-glucoside on doxorubicin-induced apoptosis in H9C2 cells*." European Journal of Pharmacology 581(1-2): 47-53.

Hanks, S. K. (2003). "*Genomic analysis of the eukaryotic protein kinase superfamily: a perspective*." Genome Biology 4(5).

Hannon, G. J.*, et al.* (1991). "*Multiple Cis-Acting Elements Are Required for Rna Polymerase-Iii Transcription of the Gene Encoding H1 RNA, the RNA Component of Human RNAse-P*." Journal of Biological Chemistry 266(34): 22796-22799.

Hantschel, O.*, et al.* (2003). "*A Myristoyl/Phosphotyrosine Switch Regulates c-Abl*." Cell 112(6): 845-857.

Hantschel, O.*, et al.* (2004). "*Regulation of the c-Abl and Bcr-Abl tyrosine kinases*." Nature Reviews Molecular Cell Biology 5(1): 33-44.

Harding, H. P.*, et al.* (2000). "*Regulated Translation Initiation Controls Stress-Induced Gene Expression in Mammalian Cells*." 6(5): 1099-1108.

Harding, H. P.*, et al.* (2000). "*Perk is essential for translational regulation and cell survival during the unfolded protein response*." Mol Cell 5(5): 897-904.

Harding, H. P.*, et al.* (1999). "*Protein translation and folding are coupled by an endoplasmic-reticulum-resident kinase*." Nature 397(6716): 271-274.

Harrison, S. C. (2003). "*Variation on an Src-like theme*." Cell 112(6): 737-740.

Hatfield, A.*, et al.* (2007). "*In reply to 'Cardiotoxicity of the cancer therapeutic agent imatinib mesylate'*." Nature Medicine 13(1): 13-13.

Haze, K.*, et al.* (1999). "*Mammalian transcription factor ATF6 is synthesized as a transmembrane protein and activated by proteolysis in response to endoplasmic reticulum stress*." Molecular Biology of the Cell 10(11): 3787-3799.

Heinrich, M. C.*, et al.* (2000). "*Inhibition of c-kit receptor tyrosine kinase activity by STI 571, a selective tyrosine kinase inhibitor*." Blood 96(3): 925-932.

Heytler, P. G. (1963). "*Uncoupling of Oxidative Phosphorylation by Carbonyl Cyanide Phenylhydrazones .1. Some Characteristics of M-Cl-CCP Action on Mitochondria and Chloroplasts*." Biochemistry 2(2): 357-&.

Hirota, H.*, et al.* (1999). "*Loss of a gp130 cardiac muscle cell survival pathway is a critical event in the onset of heart failure during biomechanical stress*." Cell 97(2): 189-198.

Holen, T.*, et al.* (2002). "*Positional effects of short interfering RNAs targeting the human coagulation trigger Tissue Factor*." Nucleic Acids Research 30(8): 1757-1766.

Homburg, C. H. E.*, et al.* (1995). "*Human Neutrophils Lose Their Surface Fc-Gamma-Riii and Acquire Annexin-V Binding-Sites During Apoptosis In-Vitro*." Blood 85(2): 532-540.

Huang, Y. Y.*, et al.* (1997). "*Pro-apoptotic effect of the c-Abl tyrosine kinase in the cellular response to 1-beta-D-arabinofuranosylcytosine*." Oncogene 15(16): 1947-1952.

Hubbard, S. R.*, et al.* (1998). "*Autoregulatory mechanisms in protein-tyrosine kinases*." Journal of Biological Chemistry 273(20): 11987-11990.

Hutvagner, G.*, et al.* (2002). "*A microRNA in a Multiple-Turnover RNAi Enzyme Complex*." Science 297(5589): 2056-2060.

I

Issels, R. D.*, et al.* (1988). "*Promotion of Cystine Uptake and Its Utilization for Glutathione Biosynthesis Induced by Cysteamine and N-Acetylcysteine*." Biochemical Pharmacology 37(5): 881-888.

Ito, T.*, et al.* (2006). "*Degradation of NFAT5, a transcriptional regulator of osmotic stress-related genes is a critical event for doxorubicin-induced cytotoxicity in cardiac myocytes*." Journal of Biological Chemistry: M609547200.

Iverson, S. L.*, et al.* (2004). "*The cardiolipin-cytochrome c interaction and the mitochondrial regulation of apoptosis*." Archives of Biochemistry and Biophysics 423(1): 37-46.

J

Jackson, A. L.*, et al.* (2003). "*Expression profiling reveals off-target gene regulation by RNAi*." Nature Biotechnology 21(6): 635-637.

Jeyaseelan, R.*, et al.* (1997). "*Molecular Mechanisms of Doxorubicin-induced Cardiomyopathy. Selective suppression of reiske iron-sulfur protein, ADP/ATP translocase, and phosphofructokinase genes is associated with ATP depletion in rat cardiomyocytes.*" Journal of Biological Chemistry 272(9): 5828-5832.

Jiang, H. Y.*, et al.* (2003). "*Phosphorylation of the a subunit of eukaryotic initiation factor 2 is required for activation of NF-kappa B in response to diverse cellular stresses*." Molecular and Cellular Biology 23(16): 5651-5663.

Johnson, L. N.*, et al.* (1996). "*Active and inactive protein kinases: Structural basis for regulation*." Cell 85(2): 149-158.

Jordanides, N. E.*, et al.* (2006). "*Functional ABCG2 is overexpressed on primary CML CD34+ cells and is inhibited by imatinib mesylate*." Blood 108(4): 1370-1373.

K

Karthikeyan, G.*, et al.* (2003). "*Reduction in frataxin causes progressive accumulation of mitochondrial damage*." Human Molecular Genetics 12(24): 3331-3342.

Kawai, T.*, et al.* (2006). "*Innate immune recognition of viral infection*." Nature Immunology 7(2): 131-137.

Kawasaki, H.*, et al.* (2003). "*Short hairpin type of dsRNAs that are controlled by tRNAVal promoter significantly induce RNAi-mediated gene silencing in the cytoplasm of human cells*." Nucleic Acids Research 31(2): 700-707.

Kerkelä, R.*, et al.* (2006). "*Cardiotoxicity of the cancer therapeutic agent imatinib mesylate*." Nature Medicine 12(8): 908-916.

Ketting, R. F.*, et al.* (2001). "*Dicer functions in RNA interference and in synthesis of small RNA involved in developmental timing in C-elegans*." Genes & Development 15(20): 2654-2659.

Kharbanda, S.*, et al.* (1998). "*Functional role for the c-Abl tyrosine kinase in meiosis I*." Oncogene 16(14): 1773-1777.

Kharbanda, S.*, et al.* (2000). "*Activation of MEK kinase 1 by the c-Abl protein tyrosine kinase in response to DNA damage*." Molecular and Cellular Biology 20(14): 4979-4989.

Kharbanda, S.*, et al.* (1995). "*Activation of the C-Abl Tyrosine Kinase in the Stress-Response to Dna-Damaging Agents*." Nature 376(6543): 785-788.

Kimes, B.*, et al.* (1976). "*Properties of a clonal muscle cell line from rat heart*." Exp Cell Res. 98(2): 367-381.

Kitamura, Y., *et al.* (2003). "*Possible Involvement of Both Endoplasmic Reticulum-and Mitochondria-Dependent Pathways in Thapsigargin-Induced Apoptosis in Human Neuroblastoma SH-SY5Y Cells*." Journal of Pharmacological Sciences 92(3): 228-236.

Kokenberg, E., *et al.* (1988). "*Cellular Pharmacokinetics of Daunorubicin - Relationships with the Response to Treatment in Patients with Acute Myeloid-Leukemia*." Journal of Clinical Oncology 6(5): 802-812.

Koong, A. C., *et al.* (2006). "*Targeting XBP-1 as a novel anti-cancer strategy*." Cancer Biol Ther 5(7): 756-9.

Kovacic, P., *et al.* (2001). "*Mechanisms of carcinogenesis: Focus on oxidative stress and electron transfer*." Current Medicinal Chemistry 8(7): 773-796.

Kozutsumi, Y., *et al.* (1988). "*The Presence of Malfolded Proteins in the Endoplasmic-Reticulum Signals the Induction of Glucose-Regulated Proteins*." Nature 332(6163): 462-464.

Kumar, S., *et al.* (2001). "*Targeting of the c-Abl Tyrosine Kinase to Mitochondria in the Necrotic Cell Death Response to Oxidative Stress*." Journal of Biological Chemistry 276(20): 17281-17285.

Kuznetsov, G., *et al.* (1993). "*Role of endoplasmic reticular calcium in oligosaccharide processing of alpha 1-antitrypsin*." J Biol Chem 268(3): 2001-8.

L

Laneuville, P. (1995). "*Abl tyrosine protein kinase*." Seminars in Immunology 7(4): 255-266.

Lasfer, M., *et al.* (2006). "*Protein kinase PKC delta and c-Abl are required for mitochondrial apoptosis induction by genotoxic stress in the absence of p53, p73 and Fas receptor*." FEBS Lett 580(11): 2547-52.

Lazebnik, Y. A., *et al.* (1994). "*Cleavage of Poly(Adp-Ribose) Polymerase by A Proteinase with Properties Like Ice 5*." Nature 371(6495): 346-347.

Lefrak, E. A., *et al.* (1973). "*A clinicopathologic analysis of adriamycin cardiotoxicity*." Cancer 32(2): 302-14.

Legros, F., *et al.* (2002). Mitochondrial Fusion in Human Cells Is Efficient, Requires the Inner Membrane Potential, and Is Mediated by Mitofusins. **13:** 4343-4354.

Lennon, S. V., *et al.* (1991). "*Dose-Dependent Induction of Apoptosis in Human Tumor-Cell Lines by Widely Diverging Stimuli*." Cell Proliferation 24(2): 203-214.

Lewis, J. M., *et al.* (1996). "*Integrin regulation of c-Abl tyrosine kinase activity and cytoplasmic-nuclear transport*." Proceedings of the National Academy of Sciences of the United States of America 93(26): 15174-15179.

Li, F., *et al.* (1996). "*Rapid Transition of Cardiac Myocytes from Hyperplasia to Hypertrophy During Postnatal Development*." Journal of Molecular and Cellular Cardiology 28(8): 1737-1746.

Li, P., *et al.* (1997). "*Cytochrome c and dATP-dependent formation of Apaf-1/caspase-9 complex initiates an apoptotic protease cascade*." Cell 91(4): 479-489.

Limaye, D. A., *et al.* (1999). "*Cytotoxicity of cadmium and characteristics of its transport in cardiomyocytes*." Toxicology and Applied Pharmacology 154(1): 59-66.

Lin, J. H., *et al.* (2007). IRE1 Signaling Affects Cell Fate During the Unfolded Protein Response. **318:** 944-949.

Liu, Q., *et al.* (1996). "*Insulin-like Growth Factor II Induces DNA Synthesis in Fetal Ventricular Myocytes In Vitro*." Circulation Research 79(4): 716-726.

Liu, Z. G., *et al.* (1996). "*Three distinct signalling responses by murine fibroblasts to genotoxic stress*." Nature 384(6606): 273-276.

Lo, Y. Y. C., *et al.* (1995). Involvement of Reactive Oxygen Species in Cytokine and Growth Factor Induction of c-fos Expression in Chondrocytes. **270:** 11727-11730.

Locksley, R. M., *et al.* (2001). "*The TNF and TNF receptor superfamilies: Integrating mammalian biology*." Cell 104(4): 487-501.

Lutter, M., *et al.* (2000). "*Cardiolipin provides specificity for targeting of tBid to mitochondria*." Nature Cell Biology 2(10): 754-756.

M

Ma, Y., *et al.* (2004). "*The role of the unfolded protein response in tumour development: friend or foe?*" Nat Rev Cancer 4(12): 966-977.

Ma, Y. J., *et al.* (2003). "*Delineation of a negative feedback regulatory loop that controls protein translation during endoplasmic reticulum stress*." Journal of Biological Chemistry 278(37): 34864-34873.

Ma, Y. J., *et al.* (2004). "*ER chaperone functions during normal and stress conditions*." Journal of Chemical Neuroanatomy 28(1-2): 51-65.

Mann, D. L. (2006). "*Targeted cancer therapeutics: the heartbreak of success*." Nat Med 12(8): 881-2.

Marques, J. T., *et al.* (2006). "*A structural basis for discriminating between self and nonself double-stranded RNAs in mammalian cells*." Nat Biotech 24(5): 559-565.

Martin, S. J., *et al.* (1995). "*Early Redistribution of Plasma-Membrane Phosphatidylserine Is A General Feature of Apoptosis Regardless of the Initiating Stimulus - Inhibition by Overexpression of Bcl-2 and Abl 2*." Journal of Experimental Medicine 182(5): 1545-1556.

Martinez, J., *et al.* (2002). "*Single-stranded antisense siRNAs guide target RNA cleavage in RNAi*." Cell 110(5): 563-74.

Mathers, C., *et al.* (2006). "*Projections of global mortality and burden of disease from 2002 to 2030*." PLoS Medicine 3: 2011-2030.

Matsumoto, M., *et al.* (1996). "*Ectopic expression of CHOP (GADD153) induces apoptosis in M1 myeloblastic leukemia cells*." FEBS Lett 395(2-3): 143-7.

Mccall, M. R., *et al.* (1999). "*Can antioxidant vitamins materially reduce oxidative damage in humans?*" Free Radical Biology and Medicine 26(7-8): 1034-1053.

Mccullough, K. D., *et al.* (2001). "*Gadd153 sensitizes cells to endoplasmic reticulum stress by down-regulating Bc12 and perturbing the cellular redox state*." Molecular and Cellular Biology 21(4): 1249-1259.

Mcmanus, M. T., *et al.* (2002). "*Small interfering RNA-mediated gene silencing in T lymphocytes*." Journal of Immunology 169(10): 5754-5760.

Menna, P., *et al.* (2007). "*Doxorubicin Degradation in Cardiomyocytes*." Journal of Pharmacology and Experimental Therapeutics 322(1): 408-419.

Minotti, G., *et al.* (2004). "*Anthracyclines: Molecular advances and pharmacologic developments in antitumor activity and cardiotoxicity*." Pharmacological Reviews 56(2): 185-229.

Mori, K. (2000). "*Tripartite Management of Unfolded Proteins in the Endoplasmic Reticulum*." Cell 101(5): 451-454.

Mu, L., *et al.* (2003). "*PLGA/TPGS nanoparticles for controlled release of paclitaxel: Effects of the emulsifier and drug loading ratio*." Pharmaceutical Research 20(11): 1864-1872.

N

Nagar, B., *et al.* (2003). "*Structural basis for the autoinhibition of c-Abl tyrosine kinase*." Cell 112(6): 859-871.

Novartis (2001). GLEEVEC (imatinib mesylate) Capsules - Draft Package Insert. East Hanover, New Jersey, Novartis Pharmaceuticals Corporation. **2008**.

Novartis. (2005, 28.08.2006). "Gleevec(R) - Tablets." 2008, from http://www.medicineonline.com/drugs/G/1333/Gleevec-Tablets.html.

O

O'brien, S. G., *et al.* (2003). "*Imatinib compared with interferon and low-dose cytarabine for newly diagnosed chronic-phase chronic myeloid leukemia*." N.Engl.J.Med. 348: 994.

Ott, M.*, et al.* (2002). "*Cytochrome c release from mitochondria proceeds by a two-step process*." Proceedings of the National Academy of Sciences of the United States of America 99(3): 1259-1263.

Oyadomari, S.*, et al.* (2004). "*Roles of CHOP/GADD153 in endoplasmic reticulum stress*." Cell Death and Differentiation 11(4): 381-389.

P

Paddison, P. J.*, et al.* (2002). "*Short hairpin RNAs (shRNAs) induce sequence-specific silencing in mammalian cells*." Genes & Development 16(8): 948-958.

Pan, G. H.*, et al.* (1998). "*Identification and functional characterization of DR6, a novel death domain-containing TNF receptor*." Febs Letters 431(3): 351-356.

Pappas, P.*, et al.* (2005). "*Pharmacokinetics of imatinib mesylate in end stage renal disease. A case study*." Cancer Chemotherapy and Pharmacology 56(4): 358-360.

Paracchini, L.*, et al.* (1993). "*The Spin Trap Alpha-Phenyl-Tert-Butyl Nitrone Protects Against Myelotoxicity and Cardiotoxicity of Adriamycin While Preserving the Cytotoxic Activity*." Anticancer Research 13(5A): 1607-1612.

Park, H. S.*, et al.* (2004). Cutting Edge: Direct Interaction of TLR4 with NAD(P)H Oxidase 4 Isozyme Is Essential for Lipopolysaccharide-Induced Production of Reactive Oxygen Species and Activation of NF-{kappa}B. **173:** 3589-3593.

Park, Y. H.*, et al.* (2006). "*BNP as a marker of the heart failure in the treatment of imatinib mesylate*." Cancer Lett 243(1): 16-22.

Pattacini, L.*, et al.* (2004). "*Endoplasmic reticulum stress initiates apoptotic death induced by STI571 inhibition of p210 bcr-abl tyrosine kinase*." Leukemia Research 28(2): 191-202.

Paule, M. R.*, et al.* (2000). "*Transcription by RNA polymerases I and III*." Nucleic Acids Research 28(6): 1283-1298.

Pawson, T.*, et al.* (1997). "*Signaling through scaffold, anchoring, and adaptor proteins*." Science 278(5346): 2075-2080.

Pendergast, A. M. (2002). "*The Abl family kinases: Mechanisms of regulation and signaling*." Advances in Cancer Research, Vol 85 85: 51-100.

Pendergast, A. M.*, et al.* (1991). "*Evidence for Regulation of the Human Abl Tyrosine Kinase by A Cellular Inhibitor*." Proceedings of the National Academy of Sciences of the United States of America 88(13): 5927-5931.

Peng, B.*, et al.* (2005). "*In Reply To 'Elimination of Imatinib Mesylate and Its Metabolite N-Desmethyl-Imatinib'*." Journal of Clinical Oncology 23(16): 3857-3858.

Peng, B.*, et al.* (2004). "*Pharmacokinetics and pharmacodynamics of imatinib in a phase I trial with chronic myeloid leukemia patients*." Journal of Clinical Oncology 22(5): 935-942.

Persengiev, S. P.*, et al.* (2004). "*Nonspecific, concentration-dependent stimulation and repression of mammalian gene expression by small interfering RNAs (siRNAs)*." Rna-A Publication of the Rna Society 10(1): 12-18.

Petit, C.*, et al.* (2005). "*Oxygen consumption by cultured human cells is impaired by a nucleoside analogue cocktail that inhibits mitochondrial DNA synthesis*." Mitochondrion 5(3): 154-61.

Plattner, R.*, et al.* (2003). "*A new link between the c-Abl tyrosine kinase and phosphoinositide signalling through PLC-[gamma]*." Nat Cell Biol 5(4): 309-319.

Plattner, R.*, et al.* (1999). "*c-Abl is activated by growth factors and Src family kinases and has a role in the cellular response to PDGF*." Genes and Development 13(18): 2400-2411.

Pluk, H.*, et al.* (2002). "*Autoinhibition of c-Abl*." Cell 108(2): 247-259.

Pollack, I. F.*, et al.* (2007). Phase I trial of imatinib in children with newly diagnosed brainstem and recurrent malignant gliomas: A Pediatric Brain Tumor Consortium report. **9:** 145-160.

Pradhan, D.*, et al.* (1997). "*Multiple systems for recognition of apoptotic lymphocytes by macrophages*." Molecular Biology of the Cell 8(5): 767-778.

Putral, L. N.*, et al.* (2006). "*RNA interference for the treatment of cancer*." Drug News & Perspectives 19(6): 317-324.

Q

Qi, X.*, et al.* (2008). "*The PKCdelta -Abl complex communicates ER stress to the mitochondria - an essential step in subsequent apoptosis*." J Cell Sci 121(Pt 6): 804-13.

R

Raina, D.*, et al.* (2005). "*c-Abl tyrosine kinase regulates caspase-9 autocleavage in the apoptotic response to DNA damage*." Journal of Biological Chemistry 280(12): 11147-11151.

Rampal, A. L.*, et al.* (1980). "*Structure of Cytochalasins and Cytochalasin-B Binding-Sites in Human-Erythrocyte Membranes*." Biochemistry 19(4): 679-683.

Rawer, D. (2005). Real-Time PCR: Optimierung und Evaluation, Etablierung von Housekeeping-Genen und die Expressionsanalyse bei Fallotscher Tetralogie, Uni Giessen.

Ren, R. (2005). "*Mechanisms of BCR-ABL in the pathogenesis of chronic myelogenous leukaemia*." Nature Reviews Cancer 5(3): 172-183.

Renshaw, M. W*., et al.* (1988). "*Differential Expression of Type-Specific C-Abl Messenger-Rnas in Mouse-Tissues and Cell-Lines*." Molecular and Cellular Biology 8(10): 4547-4551.

Ridnour, L. A*., et al.* (2005). "*Nitric oxide regulates angiogenesis through a functional switch involving thrombospondin-1*." Proceedings of the National Academy of Sciences of the United States of America 102(37): 13147-13152.

Robbins, M. A*., et al.* (2006). "*Stable expression of shRNAs in human CD34+ progenitor cells can avoid induction of interferon responses to siRNAs in vitro*." Nat Biotech 24(5): 566-571.

Romano, G. (2006). "*The controversial role of adenoviral-derived vectors in gene therapy programs: where do we stand?*" Drug News Perspect 19(2): 99-106.

Ron, D. (2002). "*Translational control in the endoplasmic reticulum stress response*." J Clin Invest 110(10): 1383-8.

Ron, D*., et al.* (1992). "*CHOP, a novel developmentally regulated nuclear protein that dimerizes with transcription factors C/EBP and LAP and functions as a dominant-negative inhibitor of gene transcription*." Genes Dev 6(3): 439-53.

Rowley, J. D. (1973). "*A new consistent chromosomal abnormality in chronic myelogenous leukaemia identified by quinacrine fluorescence and Giemsa staining*." Nature 243: 290.

S

Samuel, C. E. (2001). "*Antiviral actions of interferons*." Clin Microbiol Rev 14(4): 778-809, table of contents.

Sarvazyan, N. (1996). "*Visualization of doxorubicin-induced oxidative stress in isolated cardiac myocytes*." American Journal of Physiology-Heart and Circulatory Physiology 40(5): H2079-H2085.

Sattler, M*., et al.* (2000). The BCR/ABL Tyrosine Kinase Induces Production of Reactive Oxygen Species in Hematopoietic Cells. **275:** 24273-24278.

Sattler, M*., et al.* (1999). Hematopoietic Growth Factors Signal Through the Formation of Reactive Oxygen Species. **93:** 2928-2935.

Savill, J. (1997). "*Recognition and phagocytosis of cells undergoing apoptosis*." British Medical Bulletin 53(3): 491-508.

Sawyers, C. L. (1999). "*Chronic Myeloid Leukemia*." The New England Journal of Medicine 340(17): 1330-1340.

Scaffidi, C.*, et al.* (1998). "*Two CD95 (APO-1/Fas) signaling pathways*." Embo Journal 17(6): 1675-1687.

Scherer, L.*, et al.* (2004). "*RNAi applications in mammalian cells*." Biotechniques 36(4): 557-+.

Scherer, L. J.*, et al.* (2003). "*Approaches for the sequence-specific knockdown of mRNA*." Nat Biotech 21(12): 1457-1465.

Scherr, M.*, et al.* (2003). "*Specific inhibition of bcr-abl gene expression by small interfering RNA*." Blood 101(4): 1566-1569.

Scheuner, D.*, et al.* (2001). "*Translational Control Is Required for the Unfolded Protein Response and In Vivo Glucose Homeostasis*." 7(6): 1165-1176.

Schindler, T.*, et al.* (2000). "*Structural mechanism for STI-571 inhibition of abelson tyrosine kinase*." Science 289: 1857.

Schliwa, M. (1982). "*Action of Cytochalasin-D on Cytoskeletal Networks*." Journal of Cell Biology 92(1): 79-91.

Scholz, W.*, et al.* (1990). "*Phenobarbital Enhances the Formation of Reactive Oxygen in Neoplastic Rat-Liver Nodules*." Cancer Research 50(21): 7015-7022.

Schwartzberg, P. L.*, et al.* (1991). "*Mice Homozygous for the Ablm1 Mutation Show Poor Viability and Depletion of Selected B-Cell and T-Cell Populations*." Cell 65(7): 1165-1175.

Schwarz, D. S.*, et al.* (2003). "*Asymmetry in the assembly of the RNAi enzyme complex*." Cell 115(2): 199-208.

Schwarz, D. S.*, et al.* (2002). "*Evidence that siRNAs Function as Guides, Not Primers, in the Drosophila and Human RNAi Pathways*." Molecular Cell 10(3): 537-548.

Shamu, C. E.*, et al.* (1996). "*Oligomerization and phosphorylation of the Ire1p kinase during intracellular signaling from the endoplasmic reticulum to the nucleus*." Embo Journal 15(12): 3028-3039.

Shaul, Y. (2000). "*c-Abl: activation and nuclear targets*." Cell Death and Differentiation 7(1): 10-16.

Shen, J.*, et al.* (2003). Oxygen Consumption Rates and Oxygen Concentration in Molt-4 Cells and Their mtDNA Depleted ({rho}0) Mutants. **84:** 1291-1298.

Shen, J. S.*, et al.* (2002). "*ER stress regulation of ATF6 localization by dissociation of BiP/GRP78 binding and unmasking of golgi localization signals*." Developmental Cell 3(1): 99-111.

Shi, Y. G. (2002). "*Mechanisms of caspase activation and inhibition during apoptosis*." Molecular Cell 9(3): 459-470.

Shi, Y. G., *et al.* (1998). "*Identification and characterization of pancreatic eukaryotic initiation factor 2 alpha-subunit kinase, PEK, involved in translational control*." Molecular and Cellular Biology 18(12): 7499-7509.

Sioud, M. (2005). "*Induction of Inflammatory Cytokines and Interferon Responses by Double-stranded and Single-stranded siRNAs is Sequence-dependent and Requires Endosomal Localization*." Journal of Molecular Biology 348(5): 1079-1090.

Smith, J. M., *et al.* (2002). "*Abl: Mechanisms of regulation and activation*." Frontiers in Bioscience 7: D31-D42.

Sokol, R. J., *et al.* (1991). "*Improvement of Cyclosporine Absorption in Children After Liver-Transplantation by Means of Water-Soluble Vitamin-e*." Lancet 338(8761): 212-215.

Sole, M., *et al.* (2000). "*Rapid extracellular acidification induced by glucose metabolism in non-proliferating cells of Serratia marcescens*." Int Microbiol 3(1): 39-43.

Soubeyran, P., *et al.* (2003). "*Cbl-ArgBP2 complex mediates ubiquitination and degradation of c-Abl*." Biochemical Journal 370(1): 29-34.

Speth, P. A. J., *et al.* (1987). "*Cellular and plasma adriamycin concentrations in long-term infusion therapy of leukemia patients*." Cancer Chemotherapy and Pharmacology 20(4): 305-310.

Stanley, W. C., *et al.* (2005). "*Myocardial substrate metabolism in the normal and failing heart*." Physiol Rev 85(3): 1093-129.

Sun, X. G., *et al.* (2000). "*Interaction between protein kinase C delta and the c-Abl tyrosine kinase in the cellular response to oxidative stress*." Journal of Biological Chemistry 275(11): 7470-7473.

Sutherland, F. J., *et al.* (2000). "*The isolated blood and perfusion fluid perfused heart*." Pharmacological Research 41(6): 613-627.

T

Thien, C. B. F., *et al.* (2001). "*Cbl: Many adaptations to regulate protein tyrosine kinases*." Nature Reviews Molecular Cell Biology 2(4): 294-305.

Thornberry, N. A., *et al.* (1998). "*Caspases: Enemies within* " Science 281(5381): 1312-1316.

Thornberry, N. A., *et al.* (1997). "*A Combinatorial Approach Defines Specificities of Members of the Caspase Family and Granzyme B. FUNCTIONAL RELATIONSHIPS ESTABLISHED FOR KEY MEDIATORS OF APOPTOSIS*." Journal of Biological Chemistry 272(29): 17907-17911.

Tirasophon, W., *et al.* (1998). "*A stress response pathway from the endoplasmic reticulum to the nucleus requires a novel bifunctional protein*

kinase/endoribonuclease (Ire1p) in mammalian cells." Genes & Development 12(12): 1812-1824.

Traber, M. G.*, et al.* (1988). "*Uptake of intact TPGS (d-alpha-tocopheryl polyethylene glycol 1000 succinate) a water-miscible form of vitamin E by human cells in vitro*." American Journal of Clinical Nutrition 48(3): 605-611.

Tuominen, E. K. J.*, et al.* (2002). "*Phospholipid-cytochrome c interaction - Evidence for the extended lipid anchorage*." Journal of Biological Chemistry 277(11): 8822-8826.

Tybulewicz, V. L.*, et al.* (1991). "*Neonatal lethality and lymphopenia in mice with a homozygous disruption of the c-abl proto-oncogene*." Cell 65(7): 1153-63.

U

Urano, F.*, et al.* (2000). "*Coupling of Stress in the ER to Activation of JNK Protein Kinases by Transmembrane Protein Kinase IRE1*." Science 287(5453): 664-666.

V

Valko, M.*, et al.* (2004). "*Role of oxygen radicals in DNA damage and cancer incidence*." Molecular and Cellular Biochemistry 266(1-2): 37-56.

Valko, M.*, et al.* (2001). "*Oxygen free radical generating mechanisms in the colon: do the semiquinones of vitamin K play a role in the aetiology of colon cancer?*" Biochimica et Biophysica Acta-General Subjects 1527(3): 161-166.

Valko, M.*, et al.* (2006). "*Free radicals, metals and antioxidants in oxidative stress-induced cancer*." Chemico-Biological Interactions 160(1): 1-40.

Van Etten, R. A.*, et al.* (1995). "*Introduction of A Loss-Of-Function Point Mutation from the Sh3 Region of the Caenorhabditis-Elegans Sem-5 Gene Activates the Transforming Ability of C-Abl In-Vivo and Abolishes Binding of Proline-Rich Ligands In-Vitro*." Oncogene 10(10): 1977-1988.

Van Etten, R. A.*, et al.* (1989). "*The mouse type IV c-abl gene product is a nuclear protein, and activation of transforming ability is associated with cytoplasmic localization*." Cell 58: 669.

Vigneri, P.*, et al.* (2001). "*Induction of apoptosis in chronic myelogenous leukemia cells through nuclear entrapment of BCR-ABL tyrosine kinase*." Nat.Med. 7: 228.

Vittal, R.*, et al.* (2007). "*Effects of the Protein Kinase Inhibitor, Imatinib Mesylate, on Epithelial/Mesenchymal Phenotypes: Implications for Treatment of Fibrotic Diseases*." Journal of Pharmacology and Experimental Therapeutics 321(1): 35-44.

W

Waalen, J. (2001). "*Gleevec's Glory Days*." HHMI Bulletin: 10-15.

Wang, B., *et al.* (1997). "*ArgBP2, a multiple Src homology 3 domain-containing, Arg/Abl-interacting protein, is phosphorylated in v-Abl-transformed cells and localized in stress fibers and cardiocyte Z-disks*." J Biol Chem 272(28): 17542-50.

Weiss, S. J., *et al.* (1982). "*Phagocyte-Generated Oxygen Metabolites and Cellular Injury*." Laboratory Investigation 47(1): 5-18.

Welch, P. J., *et al.* (1993). "*A C-Terminal Protein-Binding Domain in the Retinoblastoma Protein Regulates Nuclear C-Abl Tyrosine Kinase in the Cell-Cycle*." Cell 75(4): 779-790.

Welch, P. J., *et al.* (1995). "*Disruption of Retinoblastoma Protein Function by Coexpression of Its C-Pocket Fragment*." Genes & Development 9(1): 31-46.

Wen, S. T., *et al.* (1997). "*The PAG gene product, a stress-induced protein with antioxidant properties, is an Abl SH3-binding protein and a physiological inhibitor of c-Abl tyrosine kinase activity*." Genes & Development 11(19): 2456-2467.

Wenzel, D. G., *et al.* (1970). "*Effects of Nicotine on Cultured Rat Heart Cells*." Toxicology and Applied Pharmacology 17(3): 774-&.

Wenzel, S., *et al.* (2006). "*Contribution of PI 3-kinase isoforms to angiotensin II- and [alpha]-adrenoceptor-mediated signalling pathways in cardiomyocytes*." Cardiovascular Research 71(2): 352-362.

Who. (2006). "Cancer, Fact sheet Nø297." Retrieved 15.06.2008, 2008, from http://www.who.int/mediacentre/factsheets/fs297/en/index.html.

Will, Y., *et al.* (2008). Effect of the Multitargeted Tyrosine Kinase Inhibitors Imatinib, Dasatinib, Sunitinib, and Sorafenib on Mitochondrial Function in Isolated Rat Heart Mitochondria and H9c2 Cells. **106:** 153-161.

Williams, B. R. G. (1999). "*PKR; a sentinel kinase for cellular stress*." Oncogene 18(45): 6112-6120.

Wittenberg, B. A., *et al.* (1985). Oxygen pressure gradients in isolated cardiac myocytes. **260:** 6548-6554.

Wong, S., *et al.* (2004). "*The BCR-ABL story: Bench to bedside and back*." Annual Review of Immunology 22: 247-306.

X

Xu, W. Q., *et al.* (1999). "*Crystal structures of c-Src reveal features of its autoinhibitory mechanism*." Molecular Cell 3(5): 629-638.

Y

Yahara, I.*, et al.* (1982). "*Correlation between effects of 24 different cytochalasins on cellular structures and cellular events and those on actin in vitro*." The Journal of Cell Biology 92(1): 69-78.

Yakes, F. M.*, et al.* (1997). "*Mitochondrial DNA damage is more extensive and persists longer than nuclear DNA damage in human cells following oxidative stress*." Proceedings of the National Academy of Sciences of the United States of America 94(2): 514-519.

Ye, J.*, et al.* (2000). "*ER stress induces cleavage of membrane-bound ATF6 by the same proteases that process SREBPs*." Molecular Cell 6(6): 1355-1364.

Yoneyama, M.*, et al.* (2004). "*The RNA helicase RIG-I has an essential function in double-stranded RNA-induced innate antiviral responses*." Nat Immunol 5(7): 730-737.

Yoshida, H.*, et al.* (2001). "*XBP1 mRNA Is Induced by ATF6 and Spliced by IRE1 in Response to ER Stress to Produce a Highly Active Transcription Factor*." Cell 107(7): 881-891.

Yoshida, K.*, et al.* (2005). "*JNK phosphorylation of 14-3-3 proteins regulates nuclear targeting of c-Abl in the apoptotic response to DNA damage*." Nature Cell Biology 7(3): 278-U97.

Youk, H. J.*, et al.* (2005). "*Enhanced anticancer efficacy of [alpha]-tocopheryl succinate by conjugation with polyethylene glycol*." Journal of Controlled Release 107(1): 43-52.

Yuan, Z. M.*, et al.* (1997). "*Regulation of DNA damage-induced apoptosis by the c-Abl tyrosine kinase*." Proceedings of the National Academy of Sciences of the United States of America 94(4): 1437-1440.

Yuan, Z. M.*, et al.* (1999). "*P73 is regulated by tyrosine kinase c-Abl in the apoptotic response to DNA damage*." Nature 399(6738): 814-817.

Yuan, Z. M.*, et al.* (1998). "*Activation of protein kinase C delta by the c-Abl tyrosine kinase in response to ionizing radiation*." Oncogene 16(13): 1643-1648.

Z

Zafari, A. M.*, et al.* (1998). Role of NADH/NADPH Oxidase–Derived H2O2 in Angiotensin II–Induced Vascular Hypertrophy. **32:** 488-495.

Zeng, Y.*, et al.* (2002). "*RNA interference in human cells is restricted to the cytoplasm*." RNA 8(7): 855-860.

Zhang, H. D.*, et al.* (2002). "*Human Dicer preferentially cleaves dsRNAs at their termini without a requirement for ATP*." Embo Journal 21(21): 5875-5885.

Zhelev, Z., *et al.* (2004). "*Suppression of bcr-abl synthesis by siRNAs or tyrosine kinase activity by Glivec alters different oncogenes, apoptotic/antiapoptotic genes and cell proliferation factors (microarray study)*." Febs Letters 570(1-3): 195-204.

Zimmermann, J., *et al.* (1997). "*Potent and selective inhibitors of the Abl-kinase: Phenylamino-pyrimidine (PAP) derivatives*." Bioorganic & Medicinal Chemistry Letters 7(2): 187-192.

Zimmermann, J., *et al.* (1996). "*Phenylamino-pyrimidine (PAP) - derivatives: A new class of potent and highly selective PDGF-receptor autophosphorylation inhibitors*." Bioorganic & Medicinal Chemistry Letters 6(11): 1221-1226.

Zou, H., *et al.* (1997). "*Apaf-1, a Human Protein Homologous to C. elegans CED-4, Participates in Cytochrome c-Dependent Activation of Caspase-3*." Cell 90(3): 405-413.

8 APPENDIX

8.1 Acknowledgements

Zunächst möchte ich mich bei meinen ehemaligen Betreuern an der TU Kaiserslautern herzlich danken, insbesondere Melanie Esselen und Silke Germer!

Ein herzliches Dankeschön sende ich nach Warnemünde zu dem Team von Bionas. Ganz besonderen Dank an Sabine Drechsler, Axel Kob und Michael Schulze. Vielen Dank für die tolle Zeit bei Euch und die gute Zusammenarbeit!

Liebe Kollegen, die Zeit mit Euch war super, ich danke Euch für Eure liebe Art und die Zeit mit Euch. Vielen Dank Euch allen!!!
Danke auch an Dr. Wilfried Frieauff und seinen Mitarbeitern für die Nutzung des Labors sowie seiner Software zur Bestimmung der Herzfrequenz als auch seiner bereitwilligen Hilfe bei anstehenden Fragen.

Christian Strupp danke ich für sein offenes Ohr, seine Ratschläge und seine Hilfe. Es war nicht immer leicht, Dich als Vorgänger zu haben.

Ein herzliches Dankeschön auch an Clivia Stalder. Die Zeit mit Dir im Labor als auch im Büro war kurzweilig und lustig – nur leider viel zu kurz!

À tous mes bonnes copins français: Je vous remercie! Merci pour votre patience, en particulaire au debut. Parler francais n'était pas facile; donc, merci pour laisser me trouver une phrase. Jean-Michel Grenet: C'était un bon temps dans le bureau avec toi ! Je ne vais jamais oublier les 5 minutes avant 4 heures..... ;) Merci á Magali Marcellin: On a bien rigoler au debut, enfin, VOUS avez rigolé plus. Merci beaucoup pour ton amitié!
Siro Perez-Alcala, I'd like to thank you for the short time we've worked together. It was so much fun. Unfortunately I've discovered too lately what a good job you have done – thanks for it, I have profited! Hope we will meet again to finally visit Madrid and all do all the other stuff we planned to do!
Jonathan Moggs I adore the way you're leading and treating people. I do honestly hope to be able to adapt your way. Thanks for that!
Cher François Pognan, je te remercie pour avoir le temps de parler avec moi, expliquer des choses et pour les discussions. Tu m'as aidé beaucoup et tu m'as fait plus confidente – en fait, je l'éspère. Merci pour tes temps et tes aides !!!
Merci à Olivier Grenet, je suis heureuse que je pourrais faire mes PCR dans ta groupe. Je te remercie pour les discussions sur PCR, les résultats et les conclusions. C'était un honneur d'être une des gens qui ont pu jouer au foot avec toi !

Magali Marcellin, je te remercie beaucoup aussi pour tes efforts de me montrer et éxpliquer le PCR, les machines et les robots, quoi. J'éspère on n'arrête pas avec « la tradition », quoi! Manuela Goetschy, l'introduction à l'éxtraction d'ARN et tous tes aides étaient superbe, je te remercie beaucoup. Aussi avec ta mode d'archiver les data et faire des etiquettes – « concatenate » et des autres choses. Á mon chef de ARNi, « Monsieur » Philippe Couttet, un grand merci pour ton aide, tes instructions, ton temps et les discussions. Et, en plus, les trainings avec toi et « mes mecs » étaient si bien !
Morgane Ravon, je te remercie pour m'apprendre et aider avec le cloning. J'aimais bien travailler et parler avec toi, même il était un temps court.
Josiane Bringel, je voulais te dire que j'aimais bien d'être ensemble avec toi. Ton pince-sans-rire est marrante. Uh-là.... Je garderai un bon souvenir de toi. Merci pour tout. Et merci Katie Darribat ! Je ne savais jamais quoi dire... je suis désolée.

Dear Min Dong, I thank you cordially!! Thanks for the time you've always taken for me. Thanks for all your precious advice!

Meiner kleinen Familie bei Novartis möchte ich von Herzen danken. Es war eine superschöne Zeit mit Euch!!! Mama, Papa, Kai-Uwe, Bubi und meine Mädels – ich hoffe, wir werden den Kontakt nicht verlieren!
Liebe Marianne Schwald. Dein Wissen, Dein Gedächtnis, Deine Erfahrungen, Deine Liebe zum Labor und zu Deiner Arbeit sind Wahnsinn. Danke für all Deine Geduld mit mir, danke, dass es Dir nie leid wurde mich zu unterstützen, mich aufzubauen und Deine Versuche, mich selbstbewusster zu machen.
Die Arbeit mit Virginie Riebel und Sabine Ackerknecht – es war sooo cool! Was haben wir alles gearbeitet (!) – aber was hatten wir auch einen Spaß im Labor! Ich danke Euch aufrichtig für all die Diskussionen und Eure Unterstützung, dass Ihr mir Eure Techniken und Ansichten beigebracht habt und immer Zeit für mich hattet. Danke für Eure Freundschaft!! Danke für die tolle Zeit im Labor!
Martin Schneider danke ich für die schöne Zeit mit ihm - speziell bei unseren gemeinsamen Wettkämpfen, für seine Aufmunterungen und die Einblicke in das Basler Leben. Und auch für den „Notfall-Zucker".

Merci à toutes « mes » francais pour m'apprendre cette jolie langue est pour la patience avec moi (especialement Jean-Mich, Magali– ouais, aussi á Virginie qui devais m'écouter toute la journée ☺). C'était *vachement* bon et j'ai eu beaucoup de plaisir avec vous !

Rico Funhoff, ik ben intens dankbaar voor al zijn steun, besprekingen evenals de motivatie hij me in het laboratorium, op de hemelen en in de kabel gaf! U

redde me meerdere keren, en, het belangrijkst, hebt u en Axel me getoond welke wetenschap betekent. Thank you so, so much!!

Maître « Excel » - ou maître « Word » ?? Axel Vicart, c'était si bien d'être avec toi dans le bureau !! Merci pour me donner des bons mots, de m'encourager et me faire rigoler. J'ai appris beaucoup beaucoup. Un grand merci - pour tout !!

Jean-Philippe Gasser, merci pour m'introduire dans la système d'invitrogen et Licor, pour ta patience et la bonne voisinage ! C'était un temps avec <beaucoup de plaisir> ! ☺
Soon-Siong Teo, thanks for all the jokes the "whole" day long!

Brigitte Greiner je te remercie pour ton effort de me montrer et expliquer ton spécialité immunohistochimie ! En plus, pour les discussions et ton aide avec la culture des cellules cardiacs.
Antonietta Langenegger-Trotta, Verena Schneider, Kurt Zimmermann und René Schaffner: Herzlichen Dank für Eure Hilfe und bereitwillige Unterstützung!

Ein Dankeschön an meine Korrekturleser Harald Stier, Sandra Gauster und Clemens Reisinger!

Claudio Gardi, Sonja Degner, Diana Correa und Yannick Geissmann, ich danke Euch für die schöne Zeit und Eure Freundschaft!
Meinen Kletterjungs und –mädels bin ich sehr dankbar für die willkommene Abwechslung nach der Arbeit: Urs Mathis, Fabienne Jäggi, Elias Lambrigger, Robin Pulfer, Fabian Dreher, Sabrina Adler, Thomas Bayer, Clemens Reisinger.

Meinen Freunden Sandra Gauster, Michael Linek, Hanna Bachhofer, Urs Mathis, Daniel Steffen, Manuela Göttel, Yvonne Fery, Silke Weyland, Sebastian Ganß, Claudia Handrich, Christian Strupp und Robert Rychtarski danke ich für Ihre moralische Unterstützung und für die Zeit, die wir miteinander verbracht haben.

Für die ehrlichen Diskussionen und Unterstützung danke ich Herrn und Frau Prof. Reisinger.

Meinen Eltern und Großeltern danke ich von ganzem Herzen, dass sie mich immer unterstützt haben und hinter mir stehen.

Clemens: Danke!

8.2 Curriculum Vitae

Anja Nussher
geboren am 26. März 1980 in Bad Friedrichshall, Deutschland

1986 – 1990	**Grund**- und Hauptschule Schefflenz
1990 – 1999	Nicolaus-Kistner-**Gymnasium** Mosbach
1999 – 2005	**Studium** der Lebensmittelchemie an der Technischen Universität Kaiserslautern
01/2004 - 03/2004	**Forschungsarbeit** im Arbeitskreis von PD Dr. Doris Marko, Fachrichtung Lebensmittelchemie, Umwelttoxikologie und molekulare Ernährungsforschung der TU Kaiserslautern *„Effekte von Phenolcarbonsäuren auf das Zellwachstum humaner Kolonkarzinomzellen und den epidermalen Wachstumsfaktor-Rezeptor (EGFR)“*
10/2004 - 03/2005	**Diplomarbeit** im Arbeitskreis von PD Dr. Doris Marko, Fachrichtung Lebensmittelchemie, Umwelttoxikologie und molekulare Ernährungsforschung der TU Kaiserslautern *„Modulation von Signalkettenelementen der mitogen aktivierbaren Proteinkinase-Kaskade durch ausgewählte Flavonoide sowie deren postulierte Abbauprodukte“*
05/2005 – 08/2008	**Doktorarbeit** in der Gruppe von Prof. Dr. Armin Wolf, Sektion investigative Toxicology der Novartis Pharma AG, Basel *„Evaluation of the Role of c-Abl in Imatinib-induced Toxicity in Cardiomyocytes*
26.02.2009	*wissenschaftliche Verteidigung*
11/2008 – 02/2009	**Praktikum** bei Nestlé Suisse S.A., Fabrik Basel Methodenentwicklung zur Eingangskontrolle von Senfsaaten, Toxikologische Bewertungen, Degustationen, Unterstützung von Projektleitern